

71-14

AD 728509

Contract No. Nonr 830 (30)
ARPA Order No. 630

Contract No. DANCO4-60-C-0077
ARPA Order No. 1412, Amendment 2
Program Code 9E30

**TURBULENT HEAT AND MASS TRANSFER
IN AXISYMMETRIC JETS**

by

Robert F. Mons and Pasquale M. Sforza

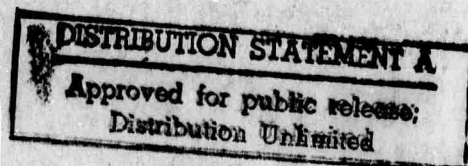


POLYTECHNIC INSTITUTE OF BROOKLYN

**DEPARTMENT
of
AEROSPACE ENGINEERING
and
APPLIED MECHANICS**

MAY 1971

Reproduced by
**NATIONAL TECHNICAL
INFORMATION SERVICE**
Springfield, Va. 22151



Distribution of this
document is unlimited.

PIBAL REPORT NO. 71-14

137

DOCUMENT CONTROL DATA - R & D

(Security classification of title, body of abstract and indexing annotation must be entered when the overall report is classified)

1. ORIGINATING ACTIVITY (Corporate author) Polytechnic Institute of Brooklyn Dept. of Aerospace Eng. and Applied Mechanics Route 110, Farmingdale, New York 11735		2a. REPORT SECURITY CLASSIFICATION Unclassified	
		2b. GROUP	
3. REPORT TITLE TURBULENT HEAT AND MASS TRANSFER IN AXISYMMETRIC JETS			
4. DESCRIPTIVE NOTES (Type of report and inclusive dates) Research Report			
5. AUTHOR(S) (First name, middle initial, last name) Robert F. Mons Pasquale M. Sforza			
6. REPORT DATE May 1971		7a. TOTAL NO. OF PAGES 121	7b. NO. OF REFS 27
8a. CONTRACT OR GRANT NO. Nonr 839(38) and DAHCO4-69-C-0077		9a. ORIGINATOR'S REPORT NUMBER(S) PIBAL Report No. 71-14	
b. PROJECT NO. ARPA Order Nos. 529 and 1442		9b. OTHER REPORT NO(S) (Any other numbers that may be assigned this report)	
c.			
d.			
10. DISTRIBUTION STATEMENT Distribution of this document is unlimited.			
11. SUPPLEMENTARY NOTES		12. SPONSORING MILITARY ACTIVITY Office of Naval Research and U.S. Army Research Office-Durham	
13. ABSTRACT The problem of turbulent mixing is examined with emphasis on mass, momentum, and energy transport in an axisymmetric free jet. An experimental investigation of the response of a pitot tube, a thermocouple, and a sampling probe to a known periodic fluctuating flow with variable intensity of fluctuations is performed. The results indicate that the pitot tube response yields an adequate measure of the mean momentum flux in the incompressible range for any level of velocity fluctuation intensity in the direction of the probe axis. On the other hand, the thermocouple and sampling probe are found to be subject to significant errors in the measurement of mean temperature and mean concentration, respectively, in the high shear regions of a turbulent free jet. An experimental examination of the flow field of a turbulent axisymmetric free jet for non-homogeneous and non-isothermal conditions is performed. The mean fluxes of mass, momentum and total enthalpy are considered to be the dependent variables. New probes are developed specifically for measuring these flux quantities. The results indicate that, for identical initial conditions, the flux of mass and the flux of total enthalpy should behave identically and that both of these variables decay faster			

14.	KEY WORDS	LINK A		LINK B		LINK C	
		ROLE	WT	ROLE	WT	ROLE	WT
	Turbulent jets Heat transfer Mass transfer Experimental techniques Theoretical analysis						

DOCUMENT CONTROL DATA - R & D

13. ABSTRACT (Contd.)

and have larger halfwidths than does the momentum flux. However, the radial coordinate at which the value of the flux variable is sensibly equal to zero, that is, the mean "edge" of the jet, is found to be the same for all flux variables.

An extended version of the Reichardt inductive theory of free turbulence is found to adequately describe the entire flow field for all of the conserved flux variables.

TURBULENT HEAT AND MASS TRANSFER IN AXISYMMETRIC JETS

by

Robert F. Mons and Pasquale M. Sforza

This research was supported in part under Contract No. Nonr 839(38) for PROJECT STRATEGIC TECHNOLOGY, by the Advanced Research Projects Agency under Order No. 529 through the Office of Naval Research; and in part under Contract No. DAHCO4-69-C-0077, monitored by the U.S. Army Research Office-Durham and supported under ARPA Order No. 1442.

Reproduction in whole or in part is permitted for any purpose of the United States Government.

POLYTECHNIC INSTITUTE OF BROOKLYN

Department

of

Aerospace Engineering and Applied Mechanics

May 1971

PIBAL Report No. 71-14

TURBULENT HEAT AND MASS TRANSFER IN AXISYMMETRIC JETS[†]

by

Robert F. Mons[‡] and Pasquale M. Sforza^{*}

Polytechnic Institute of Brooklyn
Preston R. Bassett Research Laboratory
Farmingdale, New York

ABSTRACT

The problem of turbulent mixing is examined with emphasis on mass, momentum, and energy transport in an axisymmetric free jet.

An experimental investigation of the response of a pitot tube, a thermocouple, and a sampling probe to a known periodic fluctuating flow with variable intensity of fluctuations is performed. The results indicate that the pitot tube response yields an adequate measure of the mean momentum flux in the incompressible range for any level of velocity fluctuation intensity in the direction of the probe axis. On the other hand,

[†]This research was supported in part under Contract No. Nonr 839(38) for PROJECT STRATEGIC TECHNOLOGY, by the Advanced Research Projects Agency under ARPA Order No. 529 through the Office of Naval Research; and in part under Contract No. DAHCO4-69-C-0077, monitored by the U.S. Army Research Office-Durham and supported under ARPA Order No. 1442.

[‡]Research Associate, Dept. of Aerospace Engineering and Applied Mechanics.

^{*}Associate Professor of Aerospace Engineering.

the thermocouple and sampling probe are found to be subject to significant errors in the measurement of mean temperature and mean concentration, respectively, in the high shear regions of a turbulent free jet.

An experimental examination of the flow field of a turbulent axisymmetric free jet for non-homogeneous and non-isothermal conditions is performed. The mean fluxes of mass, momentum and total enthalpy are considered to be the dependent variables. New probes are developed specifically for measuring these flux quantities. The results indicate that, for identical initial conditions, the flux of mass and the flux of total enthalpy should behave identically and that both of these variables decay faster and have larger halfwidths than does the momentum flux. However, the radial coordinate at which the value of the flux variable is sensibly equal to zero, that is, the mean "edge" of the jet, is found to be the same for all flux variables.

An extended version of the Reichardt inductive theory of free turbulence is found to adequately describe the entire flow field for all of the conserved flux variables.

TABLE OF CONTENTS

<u>Section</u>		<u>Page</u>
I	Introduction	1
II	Discussion of the Extended Reichardt Analysis	10
III	Investigation of Conventional Experimental Devices	16
IV	Development of Experimental Techniques to Measure Flux Variables	37
V	Experimental Results and Comparison to Theory	52
VI	Summary	75
VII	References	78

LIST OF ILLUSTRATIONS

<u>Figure</u>		<u>Page</u>
1a	Summary of Data for Centerline Decay of Concentration and Temperature from Ref. 17	81
1b	Summary of Data for Halfwidths of Concentration, Temperature and Velocity from Ref. 17	82
2	Schematic Diagram of Oscillating Probe Facility	83
3	Typical Velocity Profile at Exit of Double Chamber for Oscillating Probe Experiment	84
4	Variation of Error in Mean Temperature Measured by a Thermocouple in Percent as a Function of Intensity of Velocity Fluctuation and Mean Temperature	85
5	Effects of Concentration Gradient on Mean Concentration Measurements Made by a Sampling Probe	86
6	Effects of Sampling Rate on Mean Concentration Measurements Made in the Flow Field of a Turbulent Axisymmetric Jet	87
7	Results from Oscillating Experiment Showing Variation of Error in Percent in Mean Concentration Measurements as a Function of Intensity of Velocity Fluctuations	88
8	Results from Oscillating Experiment Showing Variation of Error in Percent in Mean Concentration Measurements as a Function of Sampling Rate	89

<u>Figure</u>		<u>Page</u>
9	Geometries Investigated for Inlet of Mass Flux Probe and Details of Final Design Chosen	90
10	Schematic of Gas Sampling and Analyzing System	91
11	Results of Temperature Measurements Made at the Exit of a Free Jet With Greyrad Calorimetric Probe	92
12a	Schematic Diagram of Greyrad Calorimetric Probe	93
12b	Schematic Diagram of Calorimetric Probe Designed to Measure Mean Enthalpy Flux, $\overline{\rho u h}$	94
13	Schematic Diagram and Photograph of Uncooled Probe Designed to Measure Mean Total Enthalpy Flux, $\overline{\rho u h_t}$	95
14	Results of Measurements of Mean Total Enthalpy Flux Made at the Exit of a Free Jet With Uncooled Probe	96
15	Schematic Diagram of Non-Homogeneous Jet Facility	97
16	Schematic Diagram of Homogeneous Jet Facility	98
17	Photographs of Non-Homogeneous and Homogeneous Jet Facilities	99
18	Initial Profile of Momentum Flux for Homogeneous, Isothermal Free Jet	100
19	Conservation of Total Momentum Flux and Growth of Total Mass Flux of Air for the Homogeneous, Isothermal Jet.	101

<u>Figure</u>		<u>Page</u>
20	Theoretical and Experimental Behavior of Centerline Values of Momentum Flux for Homogeneous, Isothermal Jet	102
21	Transformation Between Physical Coordinate \bar{x} and Transform Coordinate $\bar{\chi}$ for Homogeneous, Isothermal Jet	103
22	Comparison Between Theory and Experiment for Complete Momentum Flux Flow Field for Homogeneous, Isothermal Jet	104
23	Results of Measurement of Intensity of Axial Velocity Fluctuations from Momentum Flux and Mass Flux	105
24	Initial Profiles of Momentum Flux and Mass Flux of CO_2 for Non-Homogeneous, Isothermal Free Jet	106
25	Conservation of Total Momentum Flux and Total Mass Flux of CO_2 and Growth of Total Mass Flux of Air for the Non-Homogeneous, Isothermal Free Jet	107
26	Behavior of Centerline Values of All Flux Variables for Non-Homogeneous, Isothermal Jet	108
27	Transformations Between Physical Coordinate \bar{x} and Transform Coordinate $\bar{\chi}$ for Momentum Flux and Mass Flux of CO_2 for Non-Homogeneous, Isothermal Jet	109

<u>Figure</u>		<u>Page</u>
28	Halfwidth Behavior of All Flux Variables for Non-Homogeneous, Isothermal Jet	110
29	Comparison Between Theory and Experiment for Complete Momentum Flux Flow Field for Non- Homogeneous, Isothermal Jet	111
30	Comparison Between Theory and Experiment for Complete CO ₂ Mass Flux Flow Field for Non- Homogeneous, Isothermal Jet	112
31	Initial Profiles of Momentum Flux and Enthalpy Flux for Homogeneous, Non-Isothermal Jet	113
32	Conservation of Total Momentum Flux and Total Flux of Stagnation Enthalpy Minus Ambient Enthalpy and Growth of Total Mass Flux	114
33	Behavior of Centerline Values for All Flux Variables for Homogeneous, Non-Isothermal Jet	115
34	Transformation Between Physical Coordinate \bar{x} and Transform Coordinate $\bar{\chi}$ for Momentum Flux and Enthalpy Flux for Homogeneous, Non-Isothermal Jet	116
35	Halfwidth Behavior of All Flux Variables for Homogeneous, Non-Isothermal Jet	117
36	Comparison Between Theory and Experiment for Complete Momentum Flux Flow Field for Homogeneous, Non-Isothermal Jet	118
37	Comparison Between Theory and Experiment for Complete Enthalpy Flux Flow Field for Homogeneous, Non-Isothermal Jet	119

<u>Figure</u>		<u>Page</u>
38	Comparison of Transformations Between Physical Coordinate \bar{x} and Transform Coordinate $\bar{\chi}$ for All Jets Investigated	120
39	Comparison of Relative Entrainment for All Jets Investigated	121

LIST OF SYMBOLS

A	area
C	concentration
d	diameter of jet orifice
$^{\circ}F$	degrees Fahrenheit
h	enthalpy
Δh_t	stagnation enthalpy minus enthalpy of ambient fluid
\dot{m}	mass flow
P	pressure
Q	quantity defined in Table 1
Q_{energy}	generalized energy creation function
r	radial coordinate
$r_{1/2}$	halfwidth: that value of the radial coordinate at which the value of some variable is one-half its value at $r=0$
\bar{r}	r/d
r'	integration variable defined by Eq. (10)
T	temperature
u	axial velocity
v	radial velocity
\dot{w}_i	rate of production of species i
x	axial coordinate
\bar{x}	x/d
x'	integration variable defined by Eq. (8)
X_i	mole fraction of species i
Y_i	mass fraction of species i
Γ	temperature or concentration

$\Lambda(x)$	transform function defined by Eq. (3)
ω	quantity defined in Table 1
ρ	density
$(\rho u)_{\text{equiv.}}$	the distribution of mass flux of ambient temperature air that would produce the initial distribution of momentum flux, $\overline{\rho u^2}$, that actually exists for a given non-homogeneous or non-isothermal jet
ω	frequency of oscillation
x	axial coordinate defined by Eq. (8)
\overline{x}	x/d

Barred Quantities

except for coordinate variables, refers to time average

Subscripts

amb.	refers to ambient value
c	refers to coolant
e	refers to value at $r=0$, $x=0$
f	refers to a species other than the ambient species
i	refers to species i
meas.	refers to a value measured by a probe
mix	refers to a non-homogeneous gas
p	refers to probe
p.c.	refers to length of potential core
s	refers to measurement made while sampling
t	refers to stagnation value
ϕ	refers to quantities ϕ defined in Table 1

∞ refers to undisturbed local flow conditions
 $o.o$ refers to measurements at $\bar{x}=0, \bar{r}=0$
 \bar{x}, o refers to measurements at $\bar{r}=0$ and a distance from
 \bar{x} from the jet exit
 \bar{r}, o refers to measurements at $\bar{x}=0$ and a distance \bar{r}
from the axis

Superscripts

' designates the fluctuating quantities in a
turbulent flow

BLANK PAGE

I. INTRODUCTION

1. Background

The problem of free turbulent mixing of fluids has elicited considerable interest from researchers both for its diversity of application and its appeal as a classical problem of the flow of real fluids. The volume of material concerning the subject is staggering, and yet, there are certain aspects of even the most simplified problems which defy understanding.

Researching the literature suggests that investigations into turbulent mixing have generally followed one of two paths; one being the "statistical" approach; the other, the "phenomenological" approach. The statistical school has utilized the mathematics of statistics to examine the details of the turbulent motions. The phenomenological school, on the other hand, has largely ignored the details of the turbulence, since such details often preclude the application of that body of fluid dynamic analysis which has been so successfully applied to the study of laminar flows. Instead, this school has primarily concerned itself with the effects of turbulence on the flow. The work presented here will be in the phenomenological line.

The familiarity of the fluid dynamicist with the formalism that is associated with the treatment of laminar flows appears to have strongly influenced the development of the phenomenological approach. The equations for turbulent flow

are cast in a form analogous to laminar flow and the variables are characterized by the sum of mean and fluctuating components. Time averaging of the equations results in additional terms which attest to the fact that the fluctuations are not truly unrelated but can be correlated. To obtain closure it becomes necessary to relate the correlations to the mean properties of the flow, and it is here that the familiarity with laminar flows appears responsible for the introduction of the concept of the eddy transfer coefficient. The formalism is now complete. Such a study of turbulent flow is reduced to the study of laminar flow of a fluid with unusual transport properties. The solution of a particular problem now hinges upon choice of the "correct" form for the eddy transfer coefficient; the criteria for deciding which model is correct being the ability of the subsequent theory to reproduce a given set of experimental data.

Regarding the development of the phenomenological approach it is important to realize that the form of the correlations generated is entirely dependent upon the choice of the dependent variables, e.g., whether one considers that ρ and u are separate variables or instead that the mass flux (ρu) is a single variable. Furthermore, there is no formal derivation which indicates that the correlations must resemble the relations for laminar transport of mass, momentum, or energy. Hence, there is no strong foundation for the "laminarization" of the turbulent flow equations.

A more thorough description of the development of the phenomenological approach and the reasons for the rejection

of the "laminarized" approach to turbulent mixing problems has been presented by Sforza et al¹. These arguments provided the motivation to seek alternate means to analyze turbulent mixing flows.

2. The Extended Reichardt Analysis

As stated in Ref. 1, "The only well-known analysis of free turbulent flows that does not follow a laminarized approach is that due to Reichardt²; i.e., the 'inductive' theory of free turbulence". Reference 1 also gives some of the background as well as a basic formulation of this theory. The inductive theory, in general, has received little attention within this country, but appears to have been developed rather well in some of the Russian literature^{3,4}. Recently, considerable effort has been expended at the Polytechnic Institute of Brooklyn to evaluate the utility of the inductive theory in modeling free turbulent flows.

There are several salient features of the inductive theory which should be pointed out:

i) The theory is truly "inductive" in that the development has depended upon experimental results to suggest the proper formulation. The practice of establishing inductive theories is quite common in the basic sciences and may help in the treatment of the complex problem that turbulent mixing presents.

ii) The inductive theory, as developed in this work, uses the flux of mass, momentum, and energy as the dependent variables. Use of these variables, in the absence of laminar

transport, renders the fluid dynamic equations in a form completely devoid of any of the usual fluctuation correlations.

iii) Under the Reichardt hypothesis, the fluid dynamic equations become analogous to the equation describing the conduction of heat in solids. For many cases, the equations are linear and thus amenable to well-developed analytic techniques for solution.

iv) The inductive theory does not distinguish between compressible or incompressible flows, hence, eliminating the considerable complexity that enters the laminarized approach for treatment of compressible flows.

As indicated in item (ii) above, the inductive theory uses the flux of mass, momentum, and energy as the dependent variables. While this leads to great simplification of the theoretical analysis, it poses a problem when comparing the results to experimental data because the existing experimental equipment has been developed to measure the variables used in "laminarized" theories, namely, velocity, temperature, and concentration. It will be demonstrated in this work that there is considerable doubt as to the accuracy of measurements of mean temperature and concentration in turbulent shear flows. These basic inaccuracies may lead to cumulative errors when products of the measured variables are formed. Furthermore, even with complete certainty of individual property measurements, products can only be accurate to within the magnitude of the corresponding correlations, e.g., the local mean mass flux of species A is $\overline{\rho_A u} = \overline{\rho_A} \overline{u} + \overline{\rho_A' u'}$. Clearly,

even when $\overline{\rho_A}$ and \overline{u} are known very accurately, the error in $\overline{\rho_A u}$ is of $O(\overline{\rho_A' u'})$. In the shear region of a free jet, one can expect the magnitude of such correlations to be appreciable. Because of these errors, it was considered imperative to develop new experimental techniques which can measure the flux quantities directly. This has been done and the equipment that has been developed will be described in detail further on.

3. Selection of the Flowfield to be Studied

The flowfield selected for investigation in this work is the turbulent, incompressible, axisymmetric free jet. In particular, this flowfield was examined for three cases; namely,

- i) isothermal, homogeneous
- ii) isothermal, non-homogeneous
- iii) non-isothermal, homogeneous

The reasons for selecting this flowfield are listed below:

i) The symmetry of the flowfield simplifies both the theoretical analysis and the experimental measurements considerably while leaving the gist of the problem of turbulent mixing exposed, namely, the rate of mixing of mass vs. momentum vs. energy.

ii) The axisymmetric free jet is a classical problem in turbulent mixing which has received considerable attention; however, there is considerable diversity of the results.

iii) The integrals across the flowfield of the mass flux of a foreign species, momentum flux, and energy flux are

conserved in a free jet. This fact provides an excellent check on the accuracy of the experimental measurements. Furthermore, for identical initial conditions, the absence of walls, injection, etc. insures that any dissimilitude in the rates of mixing of mass vs. momentum vs. energy is a result only of the turbulent mixing process.

4. Results from Previous Investigations

The purpose of this section is to indicate the major conclusions of previous investigations and to present some observations concerning those results. Presentation of a complete bibliography on free turbulent mixing would serve little purpose for the present investigation and the reader is referred to works from Goldstein⁵, Schlichting⁶, Townsend⁷, Pai⁸, Hinze⁹, Abramovich¹⁰, Kryzwoblocki¹¹, Halleen¹², Zakkay and Fox¹³, Smoot¹⁴ and Harsha¹⁵ for such information.

The single universal conclusion derived from previous investigations is the apparent preferential transport of scalar fluid properties; namely, mass and heat, over vector properties; namely, velocity. There is great diversity of results for the quantitative behavior of all the variables; there has been little effort expended studying the development of the jet; and as Trentacoste and Sforza¹⁶ point out, "Blatant inconsistencies exist in the vast collection of experimental data on turbulent mixing problems", but there is universal agreement that scalar quantities "mix" faster than the velocity.

The axisymmetric jet is usually treated as consisting of three regions, namely, potential core, transition region, and self-preserving region. As the name suggests, the profiles in this last region are assumed to be self-preserving in nature and, thus, the bulk properties such as centerline decay rate and halfwidth growth rates can be predicted from conservation principles. It is not surprising, then, that researchers have come to agree on the power-law behavior of the jet far from the exit.

Considerable disagreement exists over the potential core length and the nature of the transition region; much of this variation probably results from differences in initial conditions. Yet, even when the x-axis is shifted to remove the potential core, there is no universal agreement on the centerline decay and halfwidth growth behavior as is shown in Fig. 1, which presents the bounds of behavior from the references quoted by Becker et al¹⁷. The diversity of the quantitative results reflects both the irregularity in experimental conditions where results should be different (e.g., initial conditions) and the difficulty in obtaining accurate measurements in turbulent shear flows.

The purpose of the present work is not an attempt to define "the" growth and decay of "the" turbulent jet, but more fundamentally to question whether scalar properties do "mix" faster than vector properties. Despite the agreement on preferential "mixing", there is, curiously, very little discussion of just what "mixing" means. The impression is

given that a quantity A mixes faster than quantity B if, at a given value of x/d , the centerline value of A, referred to the exit value, is less than that of B and the A halfwidth is greater than the B halfwidth. Of importance is whether it is meaningful to compare the quantities \bar{u} , \bar{T} , and \bar{X}_i when speaking of mixing. What is the physical significance of these quantities? Are these the variables which best describe the condition of mixedness in a turbulent flow? It is the authors' contention that these are not necessarily the most pragmatic variables available. A number of examples are presented below to support this contention.

Consider a free jet in which the flux of mass of a foreign species, the total momentum flux and the flux of energy must be conserved. The variables \bar{u} , \bar{T} , and \bar{X}_i are usually suggested as a measure of momentum, energy, and mass respectively, and yet integration of the profiles of these quantities alone is meaningless. It is the integration of $\overline{\rho u^2}$, $\overline{\rho u(h_t - h_{amb})}$ and $\overline{\rho_i u}$ that should be used to demonstrate conservation principles.

Suppose one is interested in determining the pollution output from a chimney and, therefore, one measures the concentration of the pollutant across the entire exit of the chimney. What is the physical significance of the concentration? Is it not the flux of the pollutant, which when integrated gives the total rate of output of the pollutant, that is significant? The thrust of a jet is found by integrating the momentum flux of the jet somewhere downstream of the exit;

knowledge of the velocity alone is insufficient.

From the above examples, it appears that for free turbulent flows, the flux variables may have superior physical significance over the usual variables. The remainder of this work concerns itself with evaluating the utility of employing these variables for analyzing free turbulent flows.

5. Objectives of the Present Work

The discussion presented up to this point indicates the motivation and direction for the work that was performed.

Listed below is a summary of the objectives:

i) To experimentally demonstrate that certain conventional measurement techniques are subject to significant errors in a fluctuating shear flow. Such errors may relate to the observed preferential transport of scalar quantities.

ii) To present a theoretical description of the non-homogeneous, non-isothermal free jet in terms of flux variables.

iii) To develop new experimental instruments to measure the flux variables accurately.

iv) To experimentally investigate the flowfield of the incompressible axisymmetric free jet in terms of flux variables to establish whether a preferential transport exists in terms of these variables and also to establish the suitability of the extended Reichardt theory.

The authors wish to express their appreciation to Prof. M.H. Bloom for his encouragement and discussions during the course of this research.

II. DISCUSSION OF THE EXTENDED REICHARDT ANALYSIS

1. Introduction

The important features of the extended Reichardt analysis which make this theory attractive for investigation of free turbulent mixing flows have been presented in Section I. The application of this theory to specific problems has been done previously by Mummolo¹⁸, Mons and Sforza¹⁹, and by Trentacoste and Sforza¹⁶. Within this section, a summary of the general development of the theory and the form of the solution for the specific cases that are investigated in this work are presented.

2. General Development of the Extended Reichardt Analysis

The differential equations which describe the motion of a fluid can be derived from considerations of the conservation of mass, momentum, and energy and may be found in many textbooks. For the condition of steady mean two-dimensional or axisymmetric flow, these equations can be expressed, with the use of the continuity equation and after the usual time-averaging, in the general form listed below:

$$\frac{\partial}{\partial x} (\overline{\rho u \varphi}) + \frac{1}{r^j} \frac{\partial}{\partial r} [r^j (\overline{\rho u \varphi})] = \overline{Q} \quad (1)$$

where $j=0$ for two-dimensional flow and $j=1$ for axisymmetric flow. Table I lists the variables which may be represented by φ and Q where laminar transport and body forces are neglected.

TABLE I		
Quantity	φ	Q
species mass	Y_i	\dot{w}_i
momentum	u, v	$-\frac{\partial P}{\partial x}, -\frac{\partial P}{\partial r}$
energy	$h_t - h_{amb.}$	Q_{energy}

Note that the system of Eqs. (1) will be devoid of the usual correlations if the quantities within the parentheses are treated as a single variable.

When Eq. (1) is integrated over all space, we obtain

$$\frac{\partial}{\partial x} \iint_0^{\infty} (\overline{\rho u \varphi}) dA = \iint_0^{\infty} \overline{Q} dA \quad (2)$$

Hence, in the absence of generation terms such as pressure gradients, chemical reactions, heat addition, etc., Eq. (2) states that the total flux of each quantity originates entirely at the initial station and is invariant.

The crux of the present theory lies in the suggestion made by Reichardt² and generalized by Baron and Alexander²⁰ that

$$\overline{\rho v \varphi} = -\Lambda(x) \frac{\partial (\overline{\rho u \varphi})}{\partial r} \quad (3)$$

Thus the system described by Eq. (1) becomes

$$\frac{\partial}{\partial x} (\overline{\rho u \varphi}) - \frac{\Lambda(x)}{r^j} \frac{\partial}{\partial r} [r^j \frac{\partial}{\partial r} (\overline{\rho u \varphi})] = \overline{Q} \quad (4)$$

This equation is analogous to the equation for heat conduction where diffusivity is a function of time and heat is generated within the system. If Q is linear in the dependent variable, then the equation is linear and may be treated by many well

known analytical techniques with the specification of the proper boundary and initial conditions. Rather arbitrary initial conditions may be specified at the initial station; this permits analysis of many geometrical configurations and the attendant initial distributions of $\overline{\rho u \phi}$.

The approximation represented by Eq. (3) is without rational foundation and can be justified only by the accuracy of the results produced.

3. Specific Development of the Analysis for Turbulent Axisymmetric Free Jets Issuing From Orifices of Finite Dimension

We shall now seek solutions for the streamwise flux of mass, momentum, and energy for turbulent axisymmetric free jets issuing from orifices of finite dimension utilizing the extended Reichardt analysis discussed in the above topic. The solutions obtained are to correspond to the three cases examined experimentally; namely, a homogeneous isothermal jet, a homogeneous non-isothermal jet, and a non-homogeneous isothermal jet. Specifically, this requires solution for the momentum flux distribution for each case, the energy flux distribution for the non-isothermal jet and the mass flux distribution of the foreign species for the non-homogeneous jet.

Solutions of the system of equations (4) have been obtained in other works^{16,18,19} so that only a brief outline of the procedure is necessary here. We seek solution of the equation

$$\frac{\partial}{\partial x}(\overline{\rho u \varphi}) = \frac{\Lambda(x)}{r} \frac{\partial}{\partial r} \left[r \frac{\partial}{\partial r} (\overline{\rho u \varphi}) \right] \quad (5)$$

where $\varphi = u, h_t - h_{\text{amb.}}$ or Y_f , and with initial conditions

$$\text{at } x=0: \quad \overline{\rho u \varphi} = \begin{cases} f_{\varphi}(r') & \text{for } r' < \frac{d}{2} \\ 0 & \text{for } r' \geq \frac{d}{2} \end{cases} \quad (6)$$

and boundary condition

$$\overline{\rho u \varphi} \rightarrow 0 \quad \text{as } r \rightarrow \infty \quad (7)$$

Here, d is the diameter of the orifice.

$\Lambda(x)$ is unknown and must be obtained by comparison between theory and experiment. For convenience, we introduce the transformation²¹

$$\chi = \int_0^x \Lambda(x') dx' \quad \text{or} \quad d\chi = \Lambda(x) dx \quad (8)$$

Under the transformation (8), Eq. (5) becomes

$$\frac{\partial(\overline{\rho u \varphi})}{\partial \chi} = \frac{1}{r} \frac{\partial}{\partial r} \left[r \frac{\partial}{\partial r} (\overline{\rho u \varphi}) \right] \quad (9)$$

The solution of (9) for arbitrary initial conditions²² is

$$\overline{\rho u \varphi} = \frac{1}{2\chi} \exp\left\{-\frac{r^2}{4\chi}\right\} \int_0^{\frac{d}{2}} \exp\left\{-\frac{r'^2}{4\chi}\right\} I_0\left(\frac{rr'}{2\chi}\right) f_{\varphi}(r') r' dr' \quad (10)$$

where $I_0\left(\frac{rr'}{2\chi}\right)$ is a modified Bessel function of order zero

and has the form $I_0(z) = \sum_{m=0}^{\infty} \frac{(z^2)^m}{m! \Gamma(m+1)}$. Nondimensionalization of the solution with respect to the exit diameter yields

$$(\overline{\rho u \varphi}) = \frac{1}{2\chi} \exp\left\{-\frac{\bar{r}^2}{4\chi}\right\} \int_0^{\frac{1}{2}} \exp\left\{-\frac{\bar{r}'^2}{4\chi}\right\} I_0\left(\frac{\bar{r}\bar{r}'}{2\chi}\right) f_{\varphi}(\bar{r}') \bar{r}' d\bar{r}' \quad (11)$$

The specific solution for each case indicated above is obtained by specification of each initial condition $f_{\varphi}(r')$ and specification of the form of the transformation (8).

The size of the apparatus employed in the present experimental study made it difficult to obtain a precise

exit profile for each of the quantities; however, reasonable profiles were obtained for momentum flux and energy flux and an analytic approximation was used in the theoretical development for each case. A good determination of the species flux at the exit was not possible; however, the measured concentration profile was flat so that the square root of the exit momentum profile was considered a good approximation for the exit species flux profile. The particular expressions used and the results obtained are presented in a future section.

4. Discussion of Preferential Mixing and the Inductive Theory

Note that $\Lambda(x)$ may be a different function for each of the dependent variables represented by φ . Such would be the case if there is a different rate of mixing, as the term is usually applied, for each of the dependent variables. Upon application of the transformation represented by Eq. (8), however, a single form for the governing equations is obtained. Thus, in the transformed system of coordinates, the only difference in the solution for each of the dependent variables is the result of different initial conditions, and for identical initial conditions, the solutions for each of the variables are identical. In the inductive theory, difference in the rates of mixing are manifested only in the form of the transformation between \bar{x} and $\bar{\chi}$.

The property of the inductive theory discussed above can be used to establish whether preferential mixing exists for the flux variables. Comparing the transformation between \bar{x}

and $\bar{\chi}$ is especially useful because of the ability of the inductive theory to account for variation in centerline decay and halfwidth growth that is a result of differences in initial conditions. Thus, in this work, a difference in the rate of turbulent mixing will be defined as a difference in the transformation between \bar{x} and $\bar{\chi}$, and a quantity A will be said to mix faster than a quantity B if for a given value of \bar{x} the corresponding value of $\bar{\chi}$ for quantity A is greater than the corresponding value of $\bar{\chi}$ for quantity B.

5. Conclusion

At this point, a complete description of the theoretical approach utilized in this paper has been given in principle. The theoretical results are compared to the experimental results in Section V.

III. INVESTIGATION OF CONVENTIONAL EXPERIMENTAL DEVICES

1. Introduction

As mentioned previously, one of the major objectives in studying non-homogeneous, non-isothermal jet flows has been to evaluate and understand the apparent preferential transport of scalar quantities in such flows. Yet, there appear to be few investigations to evaluate the response of the commonly used probe designs in fluctuating high shear regions as are encountered in jet flows. Without certainty of the probe's response, one can question whether there really is a preferential transport of scalar quantities in the turbulent jet or whether the measuring techniques bias the readings of concentration, temperature, and velocity in such a way that there only appears to be a preferential transport.

To obtain some knowledge of the response of pitot tubes, thermocouple probes, and sampling probes to a fluctuating flowfield an experiment was conducted subjecting these probes to a known periodic flowfield of variable velocity, temperature, and concentration fluctuation intensities. Since the true time average value of each quantity was known, the errors in mean values measured were easily computed. The results from this experiment are presented in this section.

In addition, some observations are presented concerning the design of thermal conductivity cell gas analyzers and the use the hot wire anemometer in non-isothermal, non-homogeneous turbulent flows.

2. Description of Experimental Apparatus

To achieve a known periodic fluctuating flowfield, a settling chamber was constructed with a splitter plate across its diameter. Two chambers with adjacent exit orifices capable of producing two parallel jets was thus formed. As shown in Fig. 2, the exit orifices are .375 inches square and the splitter plate is machined to a sharp edge resulting in an effective exit .375 inches wide by .750 inches high. Each settling chamber is fed by a separate air supply; one supply is always air at room temperature, the other is varied to achieve the desired non-isothermal or non-homogeneous conditions.

Fluctuation was achieved by mounting the probe on an oscillating piston driven by a crankshaft with a total stroke of .375 inches. With the probe at the exit of the chamber, this results in the probe moving between the centers of the two orifices. The center-to-center length of the connecting rod employed is 2.000 inches with a resulting rod length to crank throw ratio of 10.67. The motion of the piston for such a ratio is very nearly sinusoidal. Point-by-point measurement of the complete (steady) exit profile of the chamber together with assumption of sinusoidal motion allows accurate numerical integration of the steady exit flow variables through one cycle to arrive at the true time average that the oscillating probe senses.

The various probes examined are also shown in Fig. 2. For the gas sampling experiment, a specially designed pitot probe

is employed; the sample is fed to a thermal conductivity cell gas analyzer and sampling rate is controlled by a calibrated fine metering valve. The results are discussed subsequently for each probe; the corresponding chamber conditions are listed also.

3. Pitot Probe

The pitot probe is probably the simplest, cheapest, and most reliable device the aerodynamic researcher has at his disposal. When aligned with the local velocity vector, it measures the stagnation pressure of the flow. For incompressible flows the difference between stagnation pressure and static pressure is $\frac{1}{2}\rho u^2$; hence, in this case the probe response is proportional to the momentum flux of the flow. Investigations have shown that the probe is relatively insensitive to misalignment and inlet geometry²³, but there is little agreement as to what the probe measures in a turbulent flow. Hinze⁹ devotes a small section to the problem and the main conclusion is that probably

$$\frac{1}{2}\rho \bar{u}^2 \leq P_{\text{total}} - P_{\text{static}} \leq \frac{1}{2}\rho [(\overline{u+u'})^2 + \overline{v'^2} + \overline{w'^2}] \quad (12)$$

with the note that these limits may be exceeded. In the ideal situation the probe should measure $\frac{1}{2}\rho \bar{u}^2$ or one-half the mean momentum flux in the direction of the axis of the probe.

To determine the effect of the intensity of streamwise velocity fluctuations on the reading of a pitot tube the double chamber facility shown in Fig. 2 was employed with room temperature air supplying both chambers. The double chamber was designed to achieve as flat an exit profile as possible;

a typical total head traverse of the exit is shown in Fig. 3. The sum of the momentum thicknesses for the boundary layers on both sides of the splitter plate was less than .002 inches; hence, the profiles were assumed flat for calculations of the average total head at the exit.

Listed in Table II below are the various chamber conditions used for the pitot tube experiments; also listed are the true average total head, the relative intensity in total head, and the average total head measured by the pitot tube oscillating at approximately 10 hz and 40 hz.

TABLE II

Test No.	P_{t_1} in. H ₂ O	P_{t_2} in. H ₂ O	Actual Av. \bar{P}_t in. H ₂ O	Relative Intensity $\sqrt{\bar{P}_t}/\bar{P}_t$		Observed \bar{P}_t in. 10 Hz.	Av. H ₂ O 40 Hz.
1	1.20	.80	1.00	.20		1.005	.995
2	1.25	.75	1.00	.25		1.005	1.000
3	1.333	1.667	1.00	.333		1.005	1.000
4	1.50	.50	1.00	.50		1.01	1.000
5	2.00	0	1.00	1.00		1.005	.995
6	2.40	1.60	2.00	.20		2.005	1.995
7	2.50	1.50	2.00	.25		2.01	2.00
8	2.667	1.333	2.00	.333		2.04	2.00
9	3.00	1.00	2.00	.50		2.005	1.995
10	4.00	0	2.00	1.00		2.005	1.985
11	3.60	2.40	3.00	.20		2.98	2.965
12	3.75	2.25	3.00	.25		2.985	2.965
13	4.00	2.00	3.00	.333		2.99	2.97
14	4.50	1.50	3.00	.50		2.99	2.96

The pressures were read on an inclined manometer. It is believed that the larger errors in observed total head for average values of 3 inches H_2O were the result of sagging of the manometer tube rather than probe errors. The observed total head readings are remarkably accurate despite relative intensities as high as 100%.

There is a noticeable decrease in observed total head readings with increasing piston frequency, which corresponds to increasing the relative intensity of the lateral velocity component. At 40 hz the magnitude of the lateral velocity intensity, $\sqrt{v'^2}$, is approximately 1 ft./sec. which is quite small compared to the streamwise velocities encountered. The equipment employed did not permit generation of lateral intensities larger than this and it remains a possibility, then, that large lateral intensities can produce significant errors in total head readings. The effect of lateral intensity is found to be a definite lowering of the observed total head readings.

In summary, the pitot tube is found to measure $\frac{1}{2}\rho u^2$ very accurately for any level of intensity that is in the streamwise direction; there is a possibility that large lateral intensity can cause significant errors and increasing the lateral intensity decreases the observed total head reading.

4. Thermocouple

The thermocouple is probably the most widely used device for measuring temperature in aerodynamic research. A wide variety of sizes, materials and probe configurations are available for

various conditions to be encountered. The electrical voltage generated is a very accurate measure of the temperature of the junction, a source of error residing in the fact that the junction is not necessarily at the same temperature as the flow in which it is immersed.

For steady laminar flow, the temperature of an unshielded junction will correspond to the recovery temperature of the flow; thus, once the recovery factor is known, the total and static temperatures can be determined quite accurately. For turbulent flows, however, the thermocouple junction never achieves any particular temperature but rather is continually heating and cooling. The average temperature recorded represents that temperature required to balance the rates of heating and cooling that are taking place. Due to thermal inertia, this temperature can deviate significantly from the true mean temperature of the flow.

Analysis of heat transfer in flowing systems indicates that convection is the dominant mechanism of transfer for moderate temperature differences, thus the velocity field becomes important in determining the mean temperature that a thermocouple senses. Consider a flow consisting of hot and cold eddies. For the case of equal residence times, the thermocouple will read higher (or lower) than the true average temperature, if, on the average, the hot (or the cold) eddies travel at higher velocity. For equal average velocities, the thermocouple will read higher (or lower) than the true average temperature if the hot (or the cold) eddies have a larger

scale length. In a jet flow there is variation in both velocity and scale length thus making for a complicated response.

To establish the magnitude of possible errors in thermocouple readings due to the above-mentioned effects, the double chamber facility described previously was employed with hot air feeding one chamber and room temperature air feeding the second chamber. The entire double chamber is constructed of bakelite to reduce heat transfer between the chambers; however, significant heat transfer did occur and the temperature profile at the exit was far from flat.

The total head profile at the exit does remain flat with heating. Point-by-point measurement of the temperature and total head profiles permits evaluation of the exit velocity profile and computation of the true average temperature and velocity as well as the relative intensity of the temperature and velocity fluctuation. Note that velocity intensity can be generated in two fashions; in one case the hot jet has the higher velocity; in the other, the cold jet has the higher velocity. Mean temperature readings were recorded at various intensities generated in both fashions.

Reference 16 indicates clearly that the thermocouple is totally ineffective in measuring temperature intensity since the junction never comes close to achieving the temperatures of an individual eddy even at extremely low frequencies; therefore, only the error in mean temperature measurement is of interest here. To this end, a mechanical pen potentiometric strip

chart recorder was used to record the thermocouple signal since the inertia of the pen effectively "integrates" the signal, thus recording only the mean measurement.

Table III below lists the various exit conditions to which the oscillating thermocouple was exposed; the frequency was the same for all tests and was approximately 40 hz.

TABLE III

Test No.	P _{t₁} in. H ₂ O	P _{t₂} in. H ₂ O	\bar{T} oF	$\sqrt{\bar{T}/a}$ oF	\bar{u} ft/sec.	$\frac{\sqrt{u'^2}}{\bar{u}}$
1	2.00	1.00	104.5	24.6	92.5	.191
2	2.00	1.00	120.0	37.4	93.9	.200
3	2.00	1.00	139.1	49.2	95.5	.207
4	2.00	2.00	99.1	25.1	107.5	.023
5	2.00	2.00	114.7	36.9	109.0	.033
6	2.00	2.00	130.6	49.1	110.5	.042
7	2.00	4.00	97.3	23.6	129.3	.152
8	2.00	4.00	113.8	37.3	130.9	.143
9	2.00	4.00	131.2	51.7	132.6	.136

The thermocouple used was chromel-alumel wire .0025 inches in diameter and was referenced to 75°F. The percent error in reading is then $100 \times \left(\frac{\bar{T}_{\text{meas}} - \bar{T}}{\bar{T} - 75} \right)$. Figure 4 presents the percent error in the measured average temperature vs. relative velocity intensity generated for the case $u_{e_1} > u_{e_2}$ and the case $u_{e_1} < u_{e_2}$. The mean temperature is considered to be a parameter in this figure. As expected, the measured average temperature is high when $u_{\text{hot}} > u_{\text{cold}}$ and low when $u_{\text{hot}} < u_{\text{cold}}$; for the conditions encountered the maximum error is about 12%. The effect of the parameter, \bar{T} ,

is strange. When $u_{\text{hot}} < u_{\text{cold}}$, there is little or no effect; when $u_{\text{hot}} > u_{\text{cold}}$, the percent error increases monotonically with increasing mean temperature. No explanation for this phenomena is available.

Let us now discuss how the results shown in Fig. 4 relate to measurements in the fully developed field of a free jet. This flowfield can be characterized as consisting of two regions; the core region and the intermittent boundary region.

The core region, $r < r_{\frac{1}{2}}$, is characterized as a "well-mixed" region; the flow is fully turbulent, relative temperature and velocity intensities are low, and mean quantity gradients are small. This corresponds to the area near the origin of Fig. 4. Hence, errors in thermocouple readings should be fairly small in the core region.

The intermittent boundary region, $3r_{\frac{1}{2}} > r > r_{\frac{1}{2}}$, is characterized as being partially turbulent and partially irrotational. The turbulent regions are large scale eddies transporting eddies an order of magnitude smaller. Between these large eddies the flow consists of the irrotational fluctuating motion of the ambient fluid whose motion is induced by the moving turbulent front. Hence, relative temperature and velocity intensities are quite large and the hot eddies, on the average, have considerably higher velocity than the unmixed cold eddies. This corresponds to the right side of Fig. 4 and thus thermocouple readings are probably consistently higher than the true average temperature. Thus, the readings suggest a greater spread in temperature than actually exists. Integration of the temperature profile to

check conservation of energy is of no value since temperature itself is not a conserved quantity for the free jet. The above arguments render the measurements of temperature, by thermocouple, in a turbulent jet subject to serious doubt, especially in the high shear region.

The results and conclusions of the thermocouple investigation are summarized below:

i) From Ref. 16 it is concluded that the thermocouple is useless for measuring temperature intensities.

ii) Thermocouple measurements of mean temperature can deviate significantly from the true mean temperature in a turbulent flow. The error in measurement is a function of both temperature intensity and the velocity intensity.

iii) The complex interaction of temperature and velocity effects in a shear flow plus the inability to measure temperature intensity preclude chances for correcting the mean temperature measurements of the thermocouple.

iv) In a heated jet the thermocouple should be reasonably accurate near the axis but will probably read higher than the true mean temperature in the shear region thus indicating a wider temperature profile than actually exists.

5. Gas Sampling Techniques

The most common method in current use for analyzing flowing gas mixtures is withdrawing a sample of the flow with a probe and feeding this sample to a remote gas analyzer. In this section the effects of the rate at which a sample is removed from the flow are investigated.

There are a number of situations where the rate of sampling

can be expected to influence the composition of the sample withdrawn. Changes in sampling rate change the area of the captured stream tube and this area change is the source of possible errors.

In a flow with no concentration gradient, changing the capture area should have no effect on the concentration of the sample since every part of the flow consists of the same gas mixture. In a flow with linear concentration gradient, different sampling rates again should not result in sensibly different gas analyses since the average composition of the sample is then roughly that at the probe axis. If the flow should have non-linear concentration gradients, however, the average composition of the sample changes as the captured area changes; the measurement can be either too high or too low, depending on the curvature of the mean distribution. The above-mentioned situations are presented schematically in Fig. 5. The accompanying problems due to concentration gradients exist for both laminar and turbulent flows.

An obvious method of avoiding the errors associated with measurements in a region of concentration gradient is to minimize the sampling rate so that the captured area is small relative to the curvature of the concentration profile. Unfortunately, this practice increases the time necessary to withdraw a given mass of the sample. More important, in turbulent flows, too low a sampling rate can produce its own errors; this is discussed below.

If the captured area differs significantly from the inside

cross section area of the sampling tube, the bounding streamlines of the captured stream tube will have a large curvature; therefore, a significant acceleration is applied to the fluid that is captured. If the flow contains discrete regions of different densities, the applied acceleration may segregate these regions. A few examples of such flows are particle laden flows, turbulent flows composed of "light" eddies and "heavy" eddies and turbulent flows composed of eddies of significantly different scales and intensity; the non-homogeneous jet usually exemplifies both latter conditions.

A discussion of the effect of sampling rate under the conditions described above is in order. Only the case where the sampling rate is too high need be discussed since the effect of too low a sampling rate is just the opposite.

If the sampling rate is too high, the streamline separating the captured flow from the by-passing flow curves towards the probe and fluid near this streamline is accelerated sharply toward the axis of the probe. This is a result of the pressure at the inlet of the probe being less than the local static pressure of the flow. A solid particle, an eddy of higher than average density, or an eddy with higher than average streamwise momentum will possess more momentum, on the average, than the surrounding fluid and will be accelerated less by the pressure gradient caused by probe suction and will not enter the probe. This results in a measured concentration lower than the true average concentration. Correspondingly, light eddies, small eddies, and eddies of lower than average

momentum are accelerated more by the pressure gradient; this results in a biasing toward a high concentration.

Once again, as was the case for the thermocouple, the reading is influenced by intensity of both concentration and velocity fluctuations and by eddy scale. The flow conditions in a jet are a complicated mixture of variations of the above nature thus making assessment of probe effects difficult on a quantitative basis.

Two different experiments were conducted to assess the effects of probe sampling rate on concentration measurements. In one, measurements of concentration were made at different sampling rates in the flowfield of a turbulent axisymmetric jet which consisted of a mixture of CO_2 and air with 20% and 80% mole fractions, respectively, at the exit. The other experiment utilized the double chamber facility, described earlier, with chamber one fed a CO_2 -air mixture, the molar CO_2 concentration being 20%, and with chamber two fed pure air. The pitot probe used earlier was used as a sampling probe and oscillated at approximately 40 hz. The results are discussed below.

In connection with the first experiment, Fig. 6 shows measured values of \bar{X}_{CO_2} as a function of sampling rate for three different locations in the flow. The first location is at the halfwidth which is a region of maximum gradient. The measured value of \bar{X}_{CO_2} is found to decrease monotonically with increasing sampling rate. The second location is in a region of reduced gradient but high intermittency; again the measured value of \bar{X}_{CO_2} decreased monotonically with increased

sampling rate. The last location is at the centerline, far downstream; here the intensities are quite low and the gradient is nil. Note the total lack of effect of sampling rate here. These results clearly manifest the effects of gradient and turbulent structure as discussed above.

The second experiment isolates the effects of velocity intensity and sampling rate on sampling accuracy. As with the thermocouple experiment, velocity intensity can be generated in two ways; in one, the air jet has the higher velocity, and in the other, the CO_2 -air mixture jet has the higher velocity. When the time of exposure to each jet is identical, it is expected that the probe will receive a greater sample from the higher momentum jet. That this occurs is clearly demonstrated by the results shown in Fig. 7, which plots % error in mean concentration measurements as a function of velocity intensity when $u_{\text{mix}} > u_{\text{air}}$ and $u_{\text{mix}} < u_{\text{air}}$; the sampling rate is considered to be a parameter in this figure. Figure 7 indicates that sampling rate is relatively unimportant when there is no velocity intensity but highly important if there is. The same data shown in Fig. 7 is presented in Fig. 8, with the sampling rate as the independent variable and velocity intensity as the parameter. Figure 8 suggests that sampling at a velocity that is slightly higher than the free stream average reduces the error from velocity intensity, but in a jet flowfield, this practice may result in errors from the gradient effects discussed earlier.

The results from the oscillating experiment support the results of the measurements in the shear region of the free

jet. There it is expected that the eddies containing CO_2 have more momentum than the entrained ambient and thus $u_{\text{mix}} > u_{\text{air}}$. When $u_{\text{mix}} > u_{\text{air}}$ the concentration measurements decrease with increasing sampling rate as shown in Fig. 8; this is consistent with the results obtained in the jet flow as shown in Fig. 6. Note also in Fig. 8 that for zero intensity, sampling rate is not so important; such is the case at the centerline fifteen diameters from the exit of the jet.

The major results of the sampling rate investigation are summarized below:

i) There are several flow situations where the rate at which a sample is withdrawn can affect that sample; these include:

- a) particle laden flows
- b) flows with non-linear concentration gradients

$$\left(\frac{\partial^2 \bar{X}_i}{\partial y^2} \neq 0 \right)$$
- c) turbulent flows where there is considerable variation in the density, scale, and/or momentum of the eddies

ii) It has been shown experimentally that mean concentration measurements in a jet vary measurably as a function of the relative sampling rate.

iii) The complex interaction of gradient, density, and velocity effects preclude chances for correcting the readings.

iv) In a non-homogeneous jet, concentration measurements made by sampling should be accurate near the axis far downstream but are subject to various errors in the high shear

region and the regions of high relative velocity intensity.

6. Design of Thermal Conductivity Cell Gas Analyzers

A commonly used device for measuring the composition of a gas is the thermal conductivity cell. Since such a device can only measure the difference in the thermal conductivity of the reference gas and the unknown gas it can analyze only binary mixtures, one component of which must be the same gas as the reference gas. In the course of designing the gas analyzer used in the present work, considerable experience was gained (sometimes in a very unpleasant manner) in the behavior of these devices. What follows is a collection of observations that may save the reader considerable grief and time should he be contemplating construction of such an analyzer.

The sensing elements of thermal conductivity cells are usually heated wire filaments or heated thermistors. The first design choice is the selection of which type to use. Listed below are some advantages and disadvantages of each.

A. Hot Filament Analyzer

Advantages: (i) Inexpensive; (ii) Resistance increases with temperature, thus the electrical behavior is stable; a simple power supply is adequate; (iii) Can achieve high resolution.

Disadvantages: (i) The filament properties can change due to oxidation, contamination, etc., thus affecting the calibration; (ii) Relatively high electric current is needed for good sensitivity; (iii) High currents result in a large heat transfer to the cell block; this can cause drifting in the output signal; (iv) The filaments are fragile; (v) Heat transfer from

the filament is very strongly related to velocity; thus precise control of rates of flow of the sample and reference gas is an absolute necessity; (vi) Heat transfer is also dependent on the temperature of the incoming gas and the temperature of the cell block. Small temperature variations can result in considerable error in the measurement.

B. Thermistor Analyzer

Advantages: (i) Good sensitivity at low operating temperatures; (ii) Little oxidation of the working element; (iii) Extremely compact; (iv) Rugged.

Disadvantages: (i) Inverse variation of resistance with temperature requires sophisticated control circuits; (ii) Output is very sensitive to flow rate; (iii) Temperature of sample and block must be precisely maintained.

In light of the above observations, the thermistor type appears to be preferable in most applications. Having selected the sensing element, one may design the analyzer as a static system, where the analysis is performed with a stagnant sample in the cell, or as a dynamic system, where the sample flows through the cell during analysis. Both designs are examined below.

A. Static Analysis System

Advantages: (i) The great advantage of static analysis is the elimination of convective cooling of the sensing element; thus the signal can only result from difference in the thermal conductivities of the reference and sample provided the temperatures are carefully controlled.

Disadvantages: (i) System must be capable of high vacuum for any accuracy; (ii) Analysis is very time consuming; (iii) The pressures in the two chambers of the cell must be carefully balanced. A U-tube manometer with mercury as the fluid is a convenient monitor of the pressure balance, but leaks or surges can force mercury into the system with devastating effects on the metal components; (iv) The use of a static system resulted in slow transients in the signal despite the immersion of the cell and connecting tubing in a carefully controlled thermal bath. The authors conclude that the difference in heat transfer caused by evacuating and then pressurizing the cell changes the temperature distribution of the block itself enough to cause these transients. This problem was not overcome and the use of a static system had to be abandoned.

B. Dynamic Analysis System

Advantages: (i) Operates at higher pressure, leaks not as serious a problem; (ii) Rapid analysis is possible; (iii) In a dynamic system, only the flowing gas receives thermal energy from the element, thus transients due to changes in the temperature distribution of the block are eliminated.

Disadvantages: (i) Since convective cooling of the element can obliterate the small effect of changes in the thermal conductivity of the sample, an extremely accurate method of measuring and controlling small flow rates is essential. This feature is lacking in many commercially made gas analyzers and should be considered very carefully; (ii) The temperature of

the sample and reference gas must be invariant as it enters the cell; this can be accomplished by immersing long inlet columns in a constant temperature bath.

7. Hot Wire Anemometer

Having investigated the more commonly used devices for measurement of mean variables in a turbulent flow, attention shall be focused on the hot wire anemometer. Whether the constant current or the constant temperature approach is employed, the hot wire responds to three flow properties; namely, mass flow (ρu), the temperature of the fluid, and the molecular transport coefficients of the fluid, which depend on the gas mixture. Clearly, if two of the properties are fixed, the third can be measured. In general, the hot wire is used in isothermal, homogeneous flows where density is a known constant and thus, the velocity is measured. Rapid advances in electronic technology have made today's hot wire anemometers very accurate instruments for measuring most of the velocity correlations of interest; this is in addition to the mean velocity. Encouraged with such success researchers are trying to extend the hot wire technology to include the measurement of flows where temperature and composition are not fixed. Within this section, some comments are presented regarding the feasibility of such measurements.

Let us first consider whether the hot wire can accurately measure mean temperature in a turbulent flow. For temperature measurements the hot wire is used as a resistance thermometer; a small constant current is fed through the wire, and the voltage across the wire gives the resistance which is a function

of temperature. The only difference from a thermocouple is the method by which a voltage signal is generated; the fluid mechanic aspects are identical. That is, the wire never attains a given temperature but rather is heated and cooled by the flow. Once again, the thermal inertia may prevent measurement of the intensity of the temperature fluctuation. Also, the mean temperature of the wire is that temperature necessary to balance the heat transfer to and from the wire; this temperature is directly coupled to the velocity field as well as the temperature field as was the case with the thermocouple.

In summary, the hot wire may be no better for temperature measurements in a turbulent flow than is the thermocouple. It is only a significantly more expensive and fragile instrument.

The other area of interest is the use of the hot wire in non-homogeneous flows. A single wire can only measure a rate of heat transfer from the wire to the flow and hence is totally incapable of differentiating heat transfer changes due to changes in gas properties from those due to changes in mass flow. Recently, Way and Libby²⁴ have combined a hot wire and a hot film in a probe that makes use of the different behavior of the wire and film. With very careful calibration they were able to differentiate the signal due to concentration changes from that due to velocity. Such a device makes it feasible to measure both the mean and fluctuating variables in a non-homogeneous turbulent flow. The results presented so far are preliminary in nature so that assessment of accuracy

is difficult; still, the technique holds promise for the future. However, the expense associated with the technique is certainly prohibitive for many applications. So, at the present time, the use of the hot wire in non-homogeneous flows remains a questionable practice.

IV. DEVELOPMENT OF EXPERIMENTAL TECHNIQUES TO MEASURE FLUX VARIABLES

1. Introduction

In Section I, the motivation for using the extended Reichardt analysis was presented. One of the features of this theory is the use of the flux of mass, momentum, and energy as dependent variables instead of the usual fluid dynamic variables. In addition, the greater physical significance and utility of the flux variables in certain mixing problems was discussed. In order to experimentally verify the accuracy and utility of the theoretical model, it was necessary to devise new experimental techniques to directly measure the various flux variables.

The key to these measurements was the invention and development of a mass flux probe which operates independently of the temperature and composition of the flow. This was accomplished by locating pressure taps at the entrance of a sampling tube; the sampling rate is varied until the pressure there matches the free stream static pressure. In a non-homogeneous flow, a portion of the sample can be analyzed to obtain the mass fraction of each species; the mass fraction, Y_i , times the total mass flux, $\overline{\rho u}$, yields the individual mass flux of each species, $\overline{\rho_i u}$. The only assumption necessary is that the individual mean species velocities all be equal.

For measurement of energy flux in a non-isothermal flow, the mass flux probe can be incorporated into a calorimetric probe thus yielding direct measurement of $\overline{\rho u h}$.

2. Design of Mass Flux Probe

The concept employed for the mass flux probe was to capture a streamtube with the same diameter as the inside diameter of the probe; to do this, the static pressure at the probe entrance should equal the free stream static pressure. By locating static pressure taps at the entrance of the probe, it is possible to determine when the above condition is satisfied. Once the condition of iso-kinetic sampling is established, a flow meter can be used to quantitatively fix the mass flow in the probe; since the area of the inside of the probe is known, this is a direct measure of the local mass flux $\overline{\rho u}$.

Because the wall of the sampling tube has a finite thickness, it is expected that the geometry of the probe entrance can seriously affect the pressure measured at the inlet. In addition, the construction of a small (.062 inch diameter) probe, which is necessary for good resolution, dictates a simple inlet design to avoid impossible manufacturing situations. To evaluate the inlet geometry a 0.250 in. O.D. probe was constructed with removable inlets and placed in the test section of a subsonic low intensity wind tunnel with a velocity range of approximately 10 f.p.s. to 75 f.p.s. A venturi was used as a flow meter and the inlet static pressure was compared to the test section static pressure on an inclined manometer with water as a working fluid.

A number of inlet geometries were investigated, and the equipment utilized is shown in Fig. 9. The design which was finally selected is also shown in Fig. 9; this shape is produced by

simply radiusing the wall of the tube. This design is also very amenable to miniaturization.

It was found that the location of the pressure taps greatly affected the pressure reading for a fixed sampling rate because of viscous losses once the flow entered the probe. The manufacturing procedure which was employed to insure that isokinetic sampling resulted in the correct pressure reading is as follows. The pressure tap was located immediately behind the end of the inlet radius; this gave a slightly low pressure reading when the sampling rate was matched to the free stream velocity. To achieve the correct pressure reading it is only necessary to enlarge the inside diameter of the probe at the pressure tap slightly with a tapered reamer. The accuracy of the final probe is limited only by the patience of the machinist who enlarges the bore.

The construction of a miniaturized mass flux probe was accomplished by using concentric tubes soldered together at the inlet and soldered to a machined mount at the rear. This assembly is shown in Fig. 9. This assembly can then be mounted on a "sickle" for positioning in a flow. The performance of this final design is discussed below.

If no sample is withdrawn, the probe becomes a pitot probe and the pressure measured by the inlet tap is the stagnation pressure of the flow. Since the pressure at the inlet tap is the free stream static pressure for iso-kinetic sampling, the sensitivity of the probe is proportional to the square of the velocity in the incompressible range. The probe should remain accurate in a subsonic compressible flow but cannot be

used in a supersonic flow due to the bow shock. The accuracy of the probe depends on the accuracy of the pressure readings and the flow meter; this can be about 1%. Sensitivity to angle of attack was also investigated and the probe was found to be insensitive to angle of attack up to about 20° or about the same as an impact probe²³.

3. Selection of Flow Meter for Mass Flux Probe.

The miniature probe described above has an inside area of $2.182 \times 10^{-6} \text{ ft}^2$. The range of velocities to be measured was from 0 to about 220 ft./sec. For air at room temperature and atmospheric pressure, this requires a mass flow through the probe that ranges from 0 to about $3.5 \times 10^{-5} \text{ lbs/sec}$. Thus it was necessary to build a system to regulate and then measure quite accurately a very small mass flow. In addition, the flow meter had to measure the flow for various gas mixtures at various temperatures.

The metering of the flow was accomplished readily by the use of a commercially available very fine needle valve. Four approaches were considered to quantitatively measure the mass flow; namely,

- i) calibrate the metering valve;
- ii) measure the pressure drop along a length of tubing;
- iii) a venturi;
- iv) a hot wire in a channel.

The relative merits of each method are discussed below.

A. Calibrated metering valve.

Advantages:

- i) Versatility - Because the valve is choked, it is very easy to correct the measurement for gas mixture, temperature, and pressure changes.
- ii) Flow metering and mass flow measurements are achieved in one operation and with one piece of equipment.
- iii) Low cost.
- iv) Simplicity - the valve has only one moving part.

Disadvantages:

- i) The calibration procedure is very tedious.
- ii) The calibration can change with wear.
- iii) The valve needle is fragile and breakage is common.

B. Measured pressure drop along a tube.

Advantages:

- i) Low cost.
- ii) Simple and rugged - there are no moving parts.
- iii) There is no change in calibration if the tube is kept clean.
- iv) Calibration is easy.

Disadvantages:

- i) It is difficult to correct the reading for changes in gas mixture and temperature.

C. Venturi.

Advantages are identical to B above.

Disadvantages:

- i) It is virtually impossible to machine a good venturi flow meter to the dimensions required in the present work.

D. Hot wire.

Advantages:

- i) Simple - no moving parts.
- ii) Good sensitivity at very low velocities.

Disadvantages:

- i) It is difficult to correct the readings for changes in gas mixture and temperature.
- ii) The wire is very fragile.
- iii) The calibration of the wire can change due to oxidation, dirt accumulation, etc.
- iv) Expensive.

Because of the intent to study nonhomogeneous, non-isothermal flows, the calibrated metering valve was chosen as the flow meter, mostly for its versatility.

The valve used was a Nupro very fine needle valve with a micrometer handle. The bore was enlarged and a new needle was machined to achieve the desired flow range. The full range of flow was accomplished through fourteen turns of the needle; the micrometer handle allowed readings to the nearest hundredth of

a turn, thus giving a reading of three significant figures.

Calibration was performed by evacuating a chamber of known volume and then filling the chamber through the valve at a constant setting to a pressure of about ten inches of mercury. Knowledge of the pressure, temperature, and volume of the chamber provide the mass of air contained; measuring the time to fill the chamber allows computation of the mass flow. To avoid errors in mass flow due to the pressure drop through the probe and connecting tubing, the valve was calibrated while connected to the probe. The curve of mass flow vs. number of turns was quite irregular due to minute machining flaws; this necessitated a considerable number of data points for good calibration. The reader is advised that there is considerable difficulty in such a calibration and an alternate flow meter is desirable; however, for the conditions of the present experiment the calibrated valve was still considered the best choice.

4. Design of Gas Analyzer

The gas analyzer constructed for the present work is a dynamic system employing a thermistor element thermal conductivity cell manufactured by Carle Instruments Inc.. The distinguishing feature of our system is that the mass flux probe metering system is incorporated so that the total mass flux of the flow is measured and then a sample of the flow is analyzed without changing the sampling rate at the probe itself. A schematic diagram of the gas analyzer is shown in Fig. 10.

As discussed previously, accurate analysis with a dynamic system requires very precise balancing of the flow rates through the cell. The pressure drop through the mass flux probe and the sample tubing changes with the sampling rate and thus affects the flow rate of the gas sample through the cell; the metering valves A and B are employed to correct for this pressure change.

The measurement procedure in the jet flow field is as follows: The probe is set at the desired location in the flow. Valves 2 and 3 are closed and valve 1 is opened allowing measurement of the stagnation pressure of the flow on the manometer; this measurement is one-half the momentum flux, $\frac{\rho u^2}{2}$. Valve 1 is closed and valve 2 is opened and the calibrated metering valve is adjusted to equate the probe inlet pressure to the static pressure of the flow; this sets the probe in the isokinetic sampling mode. The position of the metering valve, as indicated by its micrometer handle, is recorded. This number would indicate the mass flux of the flow if the flow consisted of room temperature air; however, the fact that the flow consists of an as yet unknown mixture of air and carbon dioxide prevents computation of the total mass flux at this step. With the valve position recorded, valve 3 is opened and the metering valve A is adjusted to equate the mass flow through the sample side of the thermal conductivity cell to the mass flow of the reference gas, air, through the reference side of the cell. The condition of matched flow is indicated by a balance of pressure across the U-tube manometer. At the

same time, the calibrated metering valve must be closed slightly to maintain a constant mass flow through the probe as indicated by the probe inlet pressure. The gas analyzer indicates the mole fraction of carbon dioxide of the sample; this provides the correction factor for the total mass flux measurement recorded previously and the mass fraction of carbon dioxide and air. The product of the mass fraction and the total mass flux gives the species mass flux of both species. Thus, all quantities of interest, the momentum flux, $\overline{\rho u^2}$, the mass flux of carbon dioxide, $\overline{\rho_{CO_2} u}$, and the mass flux of air, $\overline{\rho_{air} u}$, are measured sequentially with the same probe at the same location in the flow.

5. Design of Calorimetric Probe

The development of a technique for measuring the enthalpy flux $\overline{\rho u h}$ is described here. It should be noted that the energy equation as developed in Section II describes the distribution of the total enthalpy flux $\overline{\rho u h_t}$, not the enthalpy flux $\overline{\rho u h}$. The probe described here can only be used in a subsonic flow for in such flows the difference between these quantities is usually negligible.

A calorimetric probe employs a coolant and simple energy conservation principle to measure the energy content of a flow. The probe is designed to draw in a sample of the flow and pass this sample through a heat exchanger section where the sample heats the coolant. The energy balance for the system

is

$$\dot{m}_s h_\infty = (\dot{m}_c \Delta h_c)_s - (\dot{m}_c \Delta h_c)_t + \dot{m}_s h_s \quad (13)$$

where \dot{m}_c is the mass flow of coolant, \dot{m}_s is the mass flow of the sample, Δh_c is the change of coolant enthalpy through the probe and h_s is the enthalpy of the sample as it leaves the probe. The enthalpies are deduced from temperatures measured by thermocouples in the probe. The subscript t refers to a tare measurement taken with no sample flowing in the probe; this is necessary to account for heat transfer to the external area of the probe. The subscript s refers to measurements taken while sampling. In an ideal probe the heat transfer during the tare measurement would be zero. When sampling, the temperature of the coolant and the sample would be equal as they reached the exit of the probe; this latter condition would insure a flat temperature profile at the location of the thermocouple, so that there would be no error in the measurement of the average temperature.

Note that \dot{m}_s in Eq. (13) is controlled by some sort of metering device in the line between the probe and vacuum and is not necessarily related to the flowfield. To obtain measurement of $(\overline{\rho u h})_\infty$ the sample mass flow must satisfy the relation

$$\dot{m}_s / A_p = (\overline{\rho u})_\infty \quad (14)$$

where A_p is the inside cross-sectional area of the probe. The incorporation of the previously described mass flux probe and flow meter into the calorimetric probe and system permits condition (14) to be satisfied. Inserting Eq. (14) into Eq. (13) gives the desired result; namely,

$$(\overline{\rho u h_s}) = \frac{1}{A_p} [(\dot{m}_c h_c)_s - (\dot{m}_c h_c)_t] + (\rho u)_s h_s \quad (15)$$

The coolant mass flow can be constant and thus for a gas coolant a sonic orifice provides an excellent means of regulating and measuring this flow. The measurement of the other quantities has been described previously.

At the time that the present investigation was begun, a commercially manufactured calorimetric probe was available from Greyrad Corp. and a model G-1-7 was purchased. This probe was designed to measure the enthalpy of extremely hot flows such as plasmas where other types of probes cannot survive. For such conditions, water is used as the coolant. The sampling rate is controlled by a sonic orifice and thus is essentially a constant.

For the present investigation the highest temperature envisioned was about 500°F and thus air was chosen as the coolant to retain sufficient sensitivity. No method for obtaining the free stream mass flux measurement was possible for this probe, but it was hoped that this probe could at least provide a more accurate temperature measurement than the thermocouple and in so doing, demonstrate the utility of the calorimetric probe concept in low temperature flows.

The accuracy of the probe was checked by locating it at the exit of a heated jet where the flow is laminar and the temperature is known quite accurately. The results of this experiment are shown in Fig. 11. As can be seen, the results are poor; the probe consistently reads a temperature about

32% too low. At first, it was thought that the sensitivity was too low for the desired temperature range and so that coolant mass flow was reduced and the exterior of the probe was insulated with fiberglass tape. The sensitivity was increased but the final reduced data was no better than before; the error was not a result of lack of sensitivity. As mentioned above, the mass flows of the sample and coolant were measured by sonic orifices, the inlet pressure being measured with a mercury manometer. The entire system was checked for leaks and found tight; the calibration of the orifices was checked and found accurate; thus the measurements of mass flow were correct. The error had to be with the temperature measurements inside the probe.

Two phenomena were indicated by the various temperature measurements and each affects the results greatly. One problem was an increase in the coolant inlet temperature between the tare measurement and the sample measurement. The purpose of the tare measurement is to remove all the uncontrollable effects of the flow on the probe such as external heat transfer, conduction through the probe supports, etc., but the measured change in inlet conditions indicated an additional amount of heat being conducted through the probe during sampling; thus the tare measurement was imperfect. If one considered the coolant inlet temperature to be room temperature at all times, the error was reduced by about a third.

The second problem was that the measurements indicated that the sample and coolant did not reach equilibrium in the probe; that is, the measurement of the sample temperature at

the exit was higher than the temperature measurement of the coolant at the exit. There are two ways that such a measurement could occur. In one case the coolant thermocouple could be located near a wall where the measured temperature would be low even if the sample and coolant were in equilibrium. In the other case, if the coolant and sample indeed did not achieve equilibrium, a non-uniform temperature profile would exist in both tubes and the location of both thermocouples would affect these readings. If one assumed that the coolant exit temperature was equal to the sample exit temperature and that the coolant inlet temperature was room temperature, the results improved remarkably.

The problems described above and the inability to measure the mass flux with the Greyrad probe prompted the design and construction of an entirely new calorimetric probe which incorporates the previously described mass flux probe and which overcomes the problem of equilibrium between sample and coolant. This probe was constructed by machining a spiral channel into the wall of a copper tube and then shrink fitting this tube into a stainless steel tube. The other differences in design are shown in Fig. 12 which compares the new probe to the Greyrad probe. Note that the new design insulates the coolant inlet as much as possible to produce an accurate tare measurement; note that the thermocouple location can be carefully controlled during assembly with the bakelite "plugs", and note the inclusion of the mass flux probe at the inlet.

The sample mass flow is matched to the flowfield to satisfy Eq. (14) as determined by the inlet pressure; the

measurement and regulation of the sample mass flow is achieved by using the same calibrated metering valve that was used previously for the mass flux and gas sampling probe.

Results of enthalpy flux measurements made with the new probe at the exit of a jet were disappointing. The mass flux measurements was found to be accurate but the energy content was grossly underestimated. It was found that the sample and coolant achieved equilibrium but that most of the energy was being conducted from the probe and not transferred to the coolant as desired.

The answer to the difficulty with the Greyrad probe and the design presented here is that the probe can conduct a certain fraction of the heat load away. When water is used as the coolant, its heat capacity overwhelms the conduction effects, but when air is the coolant, the conduction loss is a significant fraction of the total signal. To eliminate the conduction loss it appears to be necessary to construct every part of the probe, except the sample - coolant dividing tube, from a very low thermal conductivity material such as a ceramic.

Due to the problems of the cooled probes, a third probe was constructed to measure the enthalpy flux. The idea of the design is to construct the mass flux probe from an insulating material and measure the temperature of the sample inside the sample tube. This probe is shown in Fig. 13. The results of enthalpy flux measurements made at the exit of a heated jet are shown in Fig. 14.

6. Conclusion

A description of the experimental devices and techniques that were developed to measure the flux of the mass of each species for a binary flow and of enthalpy in a non-isothermal flow has been presented. The results of measurements taken in the flowfield of a free jet with these probes are presented and discussed in the following section.

V. EXPERIMENTAL RESULTS AND COMPARISON TO THEORY

1. Introduction

The results of the theoretical and experimental investigation of the flowfields of incompressible axisymmetric turbulent free jets are presented in this section. The various conditions investigated were: i) isothermal, homogeneous; ii) isothermal, non-homogeneous, and iii) non-isothermal, homogeneous.

To achieve the various conditions, two different facilities were employed. The non-homogeneous investigation was performed on the jet facility described in Ref . 16

with an injection section added to mix the carbon dioxide with the air supply. The injector consisted of three 0.1875 inch diameter tubes, fed from a manifold , passing radially through the chamber wall. A series of 0.032 inch holes are located around the circumference of each tube and spaced 0.250 inches apart along the entire length within the chamber.

The carbon dioxide was supplied from a bank of six standard welding CO₂ bottles and was regulated at about 200 psi, to a 1 cubic foot settling tank. From there the gas passed through a hot water bath, which insured final injection at room temperature, then through a second regulator to a sonic orifice and then into the chamber. The sonic orifice was the flowmeter and the inlet pressure was measured on a Heise gauge. The mass flow of the air supply was also measured with a sonic orifice in connection with a Heise gauge. Typical inlet pressures were 70 psi and the accuracy of the gauges was about 0.1 psi. A schematic diagram of the facility is shown in

Fig. 15 and a photograph is shown in Fig. 17.

The diameter of the exit orifice is 0.400 inches. An accurate measurement of the total head profile at the exit was performed. The concentration profile at the exit was found to be flat within the accuracy of the equipment; however, the probe size did not permit good resolution at the edges, thus no accurate profile for $\overline{\rho_{CO_2} u}$ was obtained at the exit.

The second facility, which was used for both the homogeneous cases, exits vertically to avoid the asymmetries reported in Ref. 16 for initially axisymmetric jets with densities different from the ambient density. The air supply is regulated and then passed through an electrical heater made from 0.1875 inch diameter nichrome wire; the temperature is regulated by a Capacitrol unit. The temperature of the air supply can be varied from room temperature to about 550°F. A schematic diagram of the homogeneous jet facility is shown in Fig. 16 and a photograph of the facility is shown in Fig. 17.

2. Isothermal, Homogeneous Jet

A. Introduction

The configuration investigated here, the axisymmetric free jet, is probably one of the oldest of classical turbulence problems. The abundance of literature on it would imply that it is about as "closed" a problem as one could find. The purpose of this investigation was to evaluate the performance of the mass flux probe described earlier.

With no internal flow, the mass flux probe becomes a pitot tube which measures $\overline{u^2}$ in a constant density flow. The

mass flux probe itself measures $\overline{\rho u}$ or \overline{u} in a constant density flow. Thus, it is possible to measure the turbulent intensity with this mean measurement device from the relation

$$\overline{u^2} - \overline{u}^2 = \overline{u'^2} \quad (16)$$

provided the measurements can be performed with sufficient accuracy. Note that Eq. (16) involves differences of squares and thus any errors will be amplified greatly. Thus, if reasonable results are obtained for the intensity, it appears safe to conclude that the mass flux probe is an accurate instrument for measuring turbulent shear flows.

B. Momentum Flux Measurements

The chamber pressure for this investigation was ten inches of water which corresponds to an exit velocity of about 210 fps. The momentum flux measurements were obtained by using the mass flux probe as a pitot tube. The exit profile was obtained by using a pitot tube .018" in diameter.

The orifice plate used for the cold jet experiment differed from the others used in that the contraction radius at the orifice was 0.0625 inches whereas the other orifices have a 0.09375 inch contraction radius. It has been shown in Ref. 16 that such a difference strongly affects the near flowfield of the jet. The sharp radius also made it difficult to obtain a good exit profile as intermittent separation occurred near the edge of the orifice. Because of the orifice used, it will be seen that the results from the cold jet are good in themselves but they do not compare readily with the results from the other jets examined.

The initial profile of momentum flux that was measured is shown in Fig. 18. The analytic curve used to fit the initial data is given by the relation:

$$\frac{(\overline{\rho u^2})_{\bar{r},0}}{(\overline{\rho u^2})_{0,0}} = \begin{cases} 1.0 & 0 \leq \bar{r} \leq .475 \\ 1.0 - 444.44 \dots (\bar{r} - .475)^2 & .475 \leq \bar{r} \leq .49 \\ 45(1 - 2\bar{r}) & .49 \leq \bar{r} \leq .50 \\ 0 & \bar{r} > .50 \end{cases}$$

Again, it must be emphasized that there were unusual conditions at the exit due to the sharp radius of the orifice plate.

i) Conservation of Momentum

For a free jet, the total momentum flux is conserved and thus the integral of the momentum flux data at any downstream station should be a constant. Figure 19a shows the results of a direct numerical integration of the raw pitot tube data at each x/d location examined divided by the integral of the exit profile shown in Fig. 18. Note that the momentum is conserved within about 2.5% beyond 12 diameters. The larger errors for the near field measurements are the result of the high shear near the edge of the jet. If the pitot measurements are corrected for shear effects, the results should improve considerably. When the data indicates excellent conservation, as in this case, one can put some faith in the accuracy of the point-by-point measurements.

ii) Centerline Decay of Momentum

The centerline value of momentum flux, non-dimensionalized with respect to the exit value, is shown in Fig. 20. from both the experiment and the theory. The data is seen to decay asymptotically as $\bar{x}^{-2.00}$ as expected. What is not expected is a potential core length of 7.2 diameters,

an unusually high value. It is believed that the orifice plate is again responsible for this result. Note that the theoretical decay is plotted as a function of $\bar{\chi}$.

By matching the centerline values of momentum flux, one can obtain the necessary relation between \bar{x} and $\bar{\chi}$. It is also possible to obtain this relation by comparing the halfwidths of the experimental and theoretical profiles, but it has been found that the centerline matching produces a more reliable result because the experimental measurements are subject to the greatest error near the halfwidth due to the large gradients there.

The relation between \bar{x} and $\bar{\chi}$ obtained from the centerline data is shown in Fig. 21. Due to the problem with the sharp radius orifice plate, this curve does not agree well with other results. To demonstrate that the orifice plate alone was responsible for the difficulties, a new plate was machined with a contraction radius of 0.09375 inches but with the same orifice diameter, 0.363 inches. The results for the centerline decay for this orifice are shown in Fig. 20. The potential core for this plate is 6.2 diameters, which will be shown to agree with the results obtained for the non-homogeneous jet and the non-isothermal jet. The \bar{x} vs. $\bar{\chi}$ relation for this orifice is shown in Fig. 21; this will also be shown to agree well with all of the other results.

From the above results it is clear that small differences in the design of the facility can alter the entire flow field significantly. Note, for example, from Fig. 20, that at 13.8 diameters the momentum at the centerline of the jet issuing

from the orifice of small contraction radius is 28% of the exit value while that of the jet from the orifice of large contraction radius is only 20.5%, of the exit value. The reason for this effect is not clear and constitutes an interesting problem.

iii) Theory Compared to Experiment

The full solution for the momentum flux field of the isothermal homogeneous jet is compared to the experimental data in Fig. 22. Note that the theory predicts the developing region well in addition to giving an excellent description of the fully developed flow where similarity occurs. Note also that the figure is in terms of physical coordinates, not similarity variables. The accuracy of the theory is felt to be quite adequate.

C. Mass Flux Measurements

The mass flux measurements were performed simultaneously with the pitot measurements to avoid any possible errors due to incorrect positioning of the probe, or to atmospheric changes, etc. Direct numerical integration of the mass flux data yields the total mass flux of air at that location which, when compared to the initial mass flux of air, is a measure of the entrainment. The results of the integrated mass flux profiles are shown in Fig. 19b, and compare favorably with the value of $.32 x/d$ reported by Ricou and Spalding²⁵, although there is some doubt about the initial profile in this case due to the possible effects of the sharp contraction radius.

D. Intensity Measurements

As explained previously, the pitot measurements were combined with the mass flux measurements to obtain a measure of the streamwise turbulent intensity $\sqrt{u'^2}$. Profiles of intensity, non-dimensionalized with respect to the centerline velocity, are shown as a function of r/x for various x/d locations in Fig. 23, and are compared to the hot wire results of Wygnanski and Fiedler²⁶ and Corrsin²⁷. While there is noticeable scatter in a given profile, the overall results are considered remarkable. It should be remembered that these intensity measurements are the result of taking a difference of the mean momentum flux and the square of mean mass flux measurements. Thus, it is possible to use the mass flux probe described earlier to measure a mean value of a fluctuation quantity using only a manometer. It is felt that the results shown in Fig. 23 would be improved with the use of a more accurate flow meter than was employed in this study which was a calibrated needle valve.

E. Conclusion

The measurements of momentum flux and mass flux in the flowfield of an isothermal, homogeneous jet are found to agree well with classical results and thus indicate the accuracy of the mass flux probe described earlier. An additional result is that the measurements of mean momentum flux and mean mass flux can be combined to obtain the streamwise turbulent intensity with some accuracy.

3. Isothermal, Non-homogeneous Jet

A. Introduction

The non-homogeneous jet investigated consisted of a mixture of carbon dioxide and air with the molar concentration of carbon dioxide being 20% at the exit. The mass flux probe used for the isothermal, homogeneous investigation was used to measure the momentum flux, $\overline{\rho u^2}$ and the species fluxes, $\overline{\rho_{CO_2} u}$ and $\overline{\rho_{air} u}$ of this jet. The facility, the probe, and the gas analyzer have all been described earlier.

B. Initial Conditions

The chamber pressure for this investigation was ten inches of water and the gas mixture was 20% CO₂ and 80% air by moles; this corresponds to an exit velocity of about 200 fps.

The exit profile of momentum flux was obtained by using an .018 inch pitot tube and water manometer. The large size of the mass flux probe did not permit measurement of an exit profile of the species fluxes. However, concentration measurements at the exit indicated that the concentration profiles were "flat" so that the profile of $\overline{\rho_{CO_2} u}$ at the exit was characterized only by the profile of velocity u . Thus, the exit profile of the mass flux of CO₂, non-dimensionalized with respect to the centerline value, was obtained by taking the square root of the momentum profile normalized with respect to the centerline value.

The measured exit profile of momentum flux and the analytic curves for momentum flux and mass flux of carbon

dioxide are shown in Fig. 24. The analytic expression for the momentum flux is

$$\frac{(\overline{\rho u^2})_{\bar{r},0}}{(\overline{\rho u^2})_{0,0}} = \begin{cases} 1.0 & 0 \leq \bar{r} \leq .4375 \\ 1.0 - 2.729536(\bar{r} - .4375)^4 & .4375 \leq \bar{r} \leq .48125 \\ 24(1 - 2\bar{r}) & .48125 \leq \bar{r} \leq .50 \\ 0 & \bar{r} > .50 \end{cases}$$

The analytic expression for the CO₂ flux is the square root of the above

$$\frac{(\overline{\rho_{CO_2} u})_{\bar{r},0}}{(\overline{\rho_{CO_2} u})_{0,0}} = \sqrt{\frac{(\overline{\rho u^2})_{\bar{r},0}}{(\overline{\rho u^2})_{0,0}}}$$

The measured exit profile of momentum flux for the CO₂-air jet was found to be identical to the exit profile of momentum for air reported in Ref. 16 using the same facility.

C. Conservation of Momentum and Mass Flux of Carbon Dioxide

For the non-homogeneous jet, two integrated quantities are conserved, namely, the total momentum flux and the total mass flux of carbon dioxide. The results of a direct numerical integration of the raw data for these two quantities is shown in Fig. 25a. The measurements indicate extremely good conservation of momentum flux, better than 5% at most locations. The conservation of carbon dioxide flux is about 15% which is acceptable.

It must be emphasized strongly that a measurement of concentration does not permit evaluation of the conservation of mass, since it is the total mass flux that is conserved. One would have to compute the local density from the concentration

measurement, divide this into the pitot measurement to obtain $\overline{\rho u^2}/\rho$, and take the square root to get what is only an approximation to the mean velocity. Next the mass fraction would be multiplied by the density to obtain ρ_{CO_2} which is multiplied by the velocity obtained above giving a mass flux. Considering the errors in each measurement, as described in Section III, and the neglect of correlations for each computation, the final result would be quite poor indeed.

D. Mass Entrainment

The remaining integral quantity is the total mass flux of air. The result of numerical integration of the raw air flux data is presented in Fig. 25b. The entrainment is found to asymptote to a linear growth as expected. Comparing the entrainment of the non-homogeneous jet to the homogeneous jet discussed earlier it appears that the non-homogeneous jet entrains more air. However, this conclusion may only be a result of the method of non-dimensionalization. The initial mass flux of air for the non-homogeneous jet is less than for a homogeneous jet of the same initial momentum flux so that non-dimensionalizing with respect to this value results in a larger number for the non-homogeneous jet. A similar problem arises for the non-isothermal jet where the decreased density at the exit requires a smaller mass flux of air for a given momentum distribution than does an isothermal jet. To compare relative rates of entrainment, the following method of data reduction is suggested. The actual dimensional value of total mass flux of air is obtained from numerical integration of

the air flux data at each value of \bar{x} . The actual mass flow of air issuing from the exit is subtracted from the above; the remainder is the amount of ambient air that has actually been entrained. To compare jets of different initial momentum levels and different areas, the remainder above is divided by the equivalent mass flux of ambient temperature air that would produce the entire momentum flux at the exit of the jet. This equivalent value for initial mass flux is suggested as a value for non-dimensionalization because it is the authors' contention that the free jet is characterized by its total momentum flux and that the ultimate entrainment of jets of equal initial momentum will be equal.

The method of comparing entrainment described above will be applied to all of the configurations investigated in this work at the end of this Section.

E. Centerline Behavior of Flux Variables

The centerline value of momentum flux, mass flux of carbon dioxide, and mass flux of air, non-dimensionalized with respect to the exit values, are plotted as a function of x/d in Fig. 26.

It is observed that the centerline values of momentum flux of the mass flux of CO_2 decay as $x^{-2.00}$ far from the exit; however, the potential core for the momentum flux is 6.2 diameters while that of the mass flux of CO_2 is 5.9 diameters. In this case, the initial profiles are believed to be nearly identical so that the more rapid decay of the CO_2 flux values is not the result of initial conditions. By the conventional

criteria for rates of mixing then, the mass flux of CO_2 is found to mix faster than the momentum flux.

The theoretical behavior of the centerline values of momentum flux and mass flux of CO_2 are presented in Fig. 26 plotted as a function of the transform variable $\bar{\chi}$. The difference in initial conditions for these two variables is so small that centerline behavior is indistinguishable in the transformed coordinate system.

As in the previous case, the \bar{x} vs. $\bar{\chi}$ transformations are obtained by matching centerline values of the dependent variables. The results of this technique are presented in Fig. 27. Two distinct transformations are generated, one for the momentum flux and the other for the mass flux of CO_2 . As discussed in Section II, the fact that these transformations are different indicates that mass flux does indeed "mix" faster than momentum flux. It appears, however, that the two transformations will merge into a single function for very large values of $\bar{\chi}$ which is reasonable in the sense that when the mass flux of the foreign species becomes an insignificant fraction of the total mass flux of the jet (this occurs because of the increasing value of the air flux) then the jet behaves like a homogeneous jet.

The centerline values of mass flux of air are also shown in Fig. 26 and are seen to decay linearly with x/d in the asymptotic limit. Because the total mass flux of air is not a conserved quantity, a theoretical development would require a source term in the air flux species equation. The approach to formulating such a source term has not yet been

developed and thus no theoretical description for the air flux was obtained.

Another important conclusion results from the observed centerline behavior of the momentum flux. The non-homogeneous facility is the same facility used for homogeneous studies in Ref. 16. The momentum decay for the non-homogeneous study is found to be absolutely identical to that of the homogeneous case; thus the change in exit concentration in no way affects the momentum field.

F. Halfwidths

The halfwidths for all of the flux variables are presented in Fig. 28 as a function of x/d . All of the halfwidths are found to asymptote to a linear growth rate. Note that there is a small but distinct difference in the behavior of the halfwidths for the momentum flux and the mass flux of carbon dioxide. Following convention it can be said that the mass flux of CO_2 "mixes" faster than momentum flux in the sense that it has larger values of halfwidths.

It is observed that the present experimental measurements indicate a preferential transport of mass over momentum in the sense that at a given x/d location, the centerline value of mass flux of CO_2 is lower than that of momentum flux and its halfwidth is larger. However, the measurements also indicate that the values of r for which no sensible measurement of each variable is obtainable are identical for each flux variable. That is, the "edge" of the jet is the same for each quantity even though the mass flux of CO_2 has a larger

value for its halfwidth and a lower centerline value than does the momentum flux. Previous experimental results, presented in terms of velocity and concentration, tended to indicate a different "boundary layer thickness" for each variable. The present results, however, show that all the flux variables are distributed differently in a mixing zone of unique width.

The momentum halfwidths shown in Fig. 28 match exactly the momentum halfwidths reported in Ref. 16 for the homogeneous condition; once again, it is found that for identical initial conditions, the momentum field is sensibly independent of the gas mixture.

G. Theory Compared to Experiment

Using the \bar{x} vs. $\bar{\chi}$ transformations shown in Fig. 27, the complete analytic description of momentum flux and mass flux of carbon dioxide was generated. Figure 29 compares the theoretical and experimental results for the entire momentum flux field of the non-homogeneous jet. Figure 30 compares the theoretical and experimental results for the entire carbon dioxide flux field. Note that the results are presented in terms of the physical coordinates, not similarity variables; also note that the theory accurately predicts the developing region of the jet in addition to the fully developed region. Also note the great similarity between the momentum profiles and the CO_2 flux profiles. Once again, the theoretical description is felt to be good.

H. Conclusion

Measurements of the species mass flux and momentum flux in a non-homogeneous free jet indicate that preferential transport of mass vs. momentum does occur for these variables in the sense that the mass flux decays sooner and has larger halfwidths. However, the "edge" of the jet is found to be identical for all of the flux variables.

The inductive theory is found to accurately describe the momentum flux and mass flux of carbon dioxide of the non-homogeneous free jet.

4. Non-Isothermal, Homogeneous Jet

A. Introduction

The non-isothermal jet facility is the same facility used for the isothermal, homogeneous study described earlier with the exception of the orifice plate. Because of the difficulties encountered with the sharp radiused plate, a new orifice plate was machined with a larger radius. The new plate was machined from bakelite to provide a "flatter" exit profile for enthalpy flux than would be possible with a metal plate.

The final design enthalpy flux probe shown in Fig. 13 was used to measure the momentum flux, $\overline{\rho u^2}$ and the total enthalpy flux, $\overline{\rho u (h_t - h_{amb.})}$ of this jet.

B. Initial Conditions - Exit Profiles

The chamber conditions for this investigation were a pressure of ten inches of water and a temperature of 300°F

corresponding to an exit velocity of about 250 fps.

The exit profile of momentum was measured with an .018 inch diameter pitot tube and water manometer. The exit profile of total enthalpy flux was computed from measurements of the pitot pressure and temperature measurements using a thermocouple. The use of a thermocouple at the exit is justified because the flow is laminar there.

The measured exit profiles of momentum flux and total enthalpy flux and the analytic curves for each are shown in Fig. 31. The analytic expression for the momentum flux is

$$\frac{(\overline{\rho u^2})_{\bar{r},0}}{(\overline{\rho u^2})_{0,0}} = \begin{cases} 1.0 & 0 \leq \bar{r}' \leq .425 \\ 1.0 - 781.25(\bar{r} - .425)^3 & .425 \leq \bar{r} \leq .465 \\ 13.571428(1 - 2\bar{r}) & .465 \leq \bar{r} \leq .500 \\ 0 & \bar{r} > .500 \end{cases}$$

The analytic expression for the total enthalpy flux is

$$\frac{(\overline{\rho u \Delta h_t})_{\bar{r},0}}{(\overline{\rho u \Delta h_t})_{0,0}} = \begin{cases} 1.0 - 0.06\bar{r} & 0 \leq \bar{r} \leq .250 \\ 0.989375 - 1.75(\bar{r} - 0.2)^4 & .250 \leq \bar{r} \leq .450 \\ 0.8987 - 23,045.26(\bar{r} - .42)^4 & .450 \leq \bar{r} \leq .500 \\ 0 & \bar{r} > .500 \end{cases}$$

C. Conservation of Momentum Flux and Total Enthalpy Flux

For the non-isothermal jet, two integrated quantities are conserved; namely, the total momentum flux and the flux of the stagnation enthalpy less ambient enthalpy, which shall be referred to as enthalpy flux. The result of a direct numerical integration of the raw data for these two quantities is presented in Fig. 32a. The measurements again indicate good conservation of total momentum flux, better than 5% at

most locations. The conservation of enthalpy flux is better than 15% everywhere. Once again, it should be noted that integration of the temperature profiles would not permit evaluation of energy conservation since temperature is not a conserved quantity.

D. Mass Entrainment

The remaining integral quantity is the total mass flux of air. The results of numerical integration of the raw mass flux data are shown in Fig. 32b. The entrainment is found to asymptote to a linear growth given approximately by $\dot{m}/\dot{m}_e = .355 x/d$. This value is higher than was obtained for the isothermal jet but is not necessarily an indication of greater mass entrainment since the initial mass flux is lower for a given total momentum flux due to the lower density at the exit. A comparison of the mass entrainment properties of all the jets examined will be presented later in this section.

E. Centerline Behavior of Flux Variables

The centerline values of momentum flux, enthalpy flux, and mass flux, non-dimensionalized with respect to the exit values are plotted as a function of x/d in Fig. 33.

It is observed that the centerline values of the momentum flux and the enthalpy flux decay as $x^{-2.00}$ far from the exit; however, the potential core for the momentum flux is 6.3 diameters while that of the enthalpy flux is 5.5 diameters. In this case, the initial profile of the enthalpy flux is considerably less "full" than that of momentum flux so that

it is expected that the enthalpy flux should decay faster. Thus, it would be difficult to apply the usual criteria for comparing rates of mixing in this case. However, the use of the inductive theory will permit a comparison of mixing rates even with an appreciable difference in the initial conditions.

The theoretical behavior of the centerline values of momentum flux and enthalpy flux are presented in Fig. 33 plotted as a function of the transform variable $\bar{\chi}$. The difference in initial conditions for these two variables does manifest itself in the theoretical result.

As was done previously, the \bar{x} vs. $\bar{\chi}$ transformations are obtained by matching centerline values of the dependent variables. The results of this technique are presented in Fig. 34. Similar to the non-homogeneous jet, two distinct transformations are generated for momentum flux and enthalpy flux. As discussed in Section II, the fact that these transformations are different does indicate that enthalpy flux "mixes" faster than momentum flux. Note that this comparison can be made despite the difference in initial conditions. Similar to the non-homogeneous case, it appears that the two curves may merge into a single function for very large $\bar{\chi}$.

The centerline values of mass flux are also presented in Fig. 33 and are seen to decay linearly with x/d in the asymptotic limit. Since the total mass flux is not conserved, no theoretical solution was developed.

An important conclusion obtained from the centerline behavior of momentum is that the momentum flux behavior is not affected by heating so long as the initial conditions

remain the same. Note that there is no sensible difference in momentum flux behavior for the isothermal homogeneous jet from the orifice of large contraction radius (refer to Fig. 20) or the isothermal non-homogeneous jet (refer to Fig. 26) or the non-isothermal homogeneous jet (refer to Fig. 33).

F. Halfwidths

The halfwidths for all of the flux variables are presented in Fig. 35 as a function of x/d . All of the halfwidths are found to asymptote to a linear growth rate. Note that the enthalpy flux halfwidths are distinctly larger than the corresponding momentum flux halfwidths so that in this sense, it can again be said that enthalpy flux "mixes" faster than momentum flux.

It is observed that the present experimental measurements indicate a preferential transport of energy over momentum in the sense that at a given value of x/d , the centerline value of enthalpy flux is lower than that of momentum flux and its halfwidth is larger. However, the measurements also indicate that the values of r for which no sensible measurement is obtainable is identical for each flux variable. That is, the "edge" of the jet is the same for each quantity even though the enthalpy flux has a larger halfwidth and a lower centerline value than does the momentum flux. Previous experimental results presented in terms of velocity and temperature, tended to indicate a different "boundary layer thickness" for each variable. The present results, however, show that the flux variables are distributed differently in a mixing zone of

unique width.

G. Theory Compared to Experiment

Using the \bar{x} vs $\bar{\chi}$ transformations shown in Fig. 34, the complete analytic description of momentum flux and enthalpy flux was generated. Figure 36 compares the theoretical and experimental results for the entire momentum flux field of the non-isothermal jet. Figure 37 compares the theoretical and experimental results for the entire enthalpy flux field. Note that the results are presented in terms of physical coordinates not similarity variables; also note that the theory accurately predicts the developing region of the jet in addition to the fully developed region. Also note the similarity between the momentum flux and energy flux profiles. Once again, the theoretical description is felt to be excellent.

H. Conclusion

Measurements of the momentum flux and the flow of stagnation enthalpy minus ambient enthalpy in the flow field of a non-isothermal free jet indicate that preferential transport of energy vs. momentum does occur for these variables in the sense that the enthalpy flux decays sooner and has larger halfwidths. However, the "edge" of the jet is found to be identical for all of the flux variables.

The inductive theory is found to accurately describe the momentum flux and enthalpy flux of the non-isothermal free jet.

5. Comparison of Rates of Mixing and Entrainment For All Configurations Investigated

Because of the measurable difference in the initial profiles of the different dependent flux variables for each jet examined, a direct comparison of the centerline decays and halfwidth growths of each variable would not necessarily indicate greater or lesser rates of mixing. However, as explained in Section II, the inductive theory manifests the effects of the initial conditions in the transformed coordinate system so that the transformation between the physical coordinate \bar{x} and the transform coordinate $\bar{\chi}$ becomes a sensitive indicator of difference in mixing rates, independent of the initial conditions.

Following the above approach, Fig. 38 presents the \bar{x} vs. $\bar{\chi}$ transformations for the momentum flux, mass flux of CO_2 , and the total enthalpy flux from all of the configurations examined in the present work, and the momentum flux results of the isothermal homogeneous investigation from Ref. 16. With the exception of the results from the orifice with sharp contraction radius, all of the momentum flux transformations are found to lie within a narrow band, thus suggesting a unique curve for momentum flux.

The transformations for mass flux of CO_2 and for enthalpy flux also lie within a narrow band which is distinct from the momentum flux curve. These results suggest a second unique curve valid for mass flux and enthalpy flux. Thus the results of the present investigation supports the contention that "mass and energy are preferentially transported over momentum".

However, the "edge" of the jet is found to be identical for all flux variables.

The relative rates of mixing of all of the flux variables from each configuration investigated in the present work have been compared above. A discussion of the relative rates of entrainment of the isothermal homogeneous jet vs. the isothermal, non-homogeneous jet vs. the non-isothermal, homogeneous jet will now be discussed.

It is not immediately evident as to how to compare entrainment for the different jets investigated. It is the authors' contention that the initial momentum flux distribution may be the best quantity to characterize a jet as regards entrainment. As a result, it is necessary to subtract the actual initial mass flux of air from downstream values since a given momentum distribution can be generated in several fashions when non-homogeneous, non-isothermal conditions exist at the exit. By subtracting the initial value of mass flux of air, the remainder is only the mass flux that has actually been entrained. This operation alone is not sufficient to allow direct comparison between the various jets, because the integral value of the total momentum flux is different for each jet. To account for this difference, the net value of air flux entrained is divided by an "equivalent" initial mass flux which is that value of mass flux of ambient temperature air which would produce the initial momentum flux distribution that existed for each jet configuration. The results of this method of data reduction are shown in Fig. 39 plotted as a function of x/d . Also shown are the results from

Ricou and Spalding²⁵ non-dimensionalized in the same fashion. It is observed that when the data is reduced in this manner, there is little sensible difference in the behavior of the two isothermal jets, but that the non-isothermal jet entrains a significantly greater amount of air near the exit of the jet. However, all of the results approach a single curve in the asymptotic limit, as would be expected.

VI. SUMMARY

The major conclusions from the investigation of the response of a pitot tube, a thermocouple, and a sampling tube to a known periodic fluctuating flow are summarized below:

1. The pitot tube accurately measures one-half the mean momentum flux, $\frac{1}{2}\rho u^2$, for any intensity of fluctuation of velocity in the direction of the probe axis.

2. The pitot tube may be affected by lateral velocity fluctuations; the effect of increasing the intensity of lateral velocity fluctuations is a decrease in the observed value of total head.

3. Thermocouple measurements of mean temperature can deviate significantly from the true mean temperature in a turbulent flow. The error in measurement is a function of both the intensity of temperature fluctuations and the intensity of velocity fluctuations.

4. The complex interaction of temperature and velocity effects in a turbulent shear flow preclude the chances for correcting the mean temperature measurements of the thermocouple.

5. In a heated jet the thermocouple should be reasonably accurate near the axis but read higher than the true mean temperature in the shear region, thus indicating a wider temperature profile than actually exists.

6. There are several flow situations where the rate at which a sample is withdrawn can affect that sample; these include:

- a. particle laden flows
- b. flows with non-linear concentration gradients

$$\left(\frac{\partial^2 X_i}{\partial y^2} \neq 0\right)$$
- c. turbulent flows where there is considerable variation in the density, scale, and/or momentum of the eddies.

7. It has been shown experimentally that mean concentration measurements in a jet are dependent upon relative sampling rate.

8. In a turbulent shear flow, the complex interaction of gradient, density, and velocity effects preclude chances for correcting the readings.

9. In a non-homogeneous jet, concentration measurements made by sampling should be accurate near the axis far downstream but are subject to various errors in the high shear regions and the regions of high relative velocity intensity.

The major conclusions from an investigation of an isothermal, homogeneous jet, an isothermal, non-homogeneous jet, and a non-isothermal, homogeneous jet in terms of the flux of mass, the flux of momentum, and the flux of total enthalpy are summarized below:

1. For the same initial conditions, the mass flux of a foreign species and the flux of total enthalpy are found to decay faster and have larger halfwidths than does the momentum flux. In this sense, it is found that mass and energy "mix" faster than momentum.

2. For the same initial conditions, the behavior of the

foreign gas mass flux and the total enthalpy flux should be identical.

3. The radial location where the flux variables become sensibly equal to zero, that is, the "edge" of the jet, is found to be the same for all of the flux variables.

4. An extended version of the Reichardt inductive theory is found to adequately describe the entire flow field of all conserved flux quantities.

5. By non-dimensionalizing the total air flux of a jet in a certain manner with respect to the initial momentum flux of the jet, it is found that a heated jet entrains more ambient air near the jet exit but that all jets ultimately entrain the same amount of ambient fluid.

VII. REFERENCES

1. Sforza, P.M., Trentacoste, N.P. and Mons, R.: "Turbulent Mixing: A Review, Revaluation and Extension", AIAA Paper No. 69-31, Presented at the AIAA 7th Annual Aerospace Sciences Meeting, N.Y., January 20-22, 1969.
2. Reichardt, H.: "On a New Theory of Free Turbulence", ZAMM Vo. 21, No. 5, October 1941.
3. Vulis, L.A. and Terekhina, N.N.: "Propagation of a Turbulent Gas Jet in a Medium with a Different Density", Zh. Tekhn, Fig., Vol. 26, No. 6, 1956.
4. Vulis, L.A., Et Al: "Transfer Processes in a Free (Jet) Turbulent Boundary Layer", Translated by Aerospace Information Div., Library of Congress, AID Rept. No. T63-73, May 1963.
5. Goldstein, S. (editor): Modern Developments in Fluid Dynamics, 2 Vols., Dover Publications, Inc, N.Y., 1965.
6. Schlichting, H.: Boundary Layer Theory, McGraw-Hill Book Co., Inc., New York, 1960.
7. Townsend, A.A.: The Structure of Turbulent Shear Flow, Cambridge University Press, London, 1956.
8. Pai, S.I.: Fluid Dynamics of Jets, Van Nostrand, New York, 1954.
9. Hinze, J.O.: Turbulence, McGraw-Hill Book Co., Inc., New York, 1959.
10. Abramovich, G.N.: The Theory of Turbulent Jets, M.I.T. Press, Cambridge, Massachusetts, 1963.

11. Kryzwoblocki, M.V.F.: "Jets-Review of Literature", Jet Propulsion, Vol. 26, pp. 760-779, 1956.
12. Hallen, R.M.: "A Literature Review on Free Turbulent Shear Flow", Dept. of Mech. Engr., AFOSR TN -5444, Stanford University, April 1964.
13. Zakkay, V. and Fox, H.: "Homogeneous and Heterogeneous Mixing in Jets and Wakes", AGARD Monograph to be published.
14. Smoot, L.G.: "(Title Unavailable), Brigham Young University, BYU-366-F, 1968.
15. Harsha, P.T.: "Free Turbulent Mixing: A Critical Evaluation of Theory and Experiment", AEDC Report TR-71-36, February 1971.
16. Trentacoste, N.P. and Sforza, P.M.: "Studies in Homogeneous and Non-Homogeneous Free Turbulent Shear Flows", PIBAL Report No. 69-36, September 1969.
17. Becker, H.A., Hottel, H.C., and Williams, G.C.: "The Nozzle-Fluid Concentration Field of the Round, Turbulent, Free Jet", J. Fluid Mech., Vol. 30, Part 2, pp. 285-303, 1967.
18. Mummolo, F.: "A Theoretical Investigation of the Mean Properties of Incompressible, Turbulent, Free Jets", Master of Science Thesis (Astronautics), Polytechnic Institute of Brooklyn, June 1969.
19. Mons, R. and Sforza, P.M.: "Chemical Reactions in Compressible Turbulent Mixing Flows", AIAA Paper No. 69-537, Presented at AIAA 5th Propulsion Joint Specialist Conference, U.S. Air Force Academy, Colorado, June 9-13, 1969.

20. Baron, T. and Alexander, L.G.: "Momentum, Mass and Heat Transfer in Jets", Chemical Engineering Progress, Vol. 47, No. 4, pp. 181-185, April 1951.
21. Crank, J.: The Mathematics of Diffusion, Oxford University Press, p. 147, 1956.
22. Carslaw, H.S. and Jaeger, J.C.: Conduction of Heat in Solids, Second Edition, Oxford Press, p. 260, 1959.
23. Dean, R.C. Jr. (editor): Aerodynamic Measurements, Eagle Enterprises, New York, 1959.
24. Way, J. and Libby, P.A.: "Application of Hot Wire Anemometry and Digital Techniques to Measurements in a Turbulent Helium Jet", AIAA Paper No. 71-201, presented at AIAA 9th Aerospace Sciences Meeting, New York, January 25-27, 1971.
25. Ricou, F.P. and Spalding, D.B.: "Measurements of Entrainment by Axisymmetric Turbulent Jets", J. Fluid Mech., 11, 1, pp. 21-32, August 1961.
26. Wagnanski, I. and Fiedler, H.E.: "Some Measurements in the Self-Preserving Jet", Boeing Scientific Research Laboratories Document D1-82-0712, April 1968.
27. Corrsin, S. and Uberoi, M.S.: "Further Experiments on the Flow and Heat Transfer in a Heated Turbulent Air Jet", NACA Report No. 998, 1950.

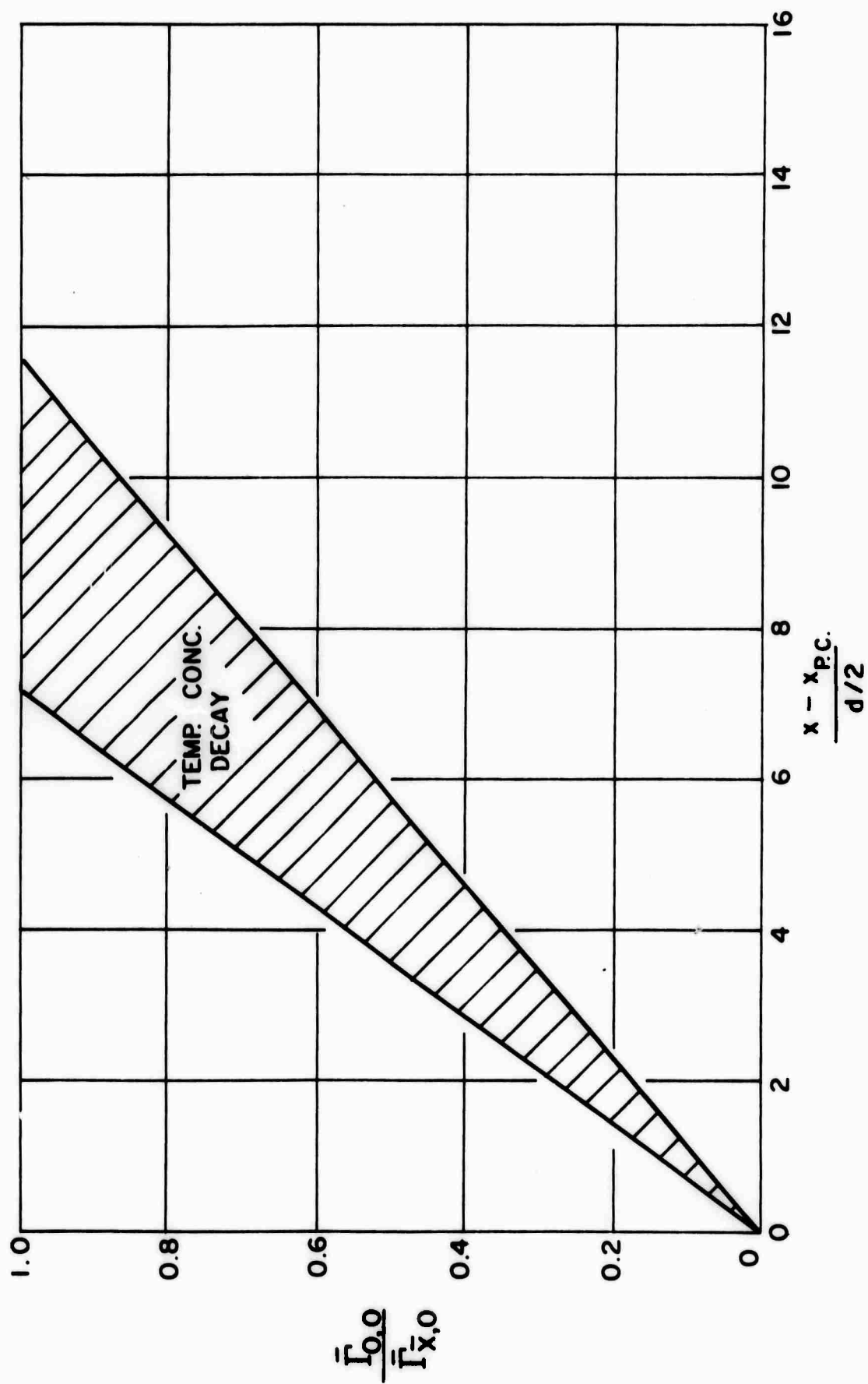


FIGURE 1a SUMMARY OF DATA FOR CENTERLINE DECAY OF CONCENTRATION AND TEMPERATURE FROM REF. 17

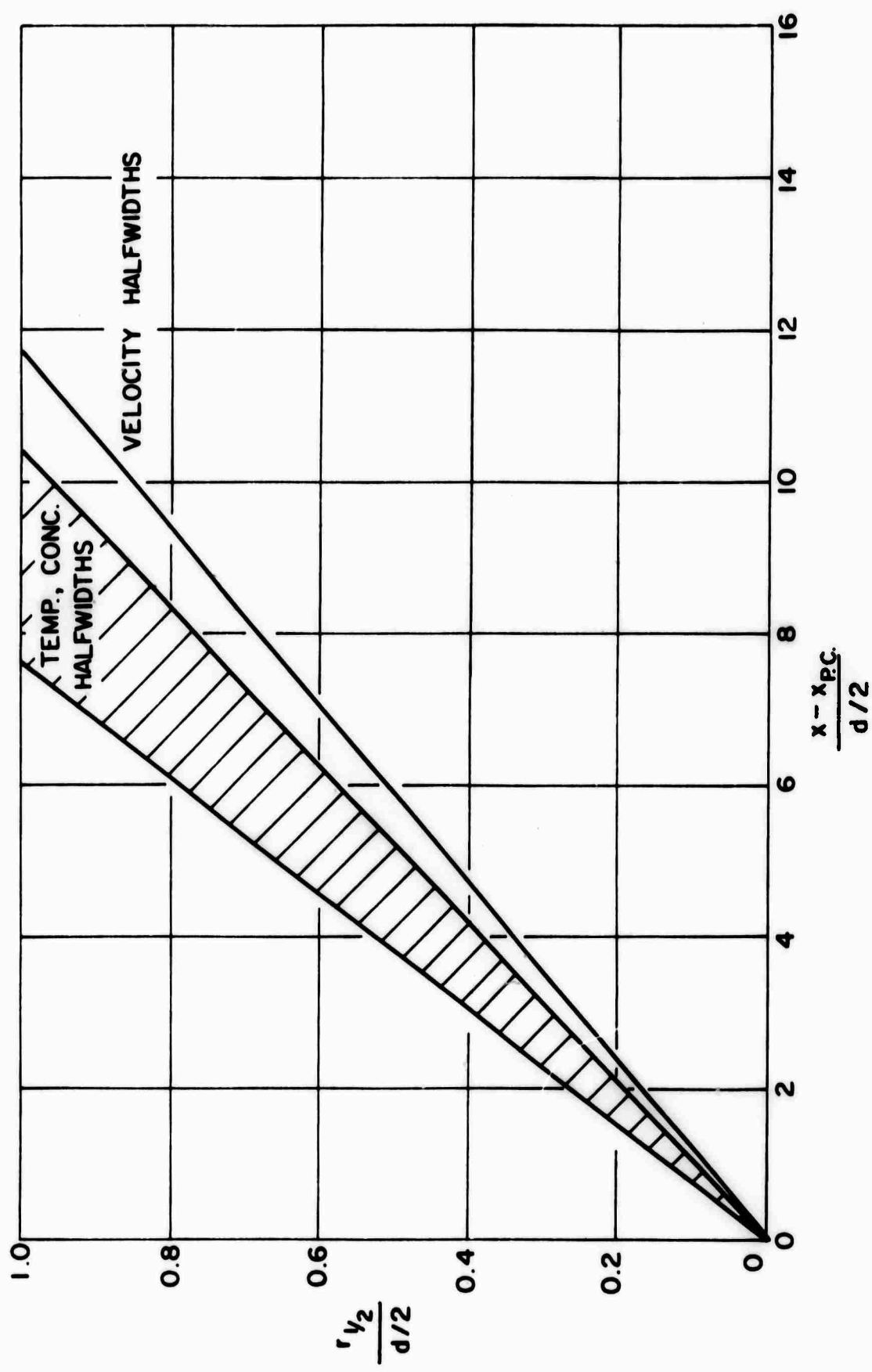


FIGURE 1b SUMMARY OF DATA FOR HALFWIDTHS OF CONCENTRATION, TEMPERATURE AND VELOCITY FROM REF. 17

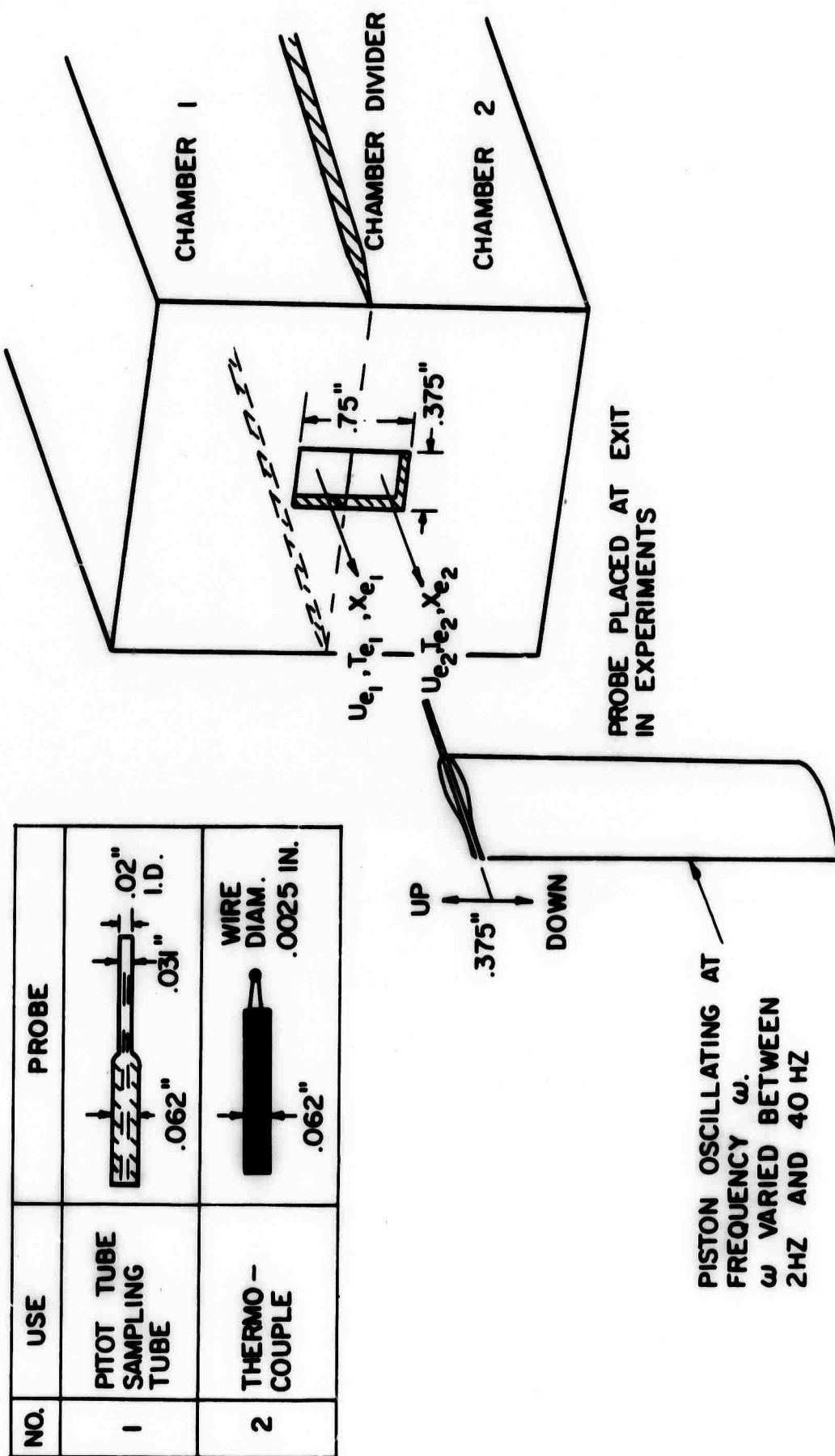


FIGURE 2 SCHEMATIC DIAGRAM OF OSCILLATING PROBE FACILITY

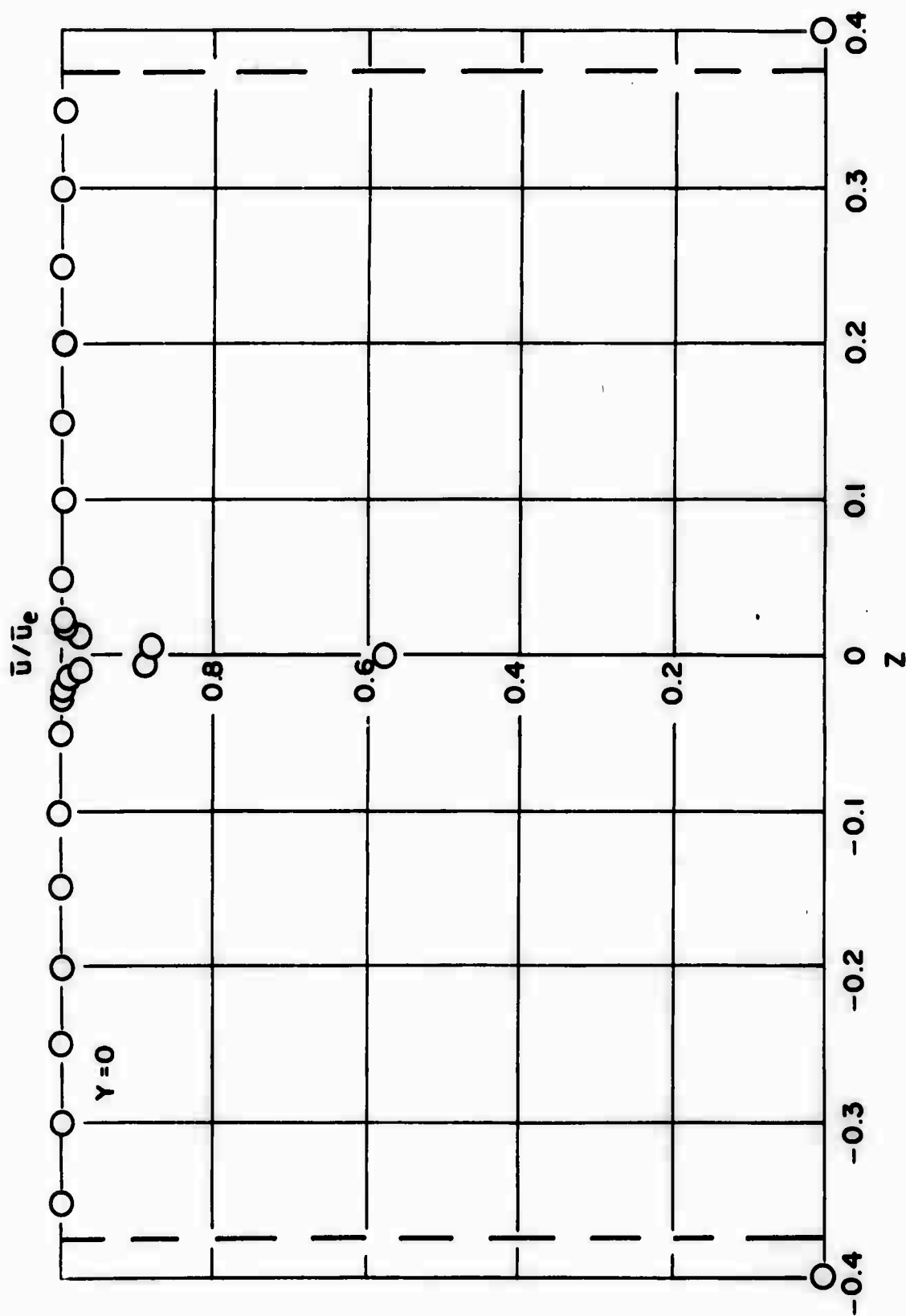


FIGURE 3 TYPICAL VELOCITY PROFILE AT EXIT OF DOUBLE CHAMBER
FOR OSCILLATING PROBE EXPERIMENT

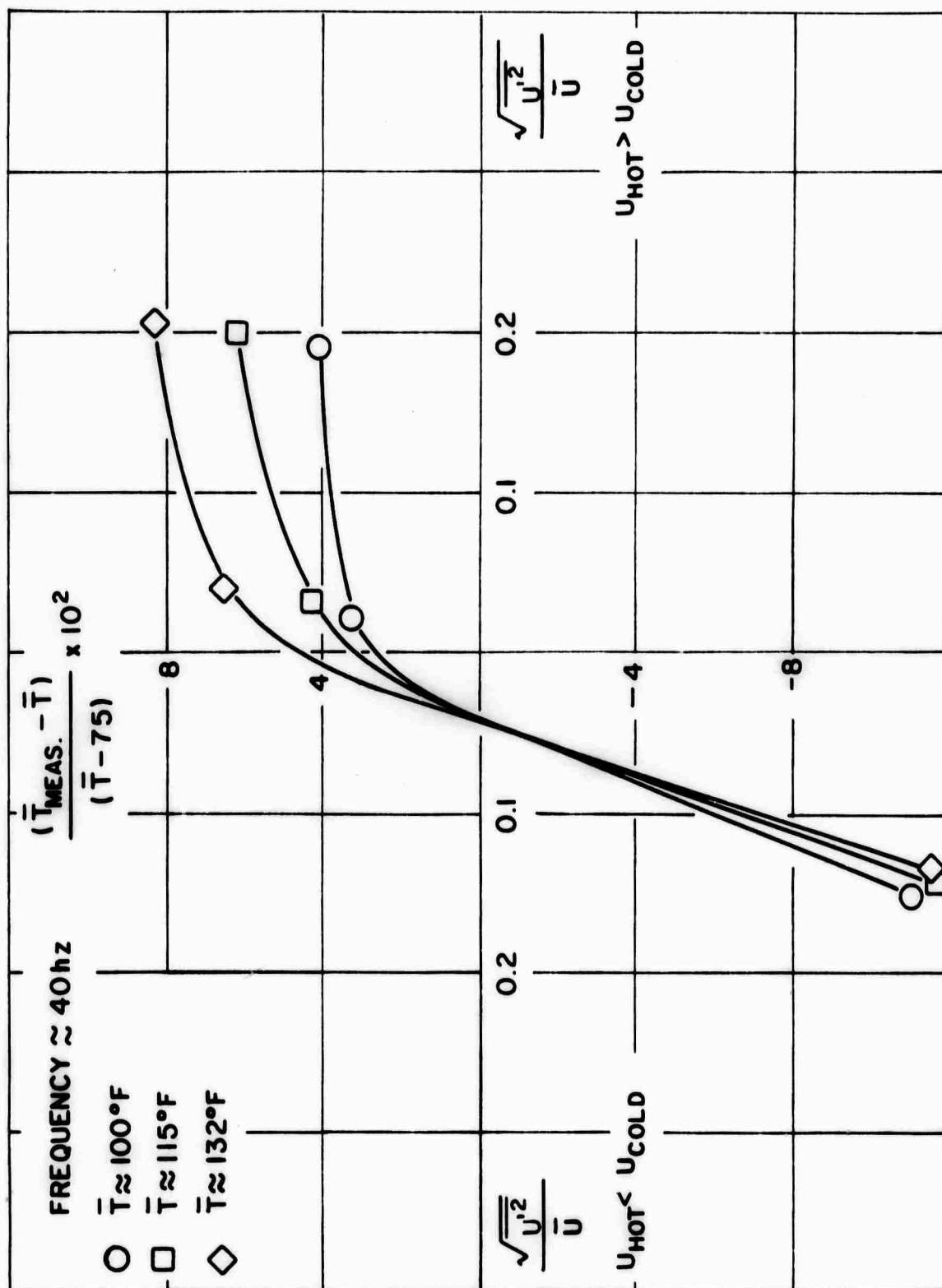


FIGURE 4 VARIATION OF ERROR IN MEAN TEMPERATURE MEASURED BY A THERMOCOUPLE IN PERCENT AS A FUNCTION OF INTENSITY OF VELOCITY FLUCTUATION AND MEAN TEMPERATURE

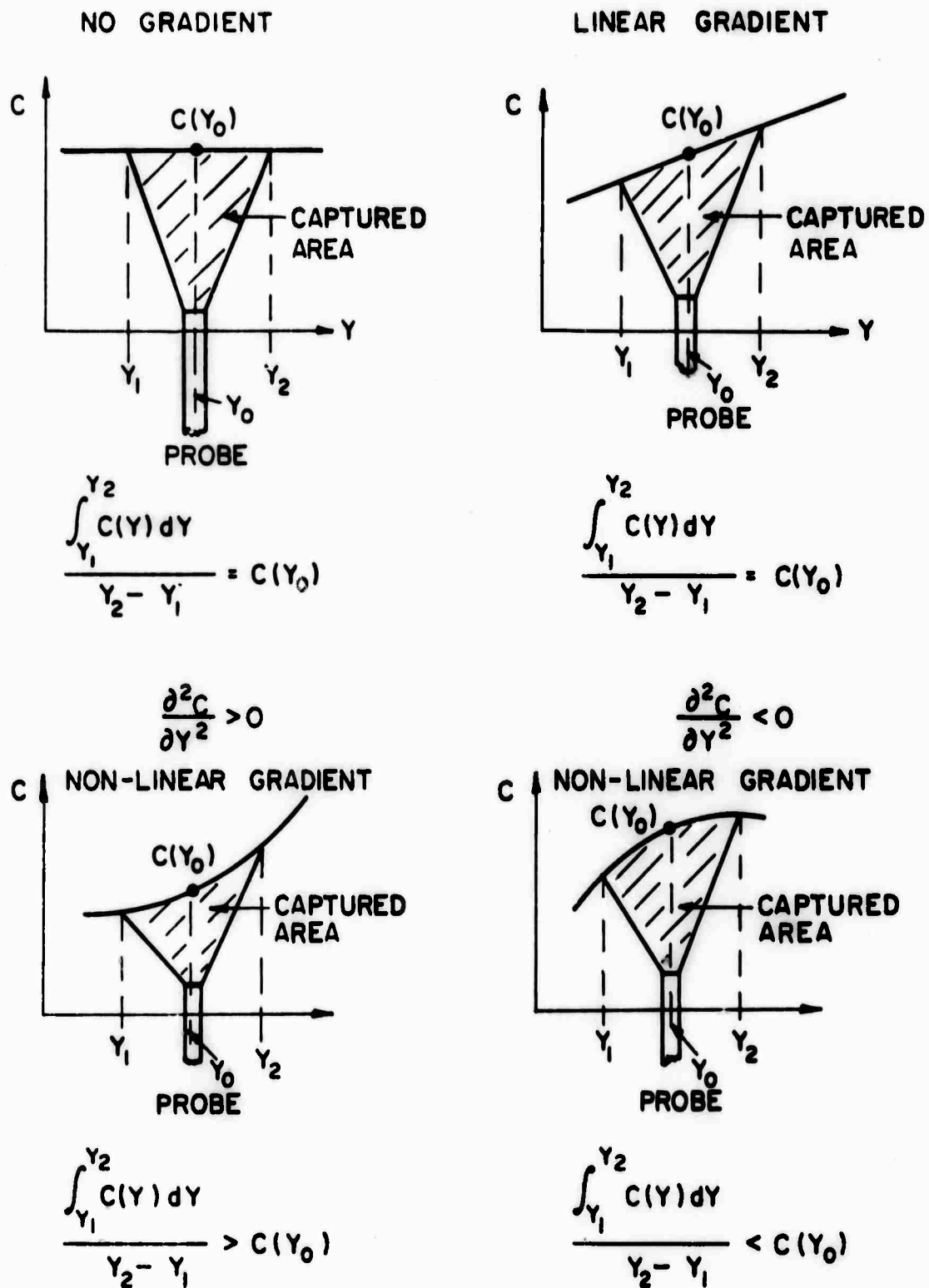


FIGURE 5 EFFECTS OF CONCENTRATION GRADIENT ON MEAN CONCENTRATION MEASUREMENTS MADE BY A SAMPLING PROBE

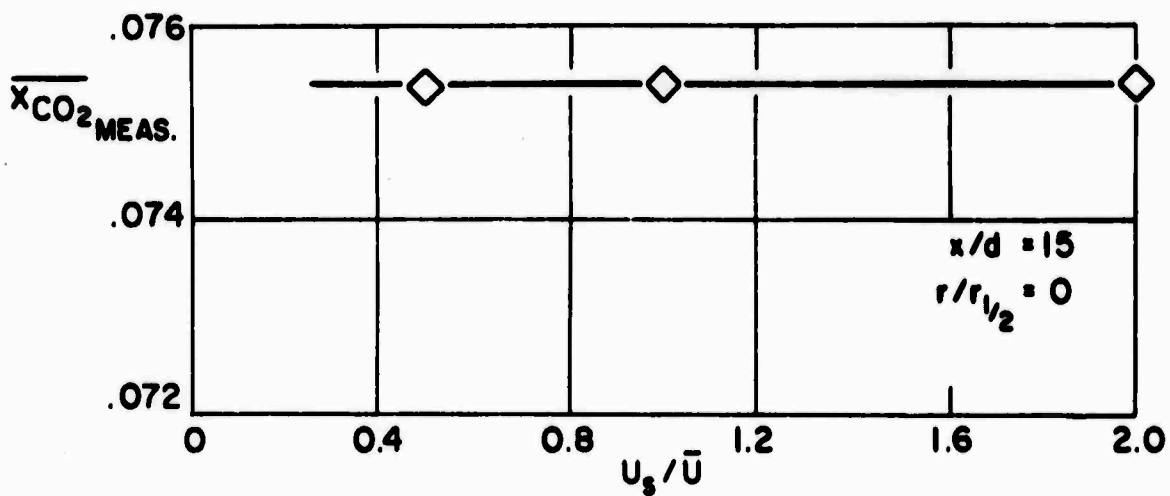
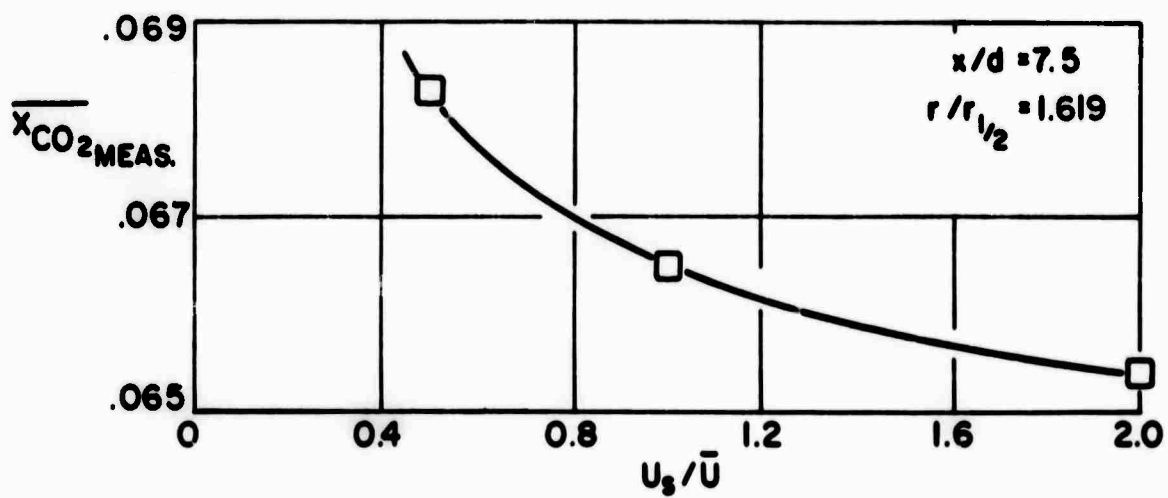
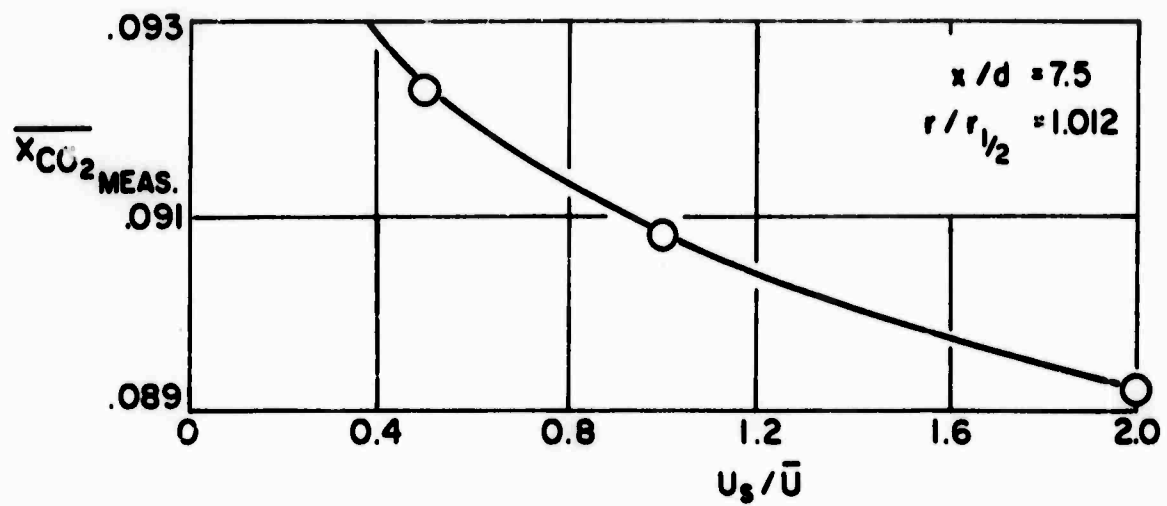


FIGURE 6 EFFECTS OF SAMPLING RATE ON MEAN CONCENTRATION MEASUREMENTS MADE IN THE FLOW FIELD OF A TURBULENT AXISYMMETRIC JET

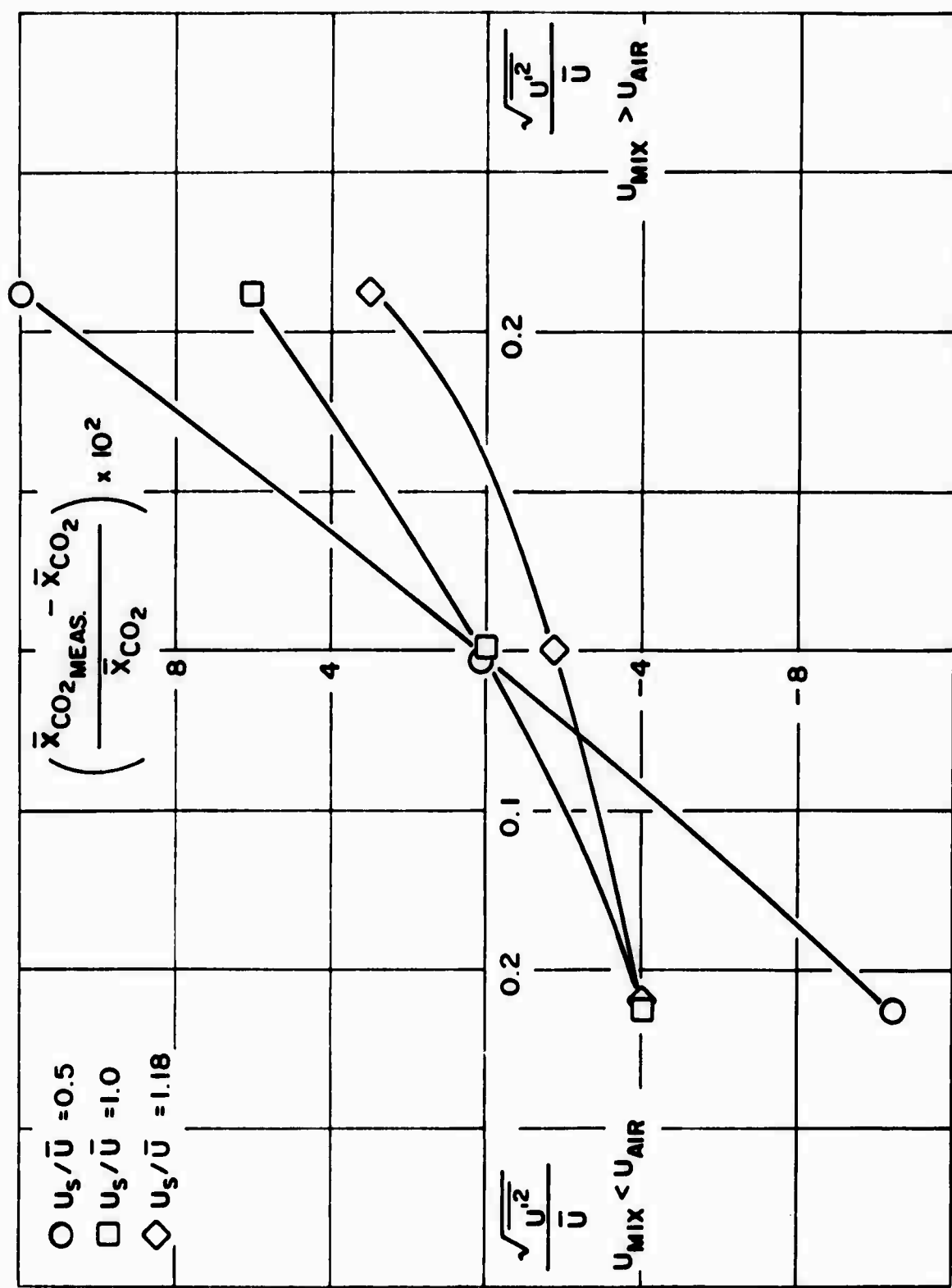


FIGURE 7 RESULTS FROM OSCILLATING EXPERIMENT SHOWING VARIATION OF ERROR IN PERCENT IN MEAN CONCENTRATION MEASUREMENTS AS A FUNCTION OF INTENSITY OF VELOCITY FLUCTUATIONS

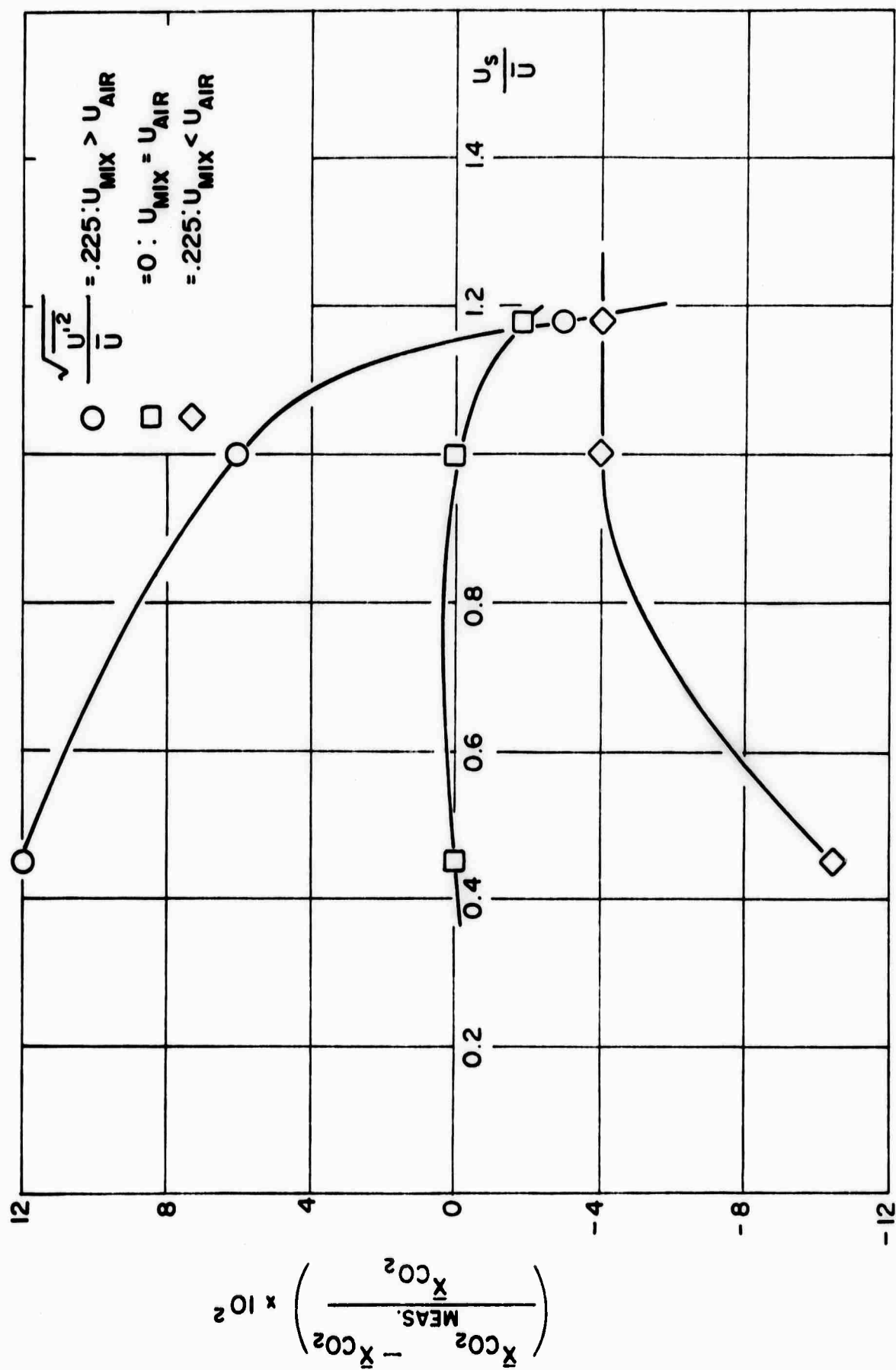
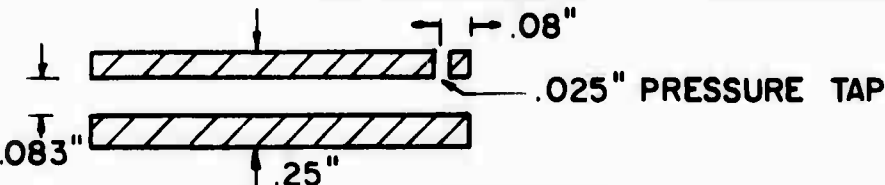
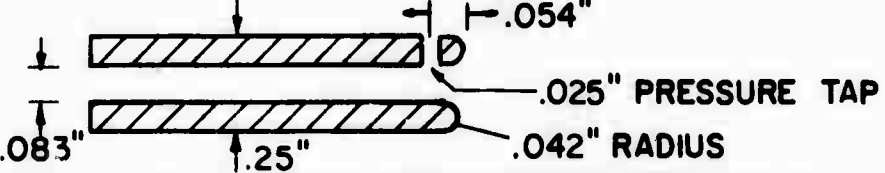
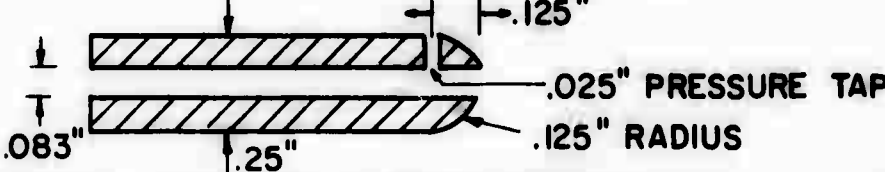
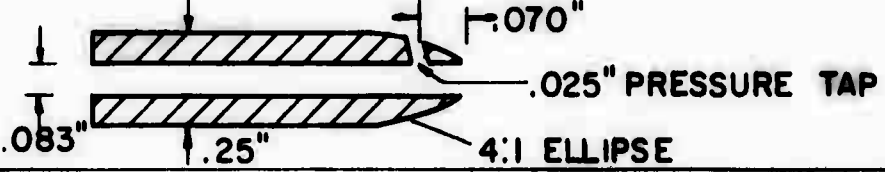
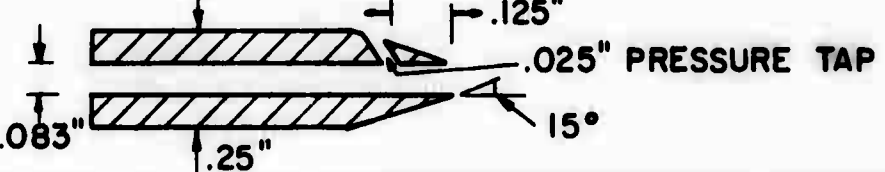


FIGURE 8 RESULTS FROM OSCILLATING EXPERIMENT SHOWING VARIATION OF ERROR IN PERCENT IN MEAN CONCENTRATION MEASUREMENTS AS A FUNCTION OF SAMPLING RATE

PROBE GEOMETRIES INVESTIGATED

NO.	
1	
2	
3	
4	
5	

FINAL DESIGN (NO. 2 ABOVE)

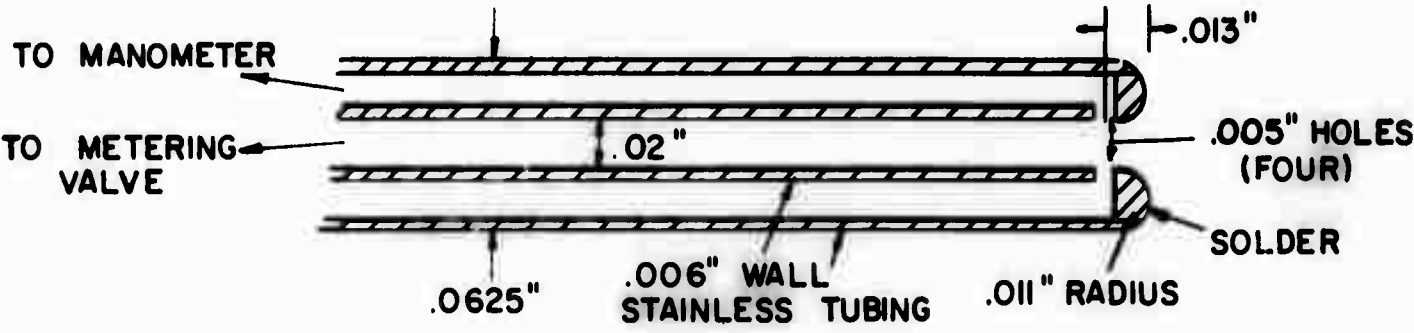


FIGURE 9 GEOMETRIES INVESTIGATED FOR INLET OF MASS FLUX PROBE AND DETAILS OF FINAL DESIGN CHOSEN

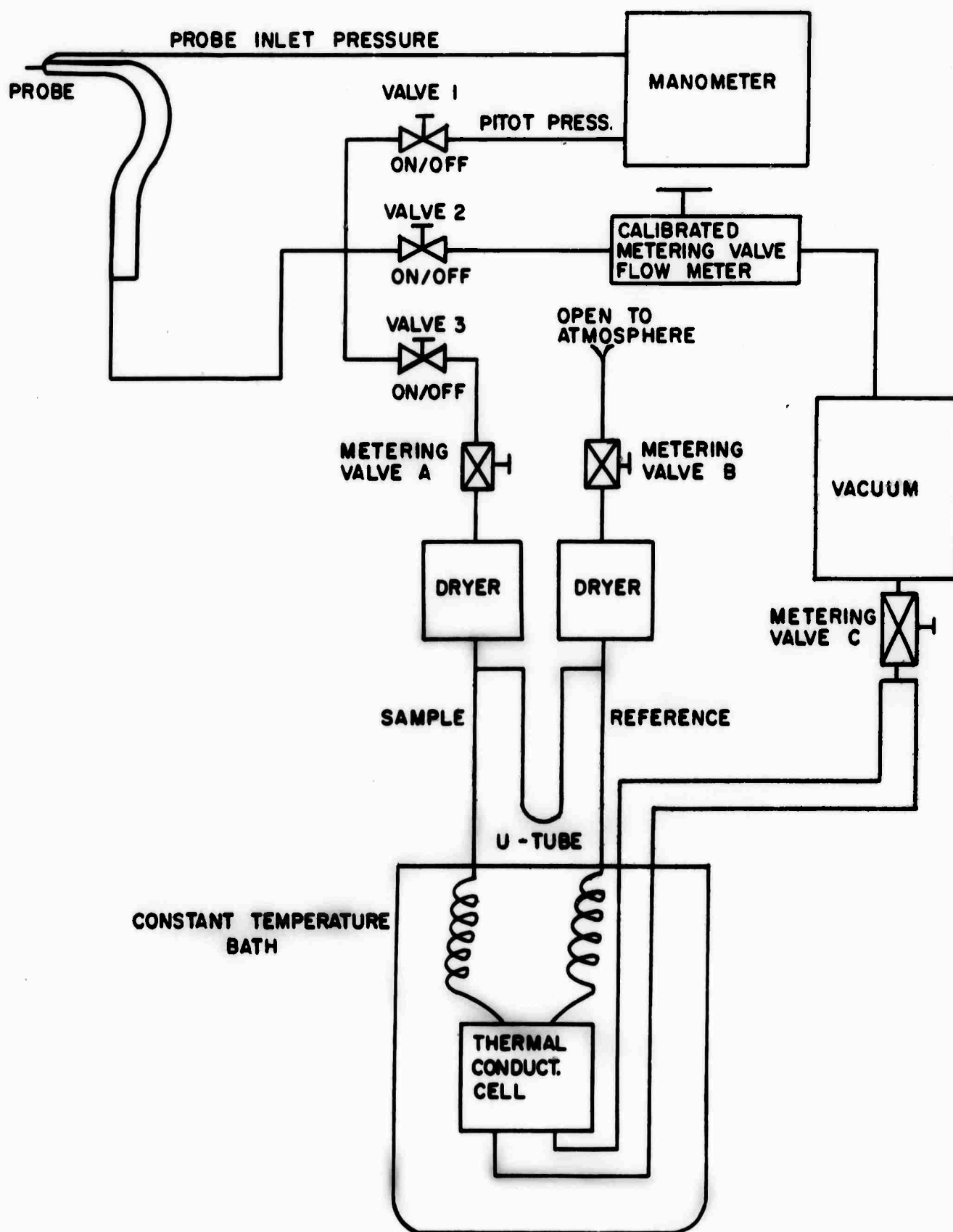


FIGURE 10 SCHEMATIC OF GAS SAMPLING AND ANALYZING SYSTEM

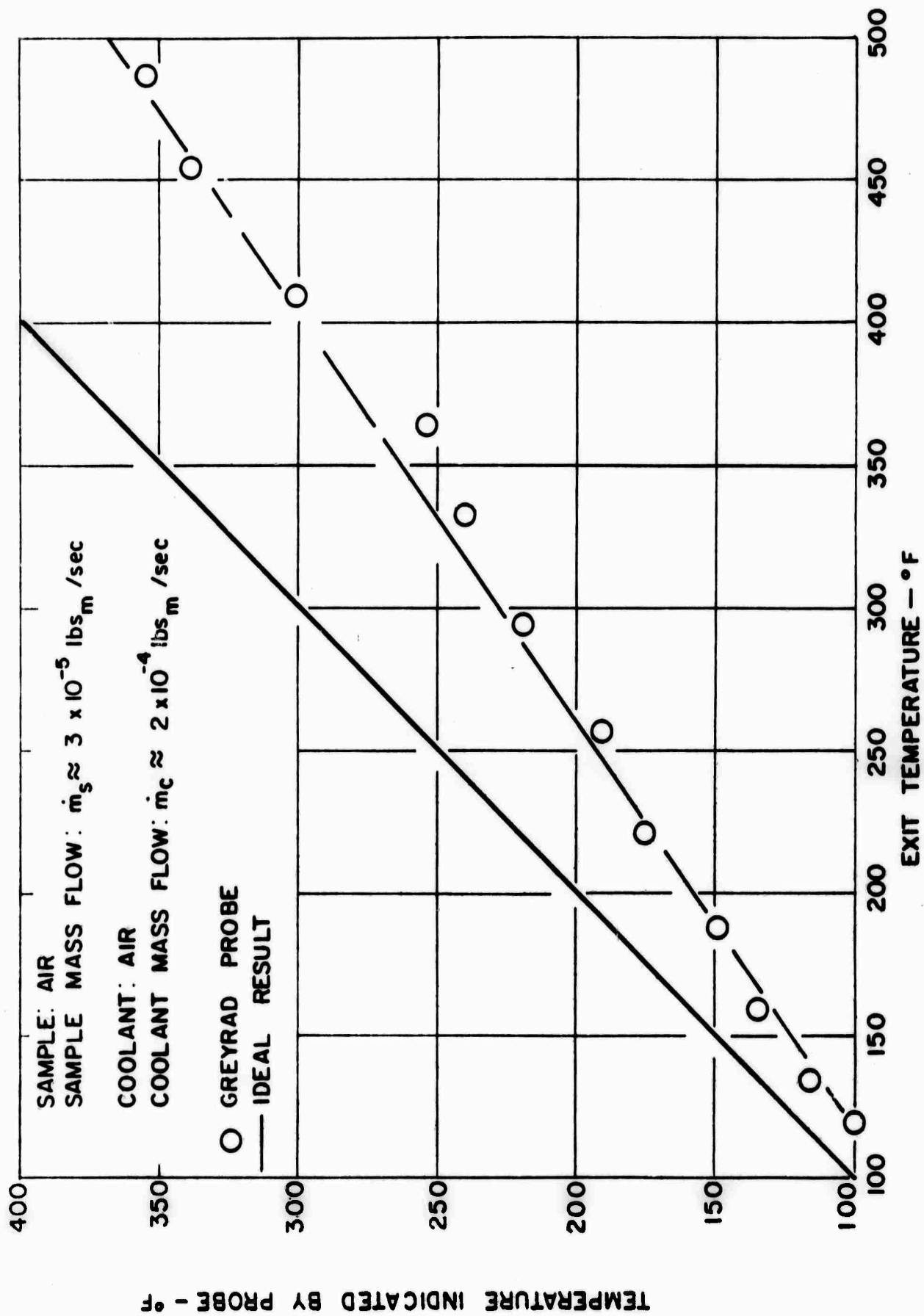


FIGURE 11 RESULTS OF TEMPERATURE MEASUREMENTS MADE AT THE EXIT OF A FREE JET WITH GREYRAD CALORIMETRIC PROBE

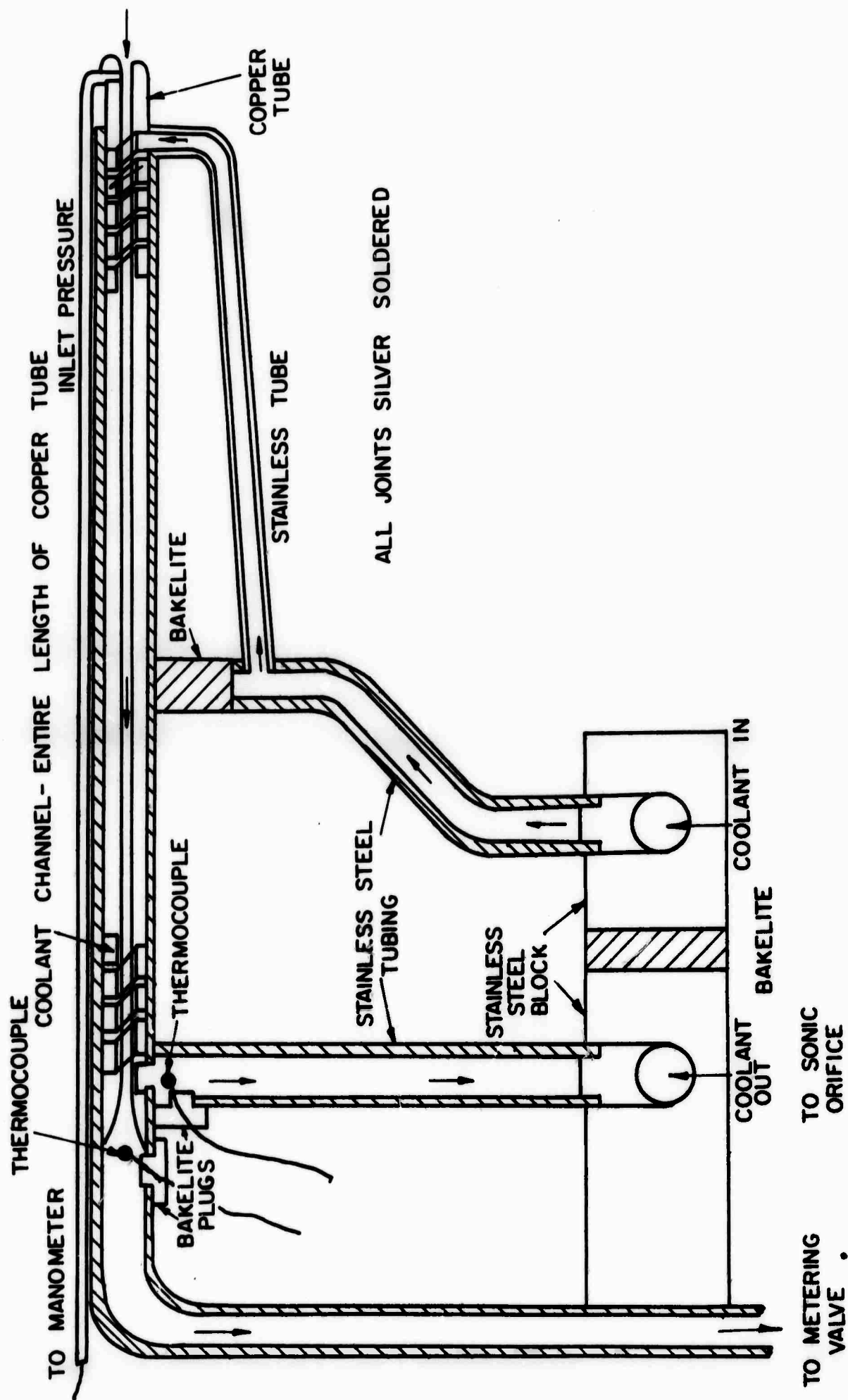
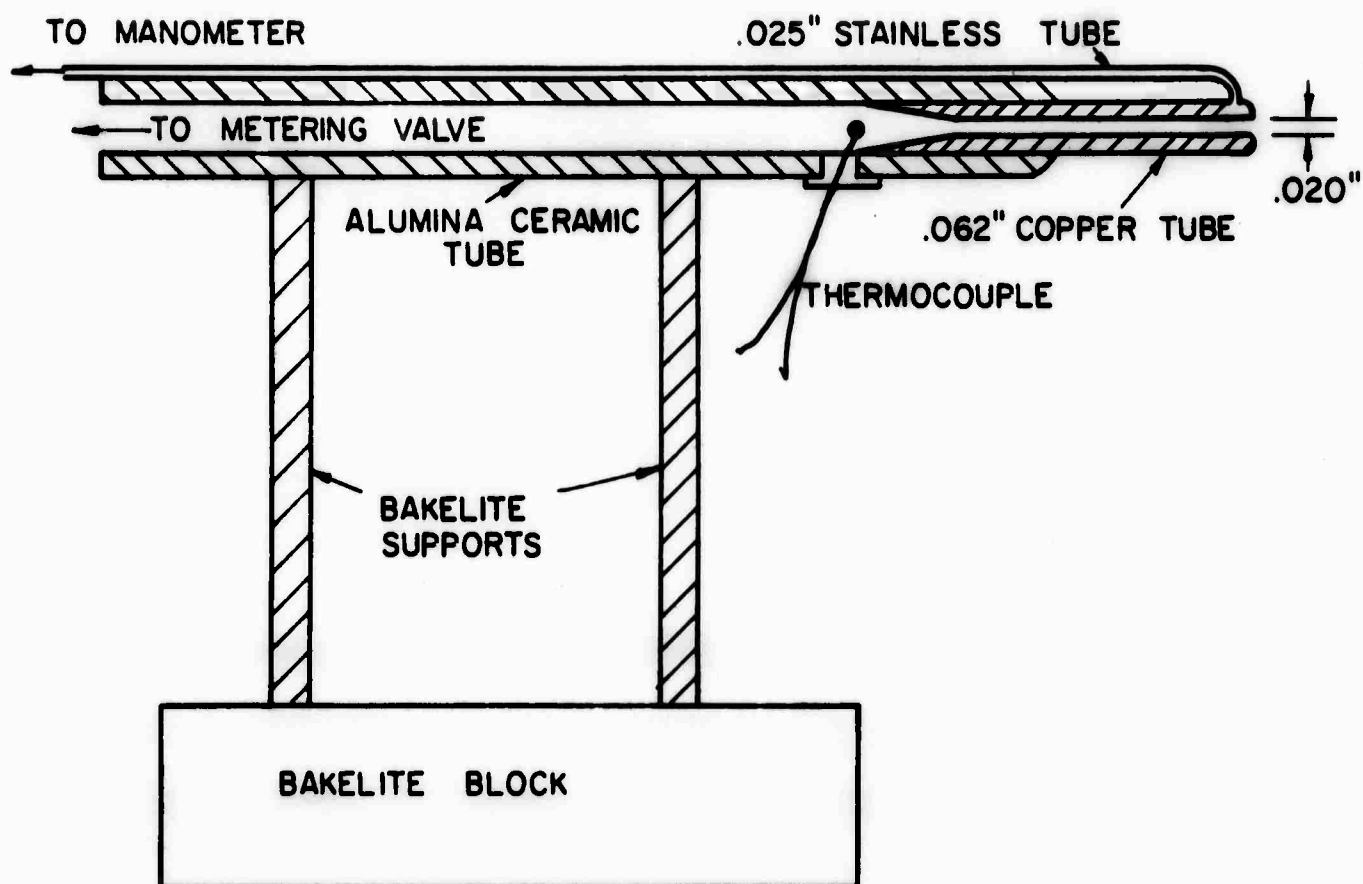


FIGURE 12b SCHEMATIC DIAGRAM OF CALORIMETRIC PROBE DESIGNED TO MEASURE MEAN ENTHALPY FLUX, cuh



SCHEMATIC OF UNCOOLED ENTHALPY FLUX PROBE

PHOTOGRAPH OF UNCOOLED ENTHALPY FLUX PROBE

FIGURE 13 SCHEMATIC DIAGRAM AND PHOTOGRAPH OF UNCOOLED PROBE
DESIGNED TO MEASURE MEAN TOTAL ENTHALPY FLUX, $\overline{\rho u h}_t$

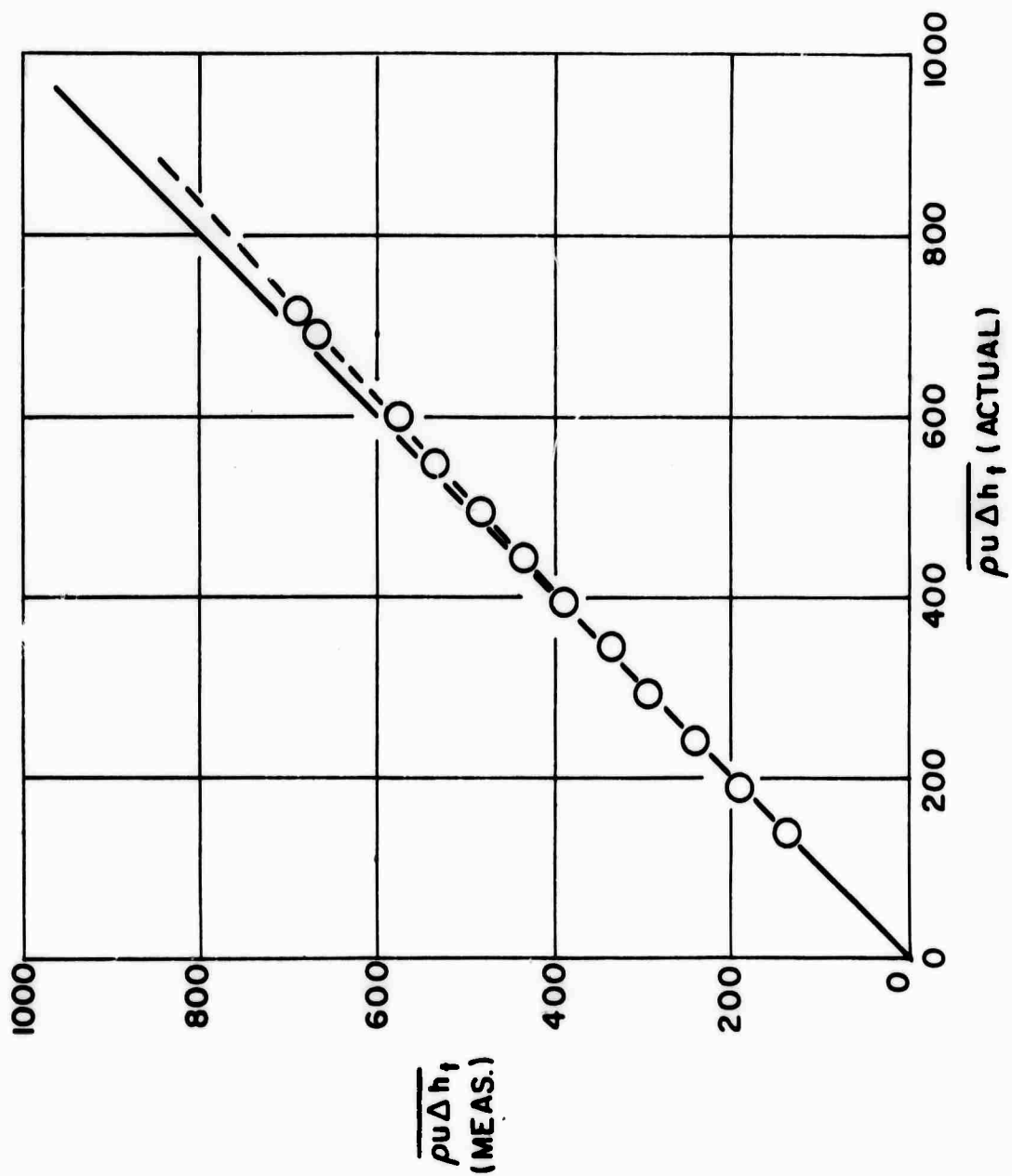


FIGURE 14 RESULTS OF MEASUREMENTS OF MEAN TOTAL ENTHALPY FLUX MADE AT THE EXIT OF A FREE JET WITH UNCOOLED PROBE

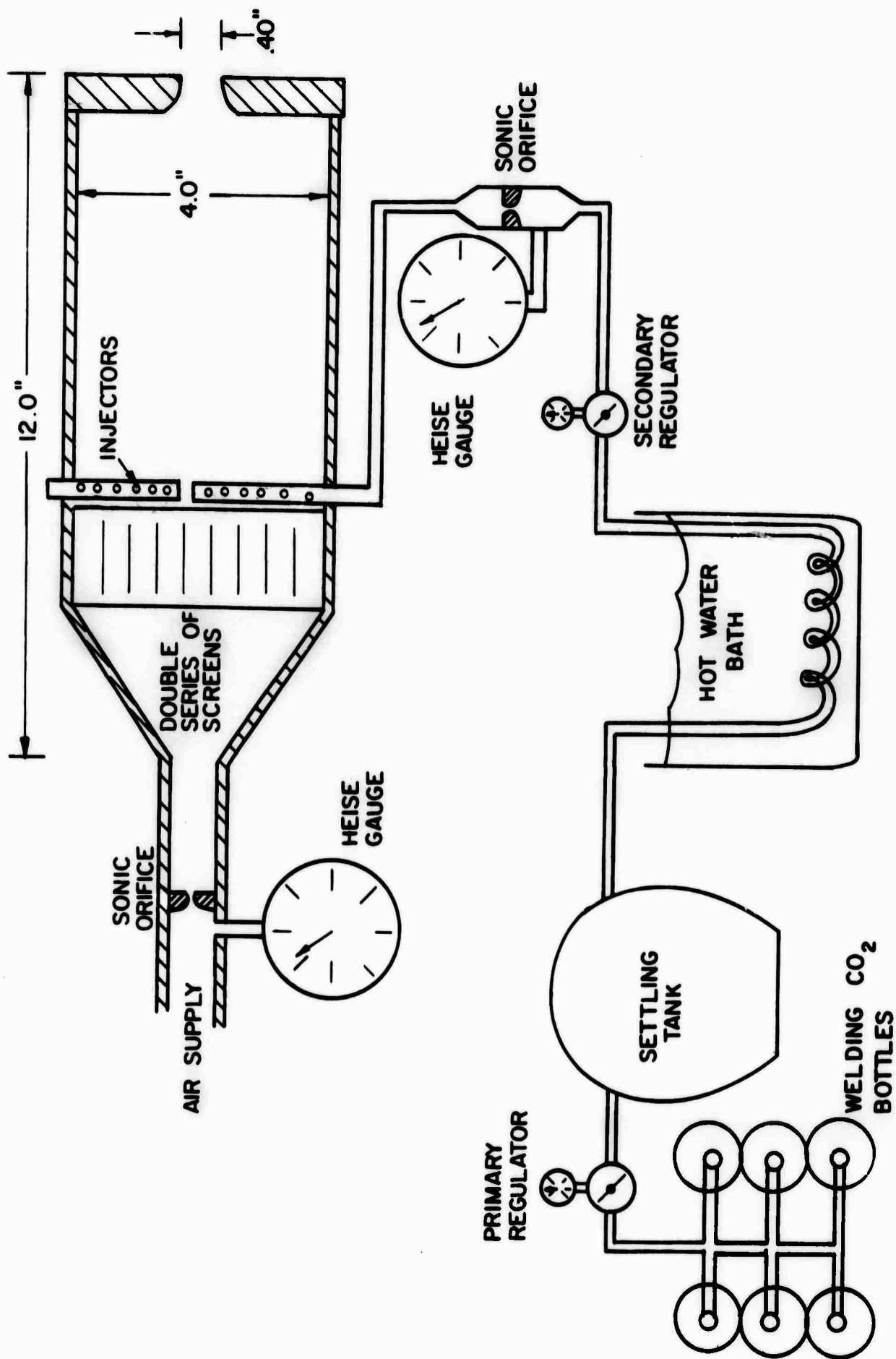


FIGURE 15 SCHEMATIC DIAGRAM OF NON_HOMOGENEOUS JET FACILITY

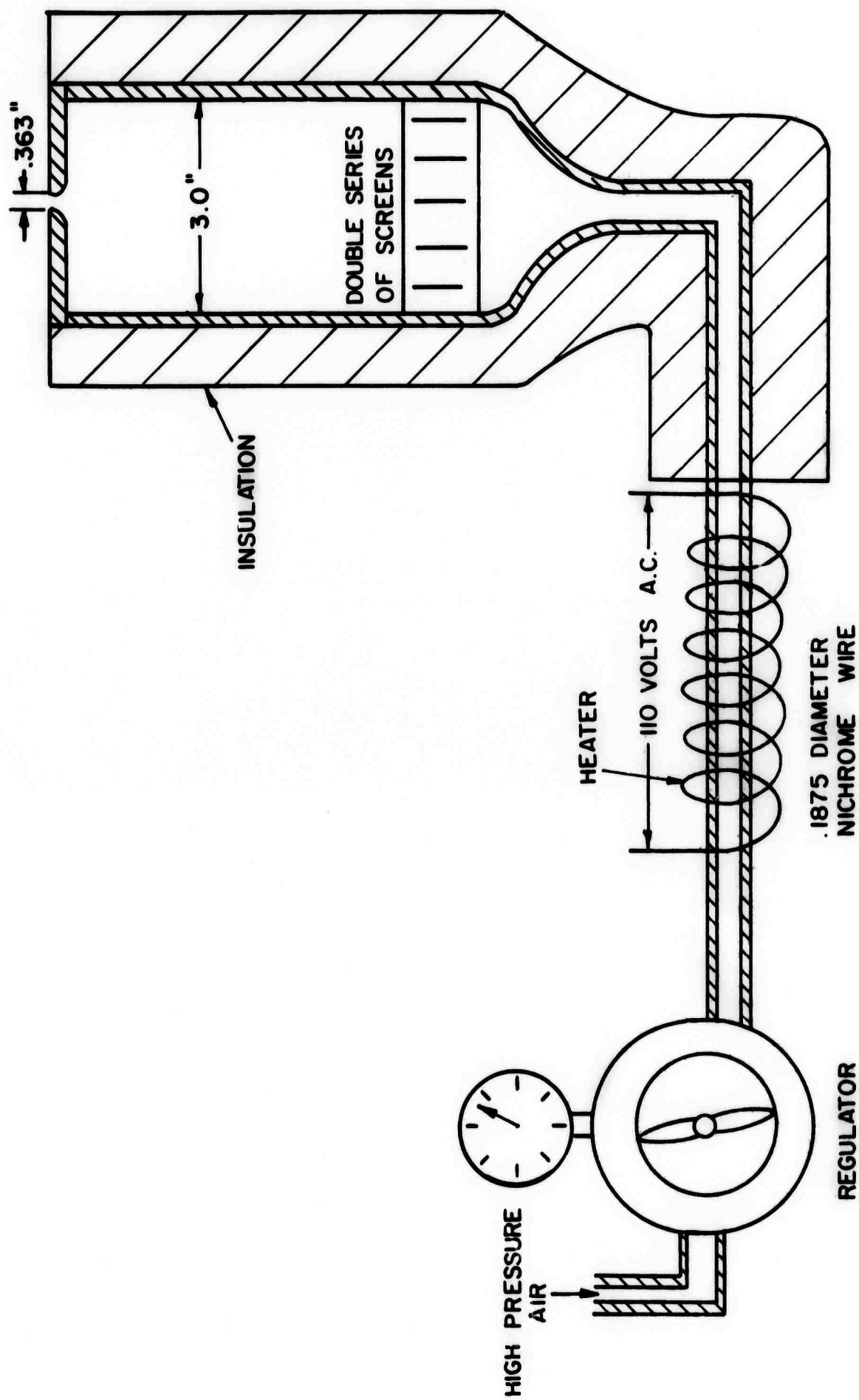
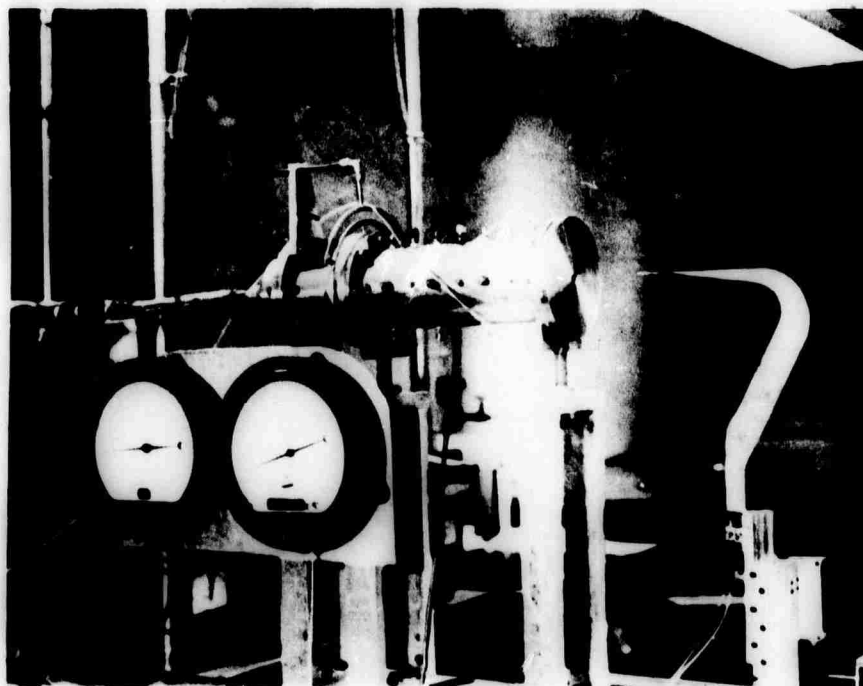
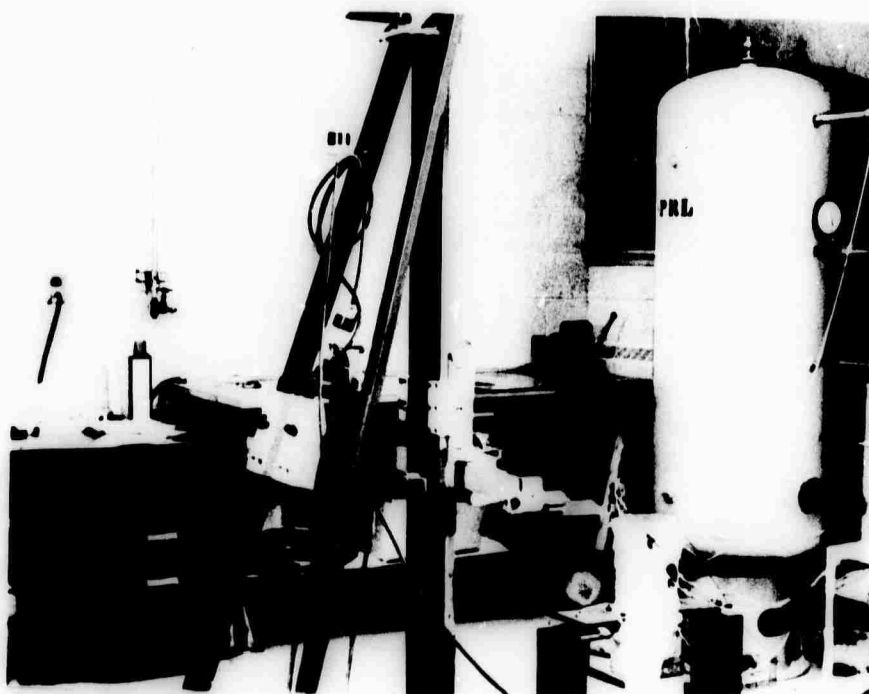


FIGURE 16 SCHEMATIC DIAGRAM OF HOMOGENEOUS JET FACILITY



NON-HOMOGENEOUS JET FACILITY



HOMOGENEOUS JET FACILITY

FIGURE 17 PHOTOGRAPHS OF NON-HOMOGENEOUS AND HOMOGENEOUS JET FACILITIES

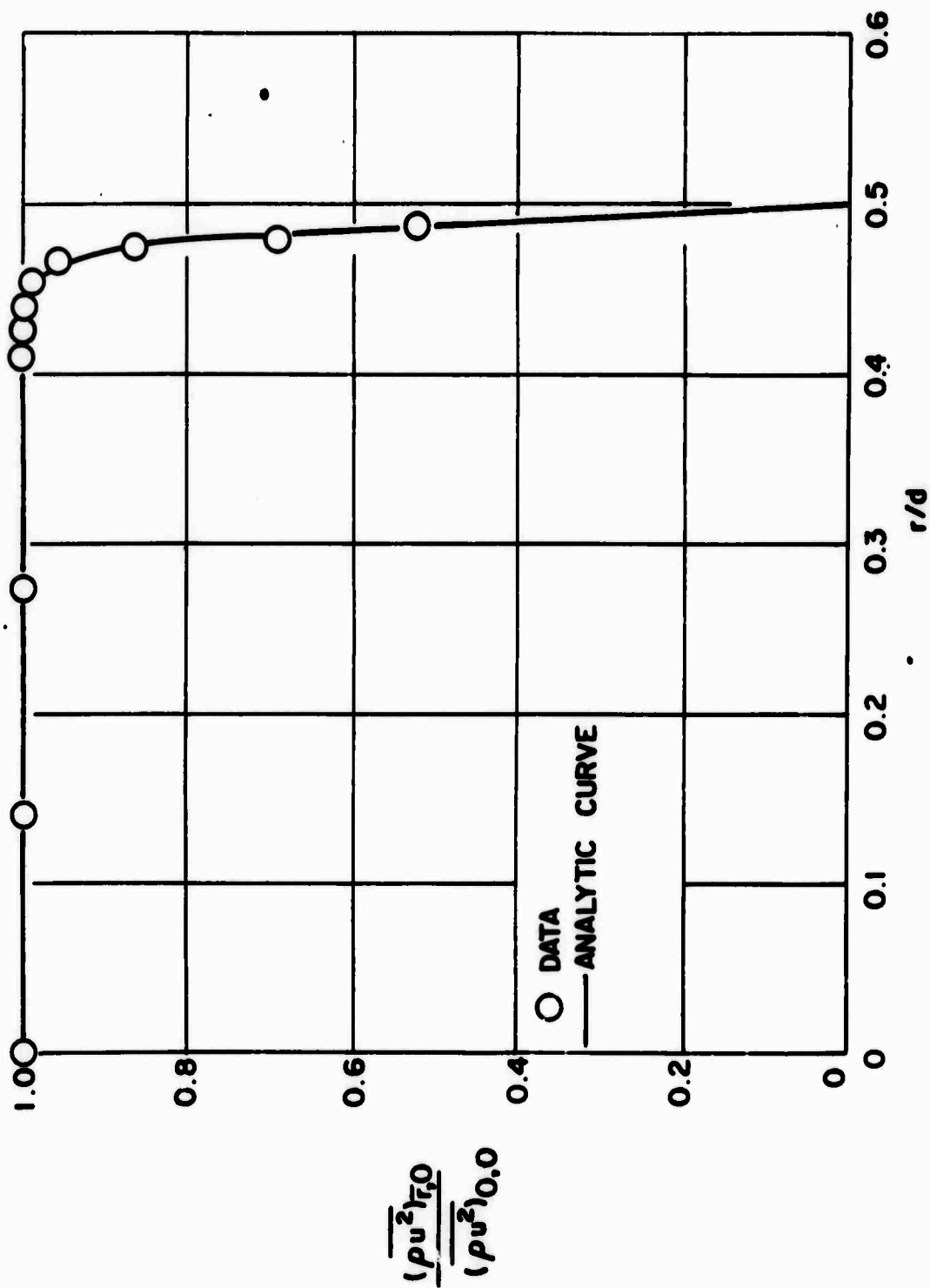


FIGURE 18 INITIAL PROFILE OF MOMENTUM FLUX FOR HOMOGENEOUS, ISOTHERMAL FREE JET

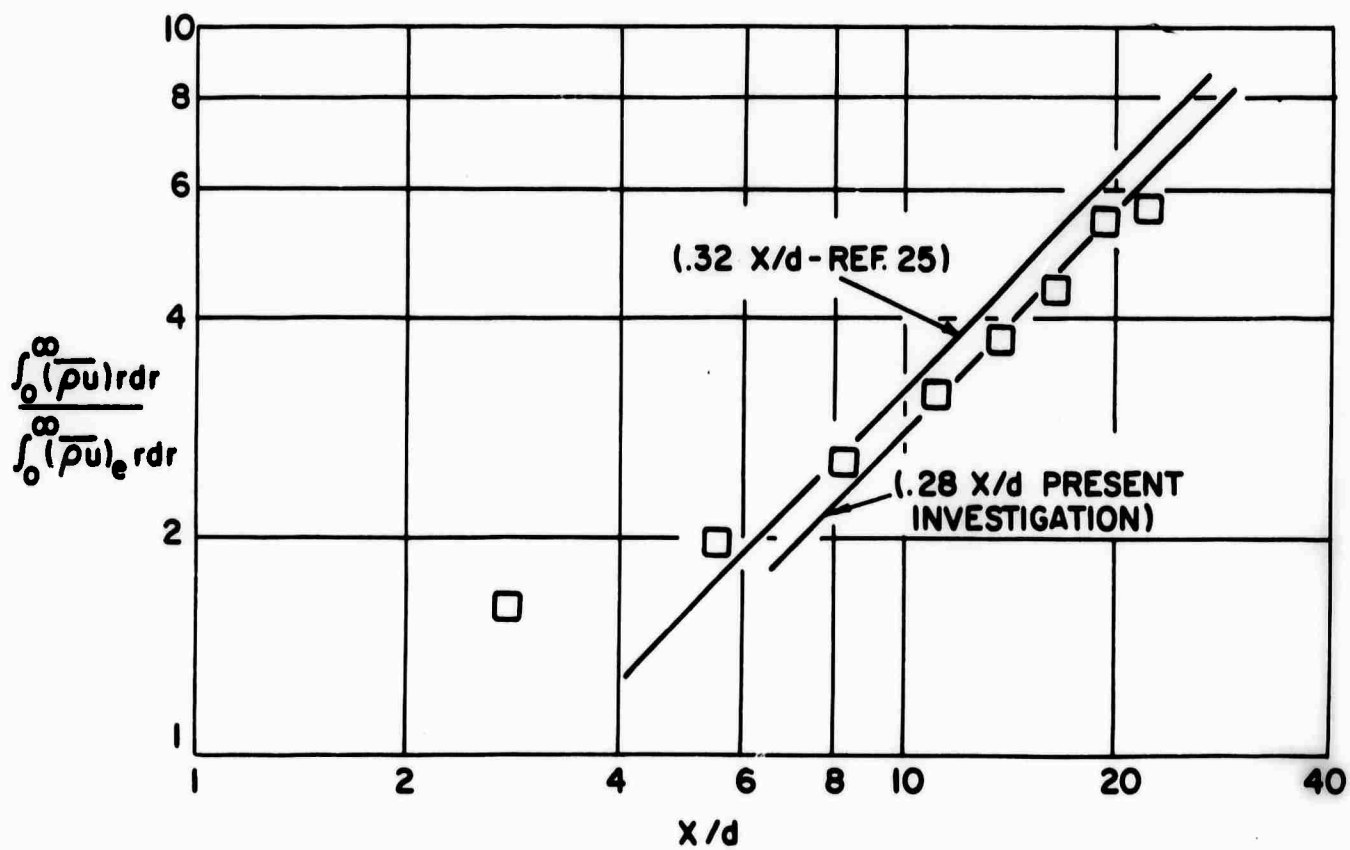
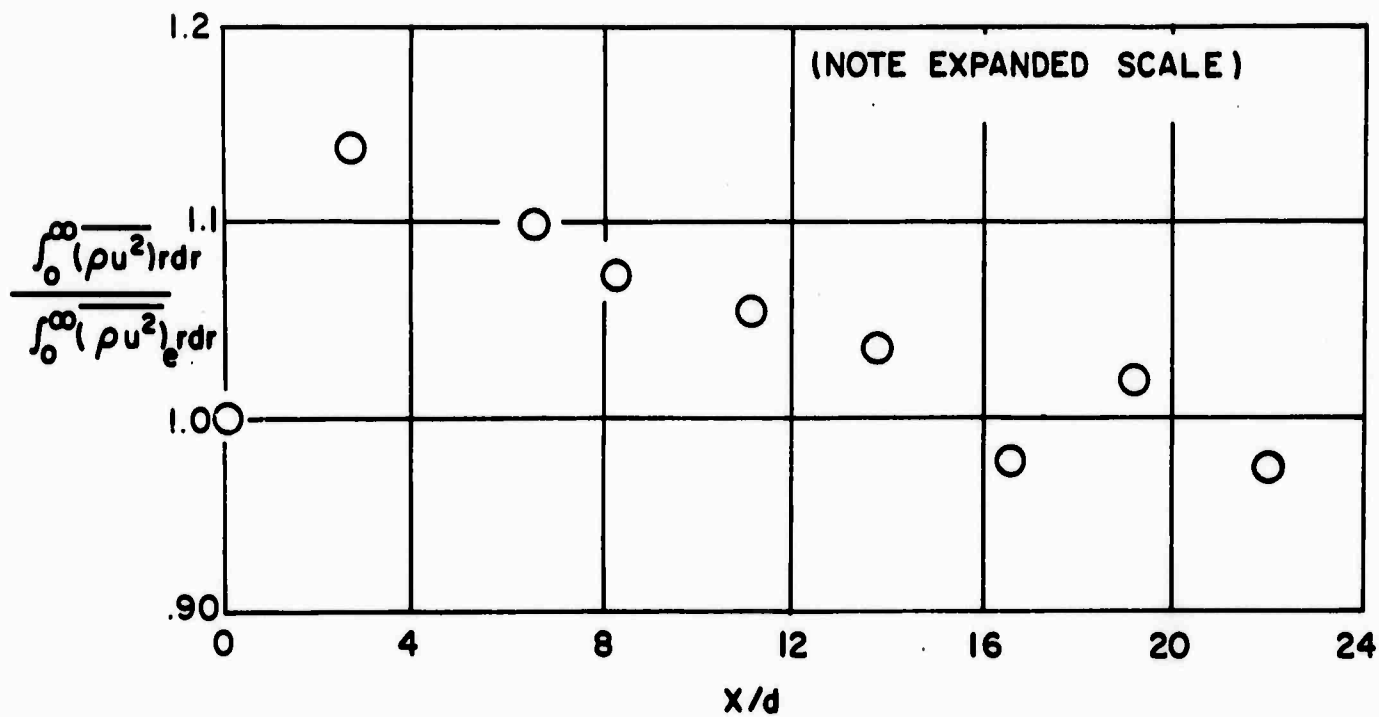


FIGURE 19 CONSERVATION OF TOTAL MOMENTUM FLUX AND GROWTH OF TOTAL MASS FLUX OF AIR FOR THE HOMOGENEOUS, ISOTHERMAL JET

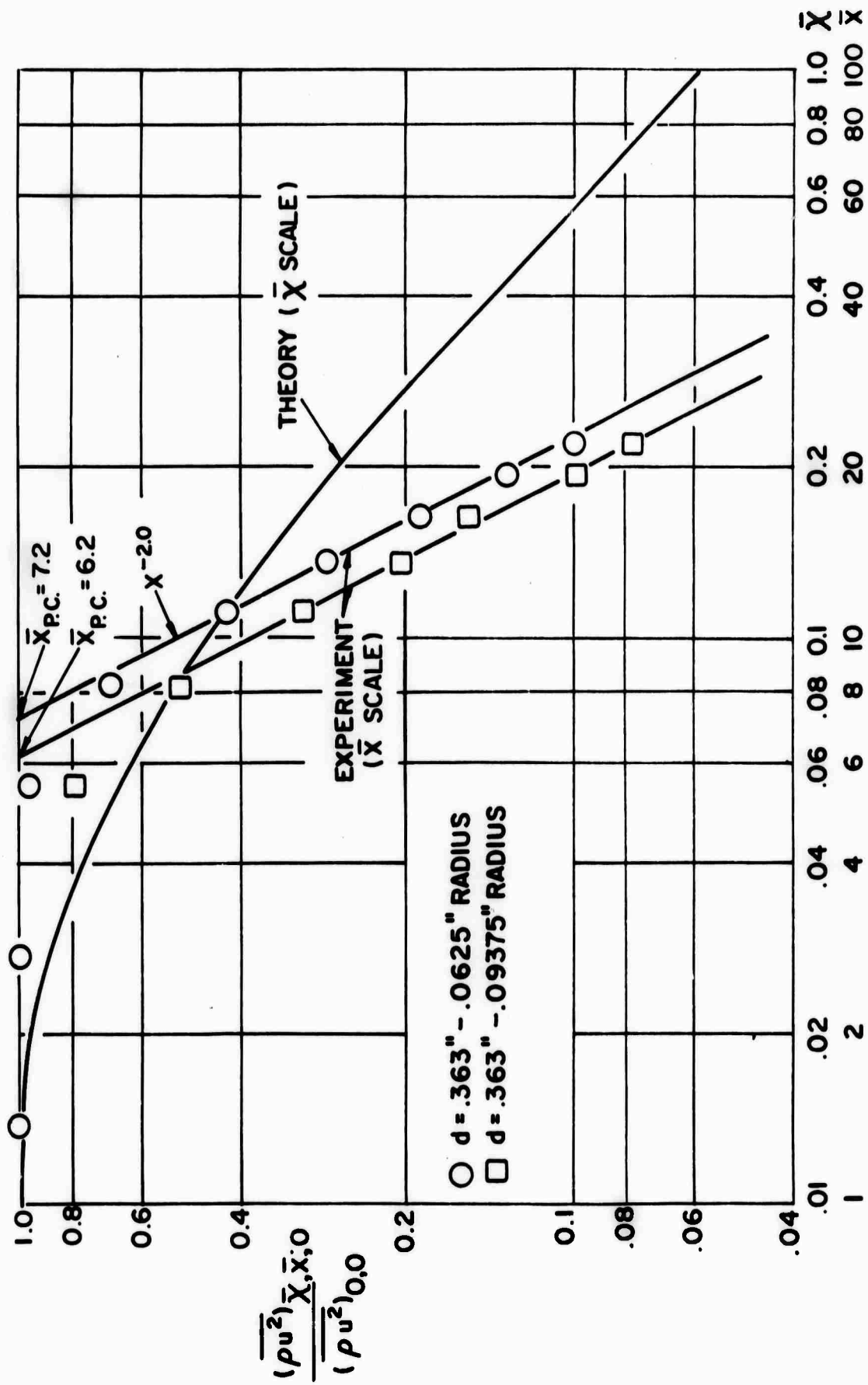


FIGURE 20 THEORETICAL AND EXPERIMENTAL BEHAVIOR OF CENTERLINE VALUES OF MOMENTUM FLUX FOR HOMOGENEOUS, ISOTHERMAL JET

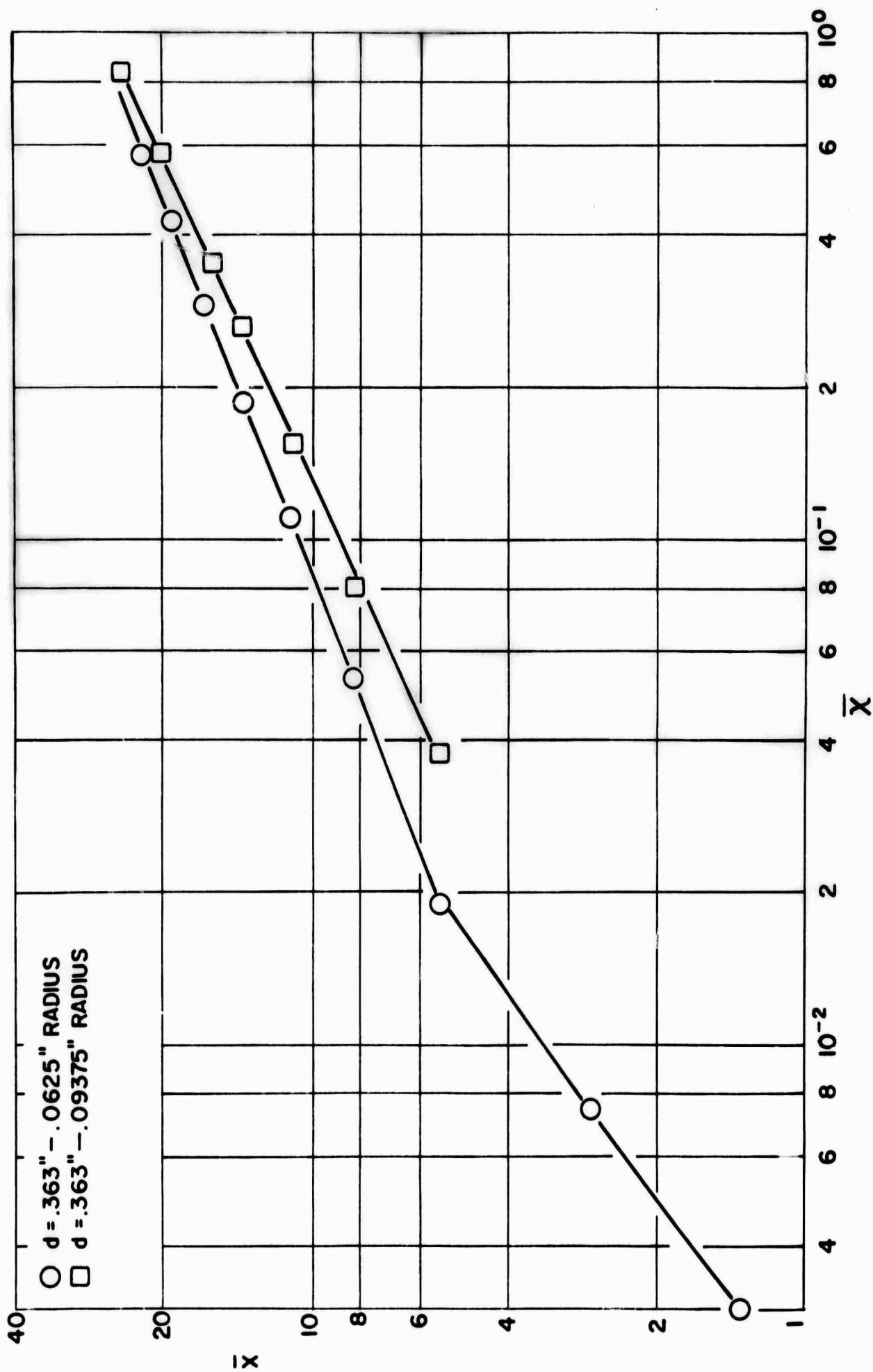


FIGURE 21 TRANSFORMATION BETWEEN PHYSICAL COORDINATE \bar{x} AND TRANSFORM COORDINATE \bar{X} FOR HOMOGENEOUS, ISOTHERMAL JET

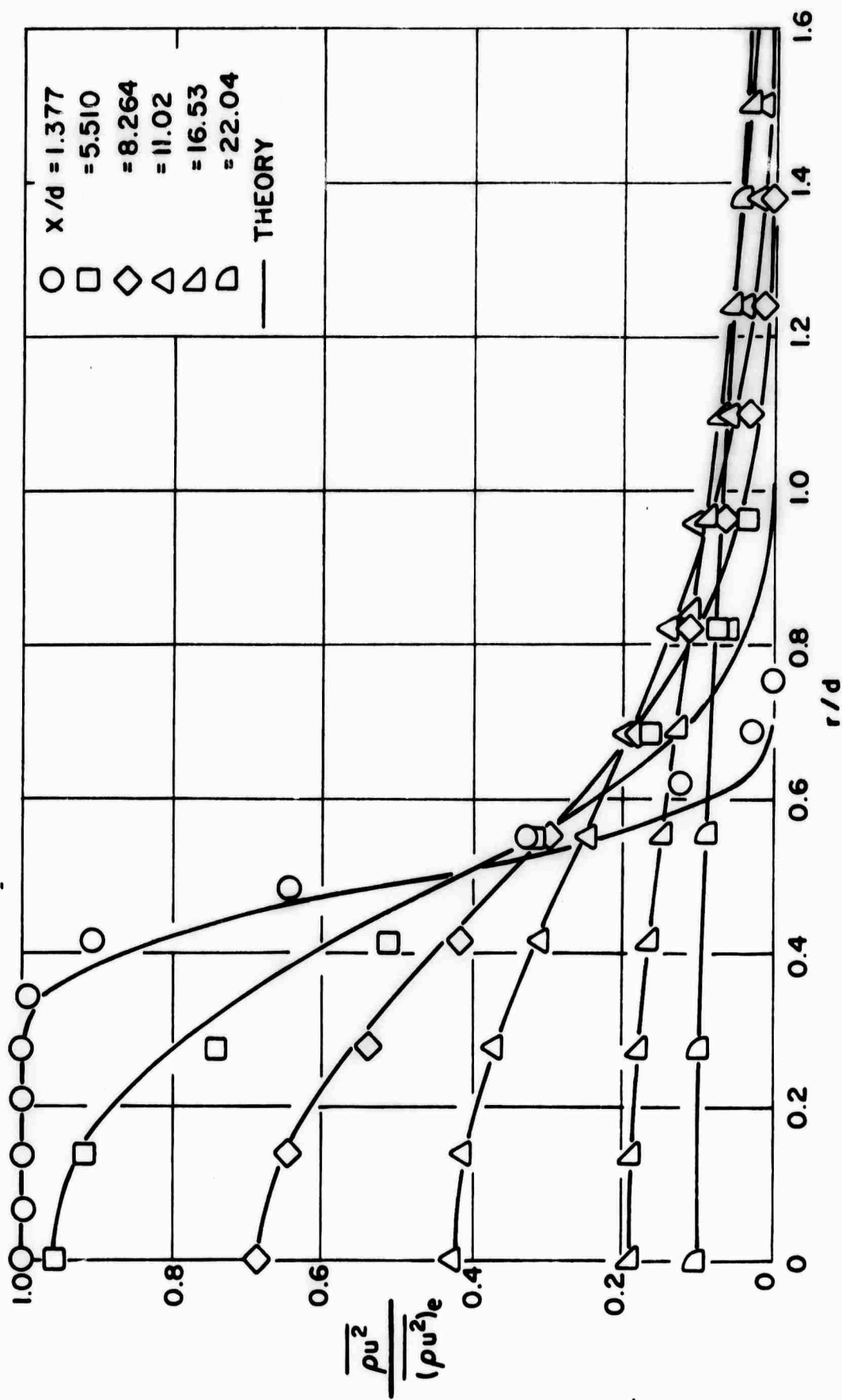


FIGURE 22 COMPARISON BETWEEN THEORY AND EXPERIMENT FOR COMPLETE MOMENTUM FLUX FLOW FIELD FOR HOMOGENEOUS, ISOTHERMAL JET

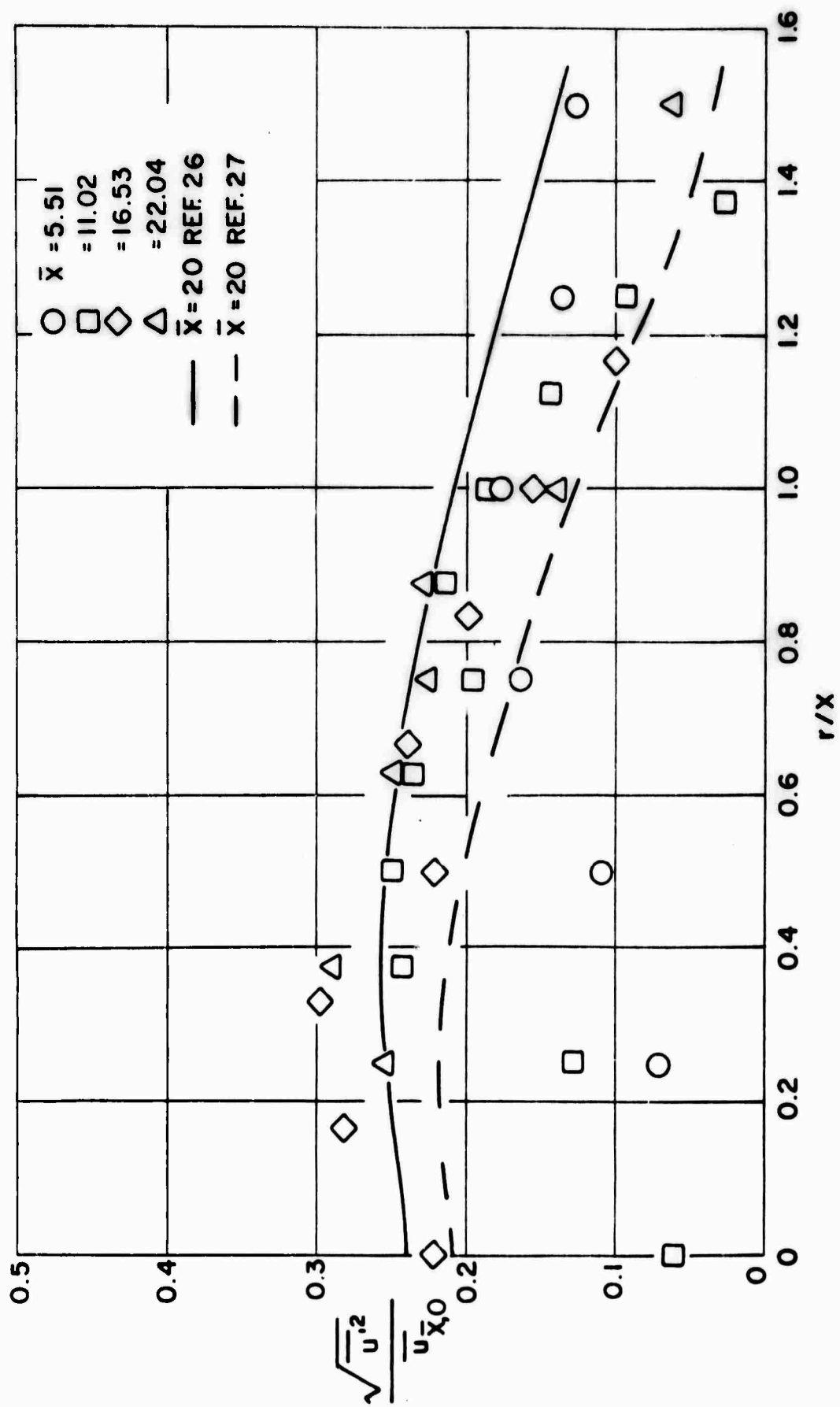


FIGURE 23 RESULTS OF MEASUREMENT OF INTENSITY OF AXIAL VELOCITY FLUCTUATIONS FROM MOMENTUM FLUX AND MASS FLUX

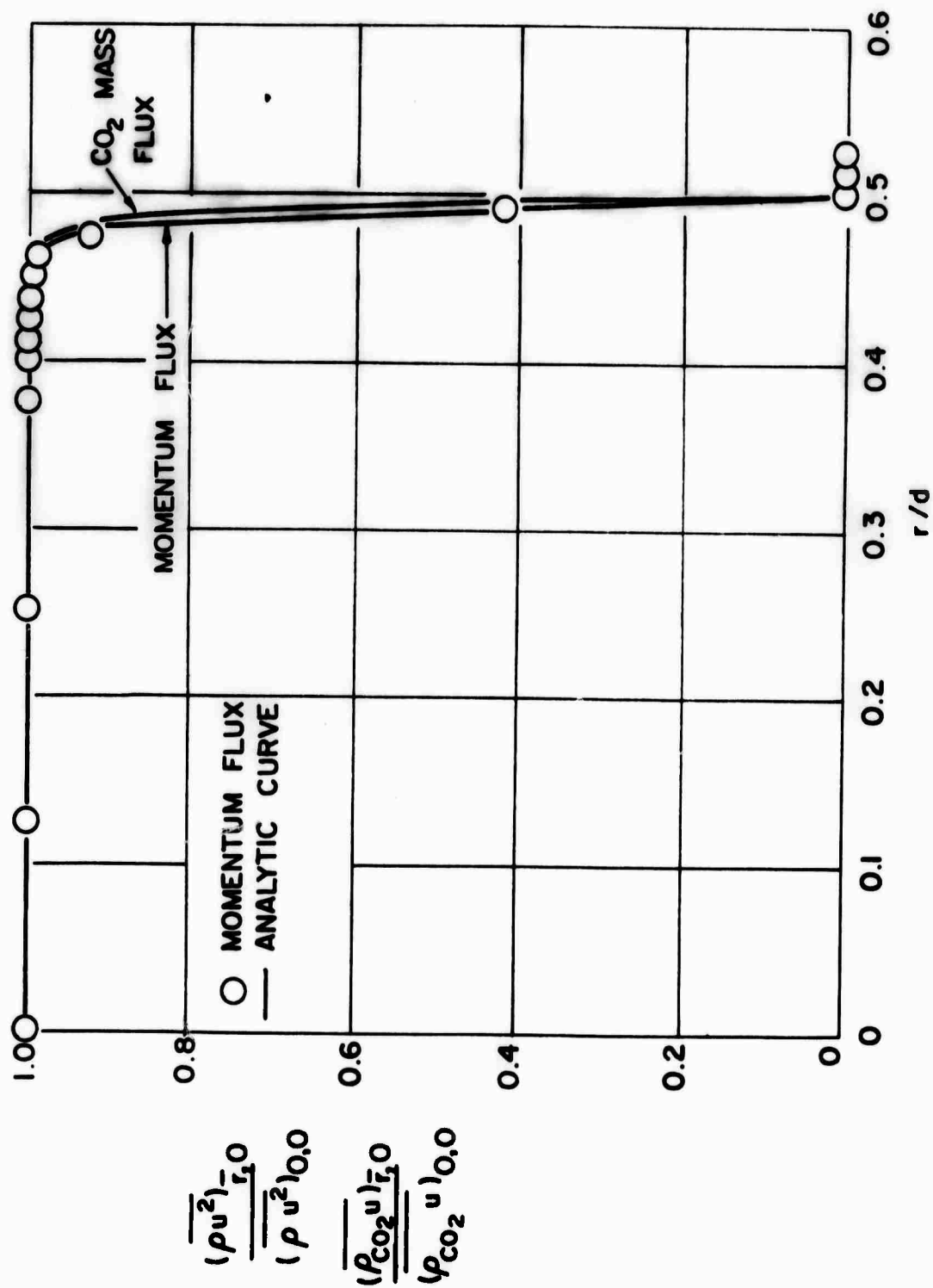


FIGURE 24 INITIAL PROFILES OF MOMENTUM FLUX AND MASS FLUX OF CO₂ FOR NON-HOMOGENEOUS, ISOTHERMAL FREE JET

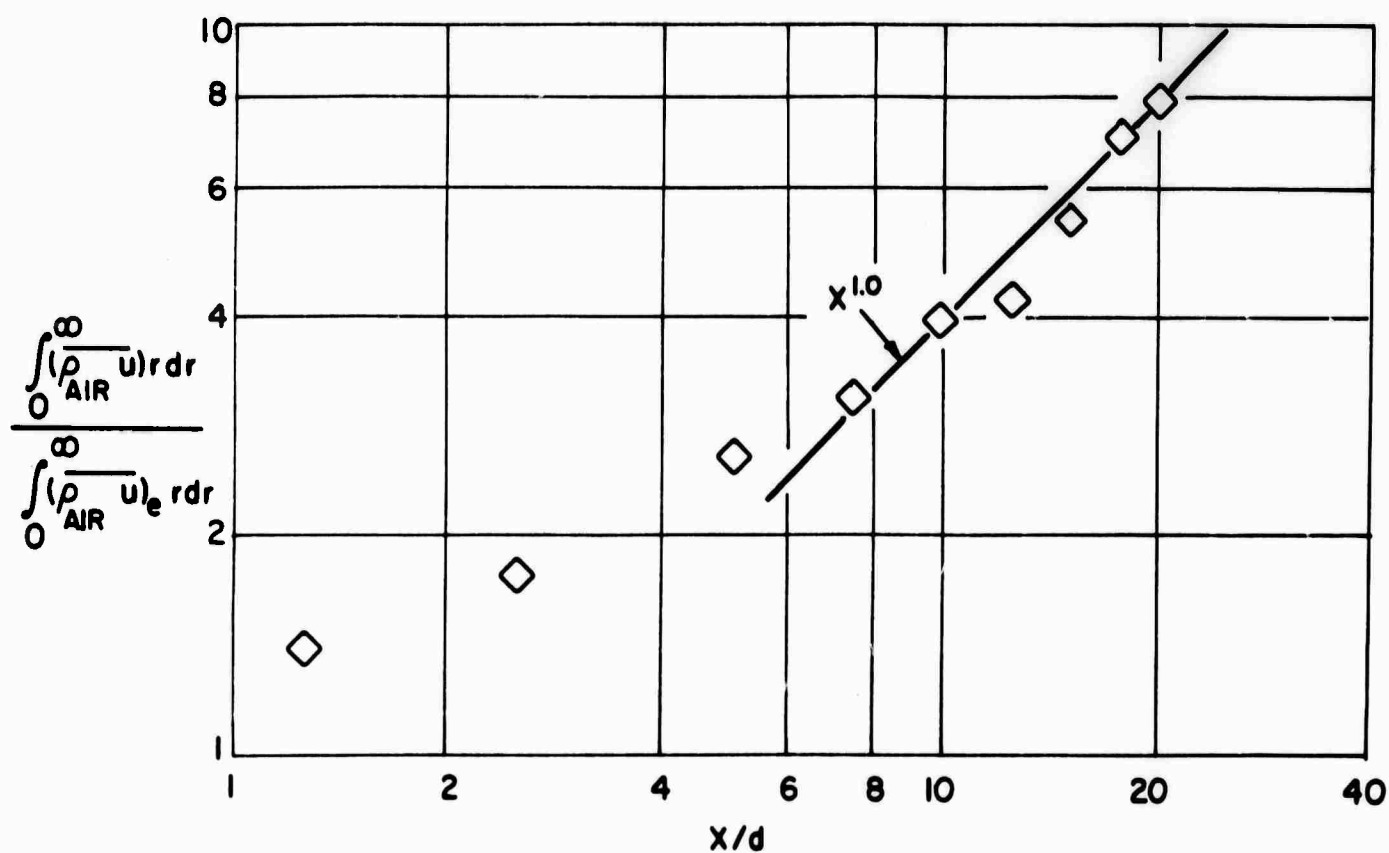
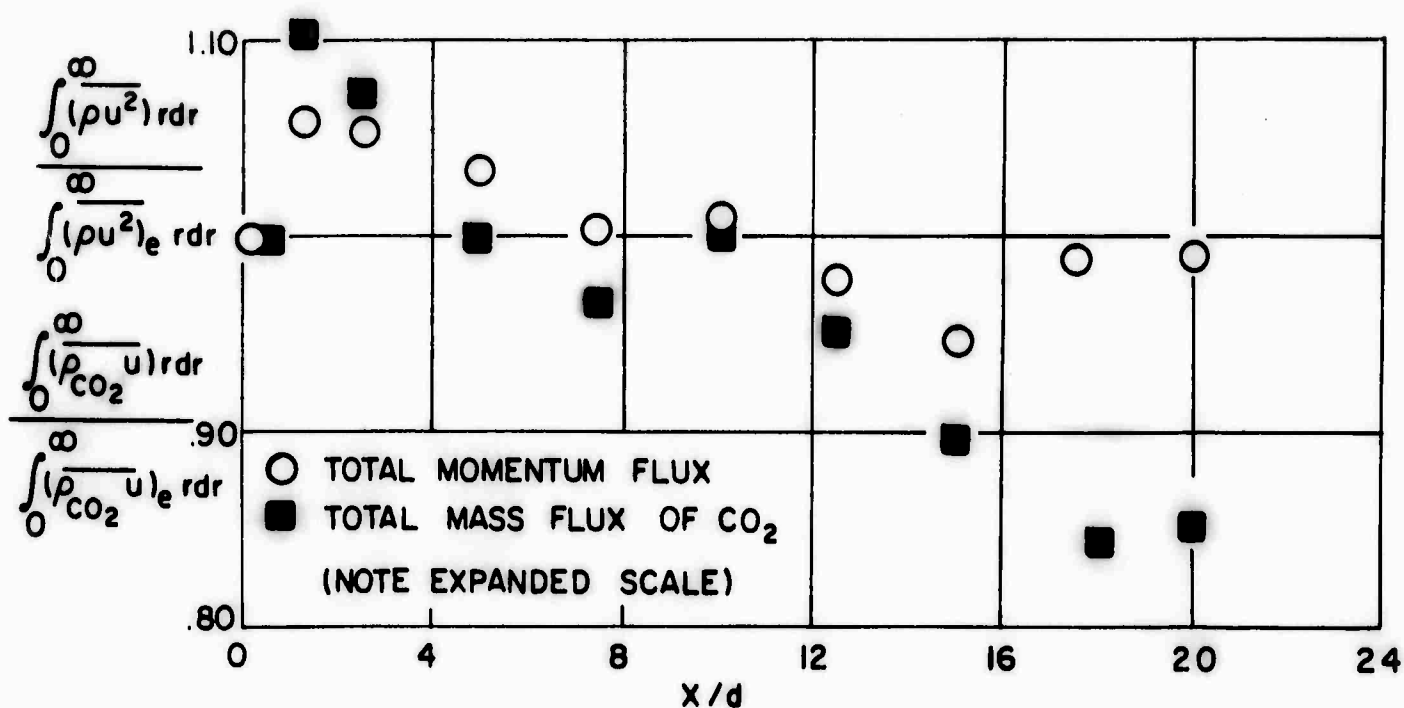


FIGURE 25 CONSERVATION OF TOTAL MOMENTUM FLUX AND TOTAL MASS FLUX OF CO₂ AND GROWTH OF TOTAL MASS FLUX OF AIR FOR THE NON-HOMOGENEOUS, ISOTHERMAL FREE JET

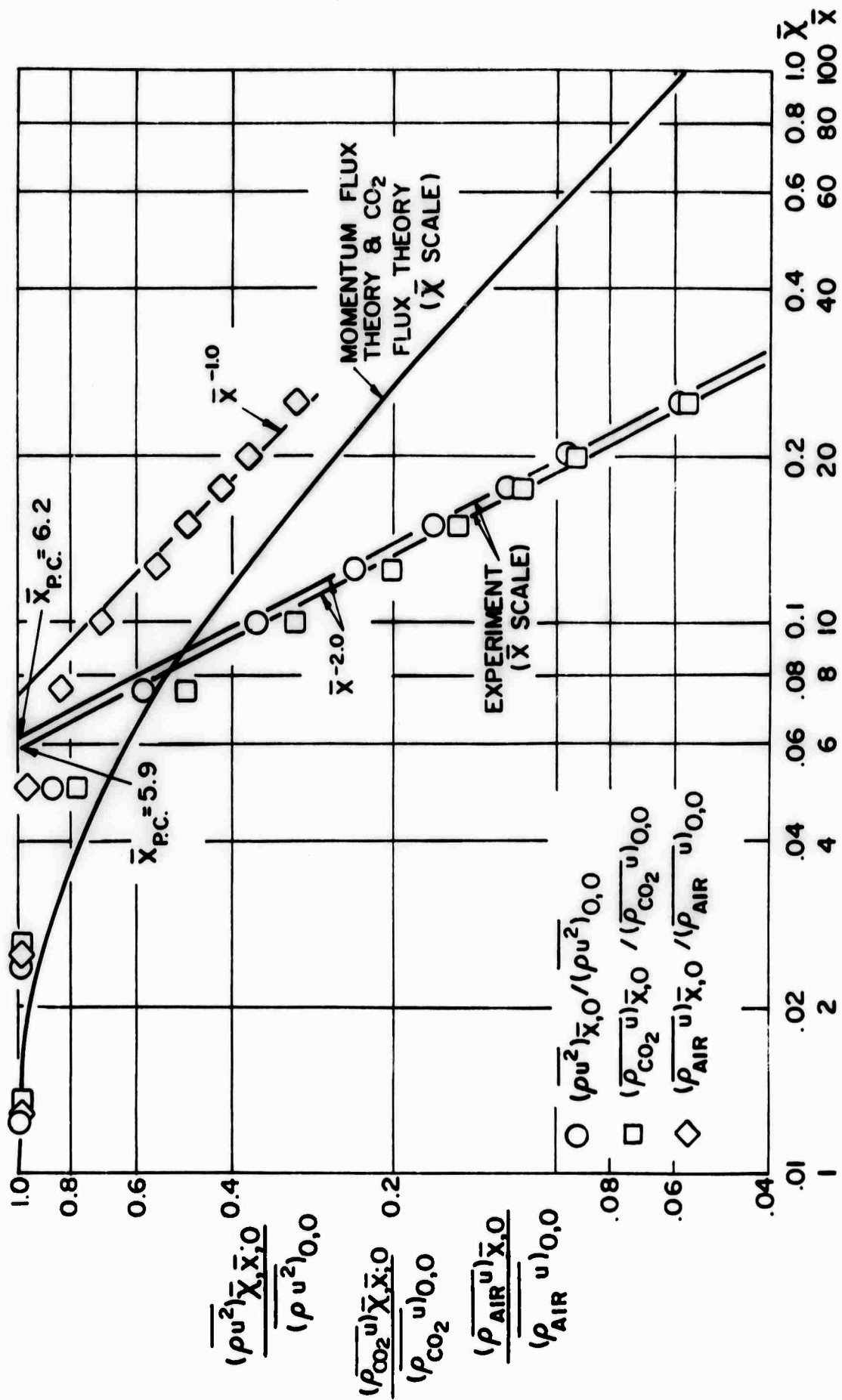


FIGURE 26 BEHAVIOR OF CENTERLINE VALUES OF ALL FLUX VARIABLES FOR NON-HOMOGENEOUS, ISOTHERMAL JET

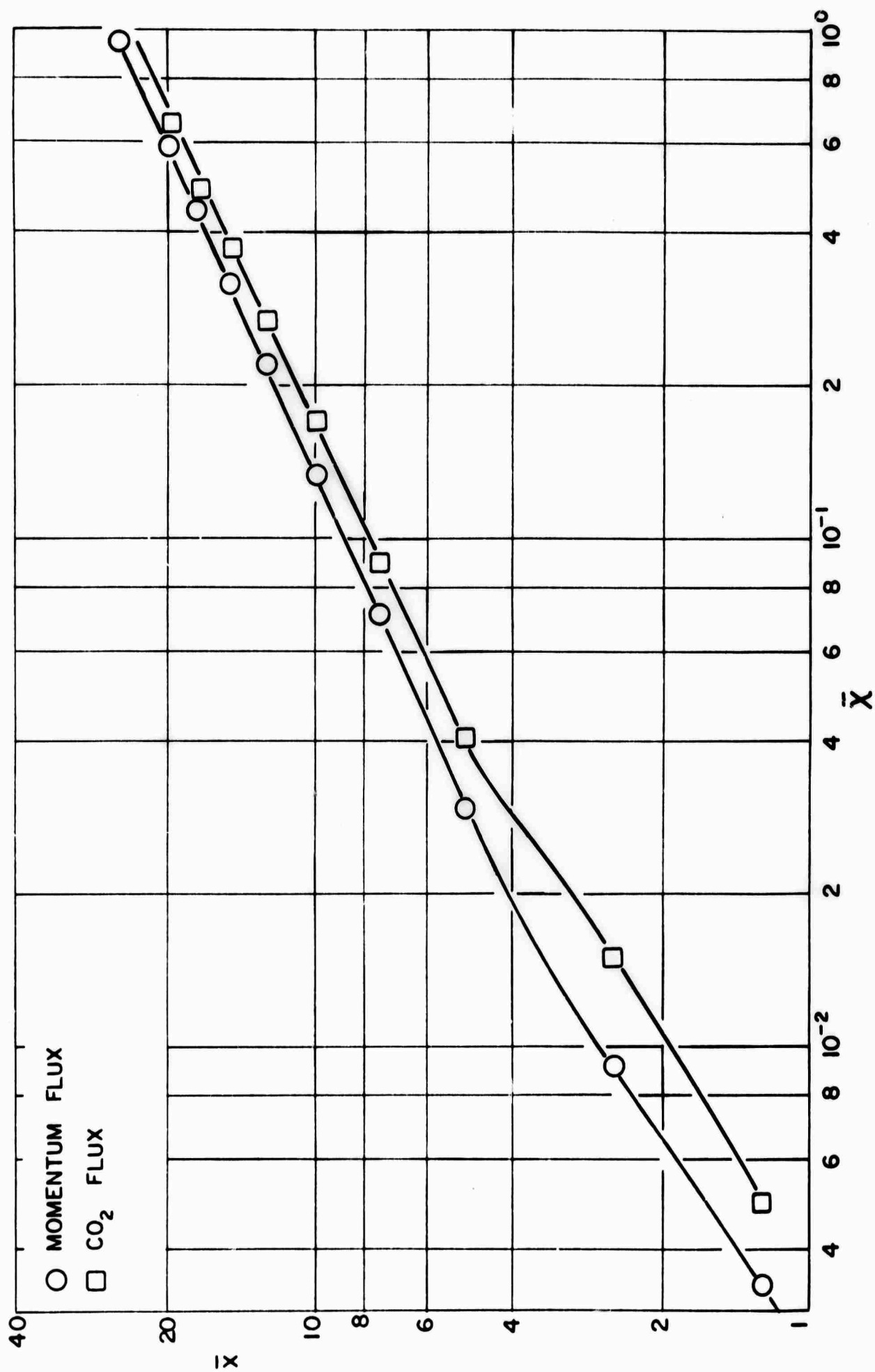


FIGURE 27 TRANSFORMATIONS BETWEEN PHYSICAL COORDINATE \bar{x} AND TRANSFORM COORDINATE \bar{X} FOR MOMENTUM FLUX AND MASS FLUX OF CO₂ FOR NON-HOMOGENEOUS, ISOTHERMAL JET

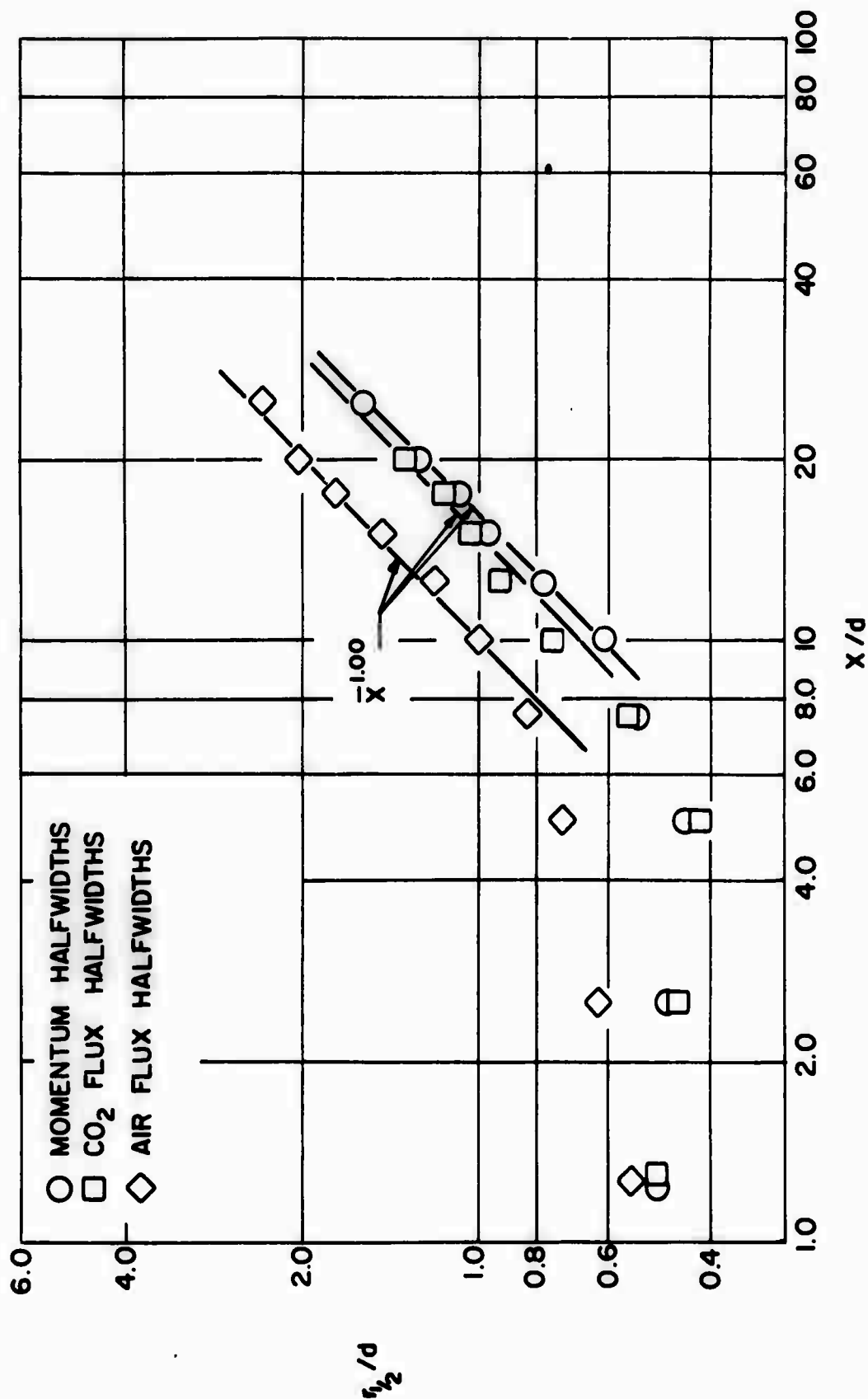


FIGURE 28 HALFWIDTH BEHAVIOR OF ALL FLUX VARIABLES FOR NON-HOMOGENEOUS, ISOTHERMAL JET

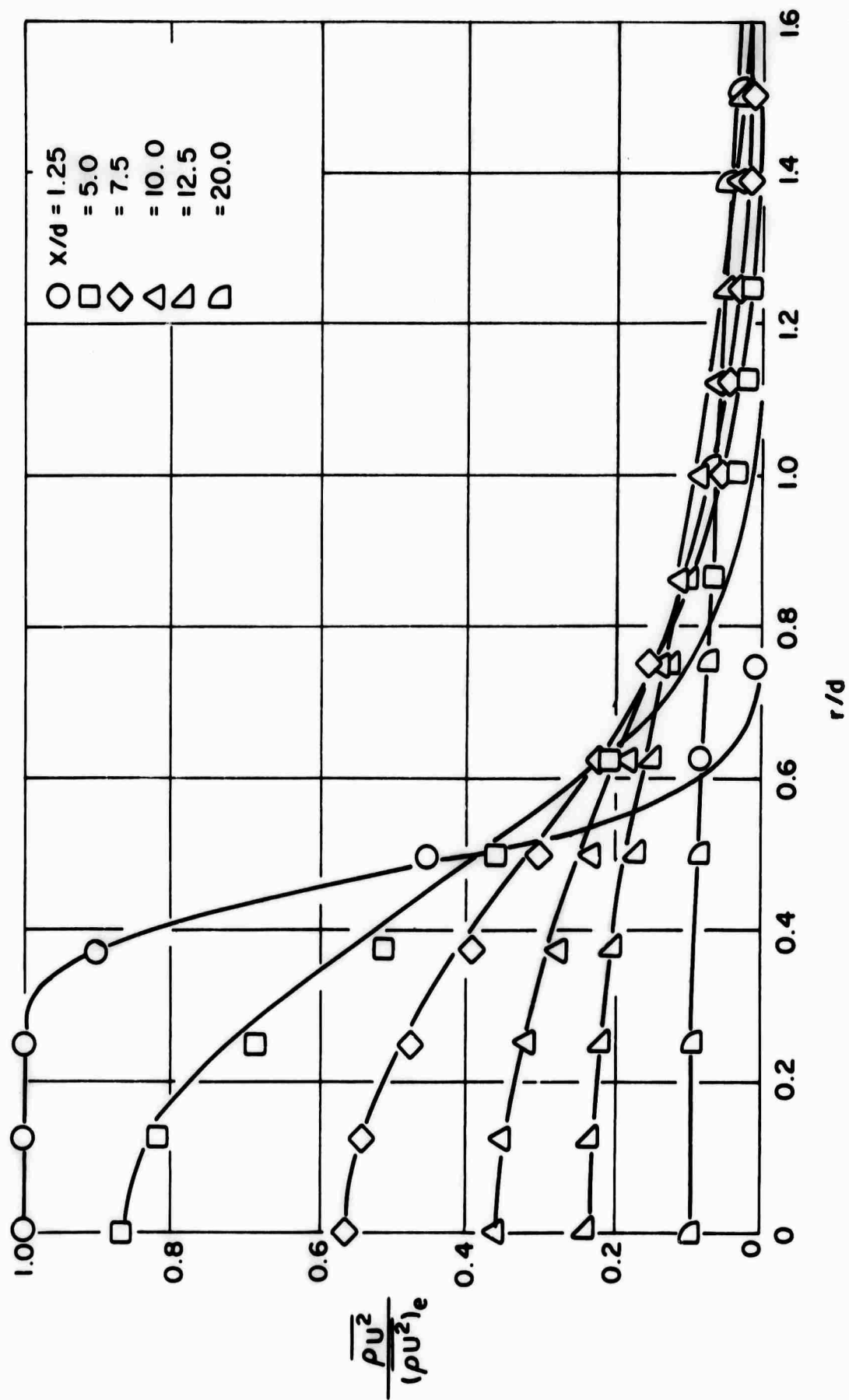


FIGURE 29 COMPARISON BETWEEN THEORY AND EXPERIMENT FOR COMPLETE
MOMENTUM FLUX FLOW FIELD FOR NON-HOMOGENEOUS, ISOTHERMAL
JET

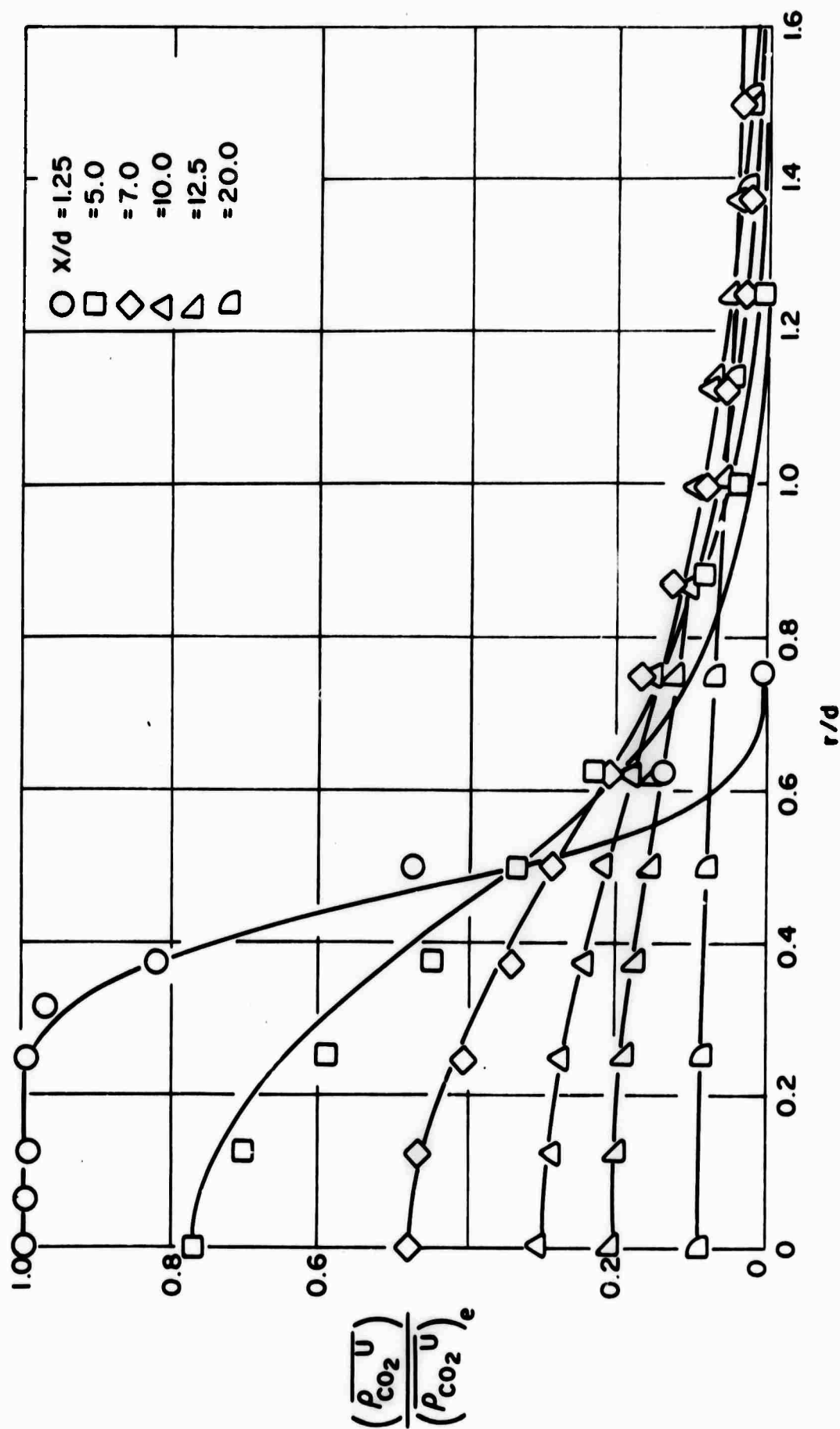


FIGURE 30 COMPARISON BETWEEN THEORY AND EXPERIMENT FOR COMPLETE CO_2 MASS FLUX FLOW FIELD FOR NON-HOMOGENEOUS, ISOTHERMAL JET

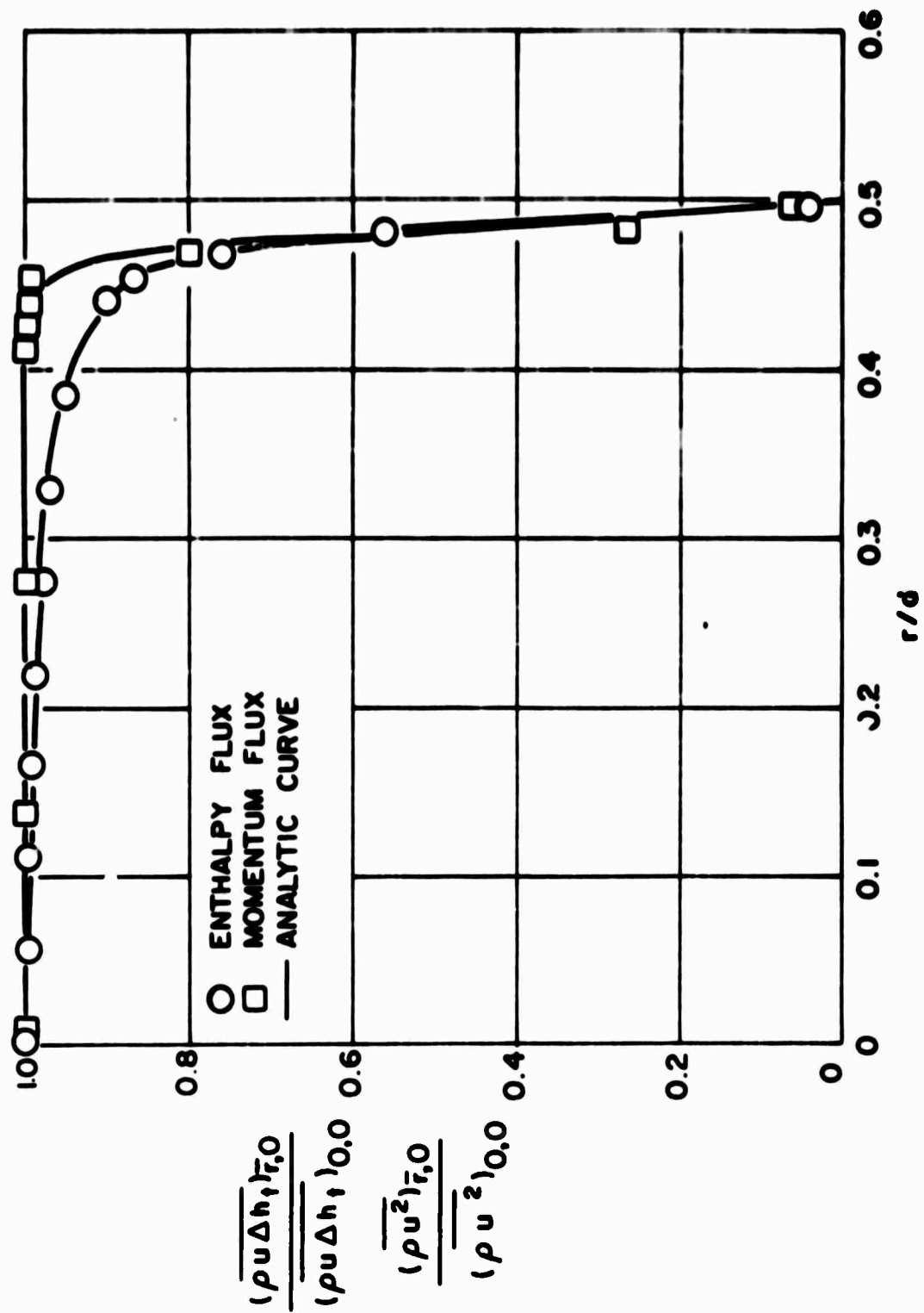


FIGURE 31 INITIAL PROFILES OF MOMENTUM FLUX AND ENTHALPY FLUX FOR HOMOGENEOUS, NON-ISOTHERMAL JET

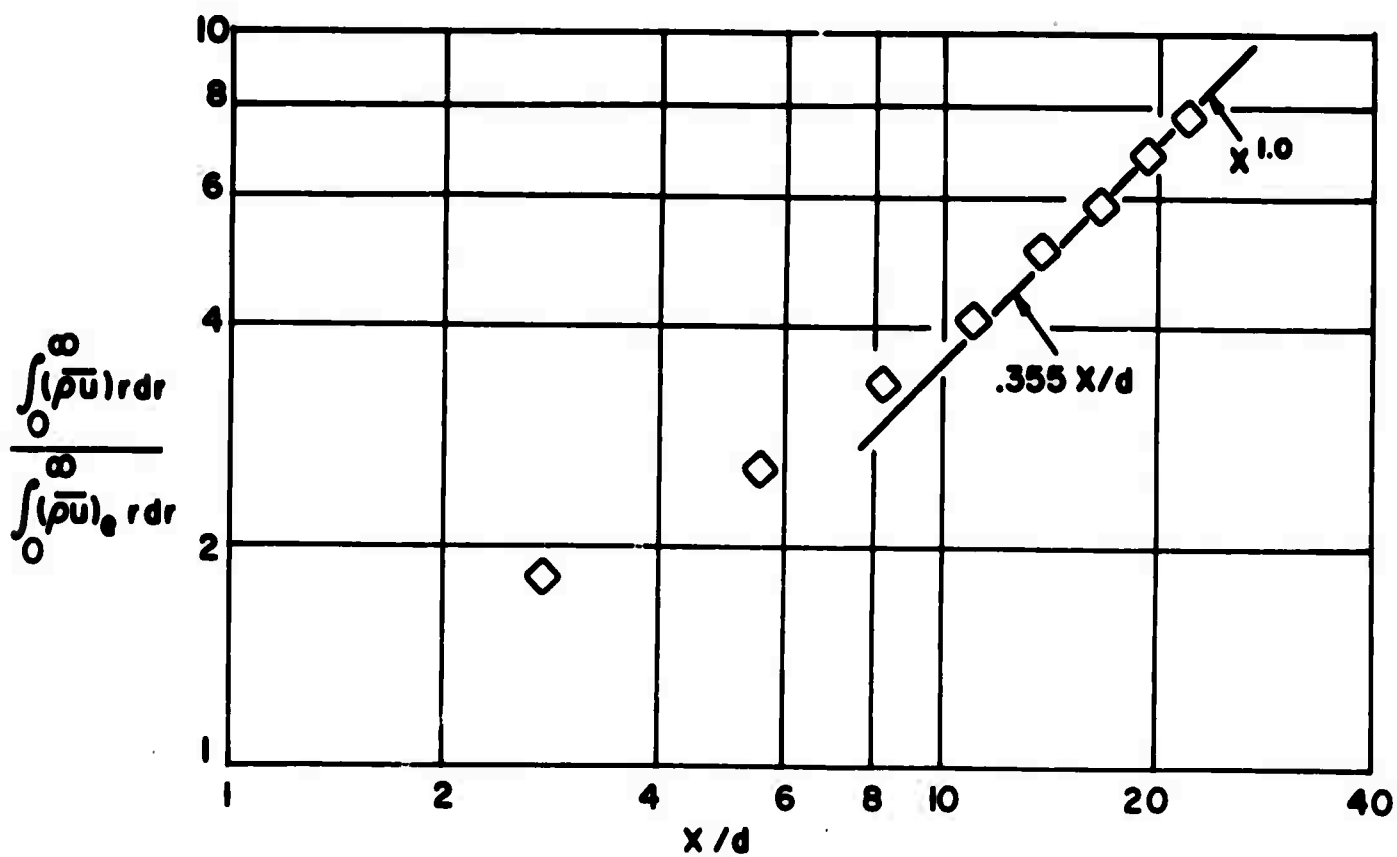
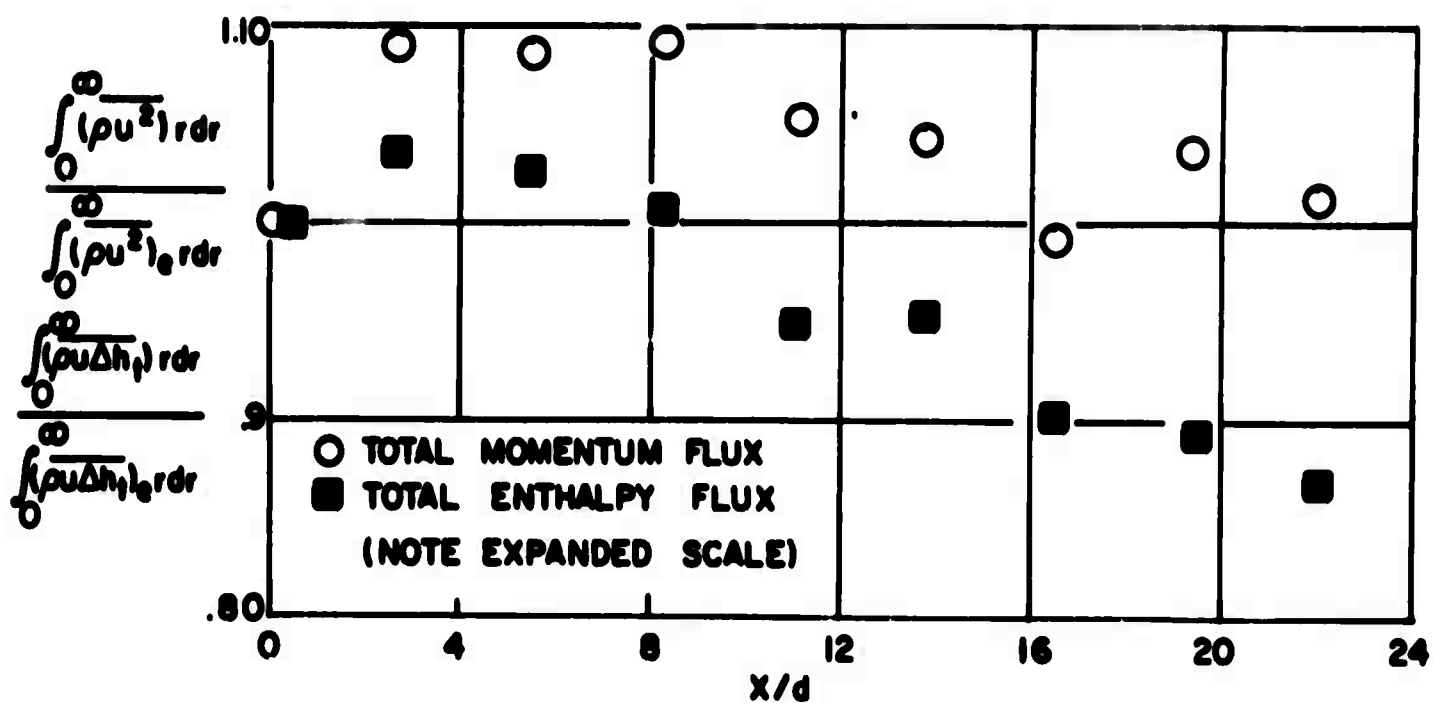


FIGURE 32 CONSERVATION OF TOTAL MOMENTUM FLUX AND TOTAL FLUX OF STAGNATION ENTHALPY MINUS AMBIENT ENTHALPY AND GROWTH OF TOTAL MASS FLUX

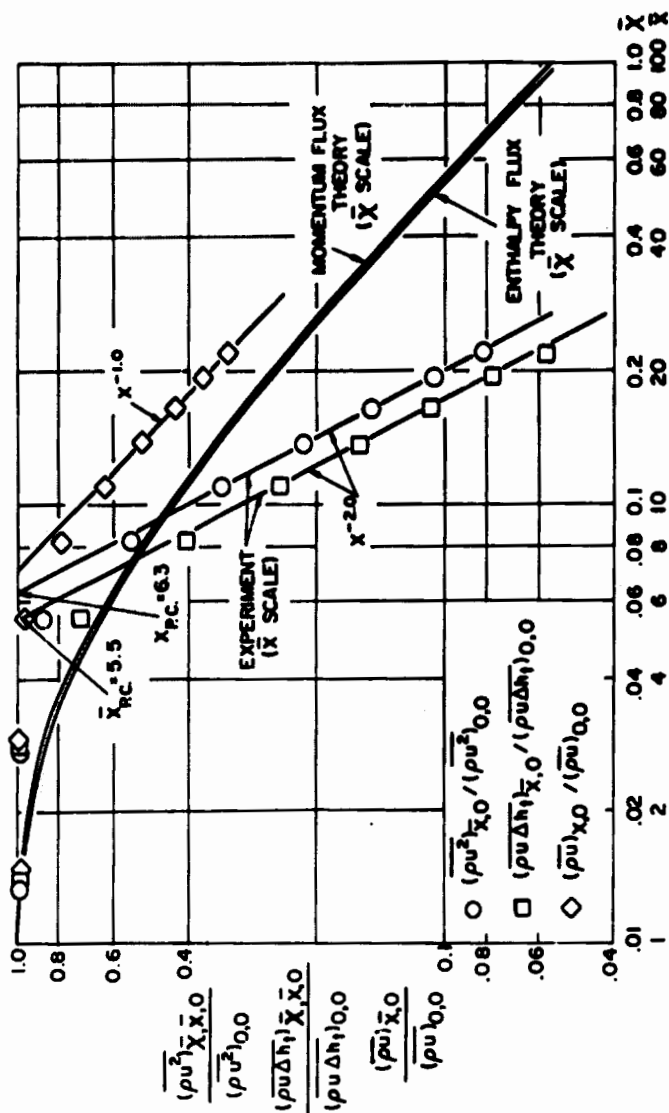


FIGURE 33 BEHAVIOR OF CENTERLINE VALUES FOR ALL FLUX VARIABLES FOR HOMOGENEOUS, NON-ISOTHERMAL JET

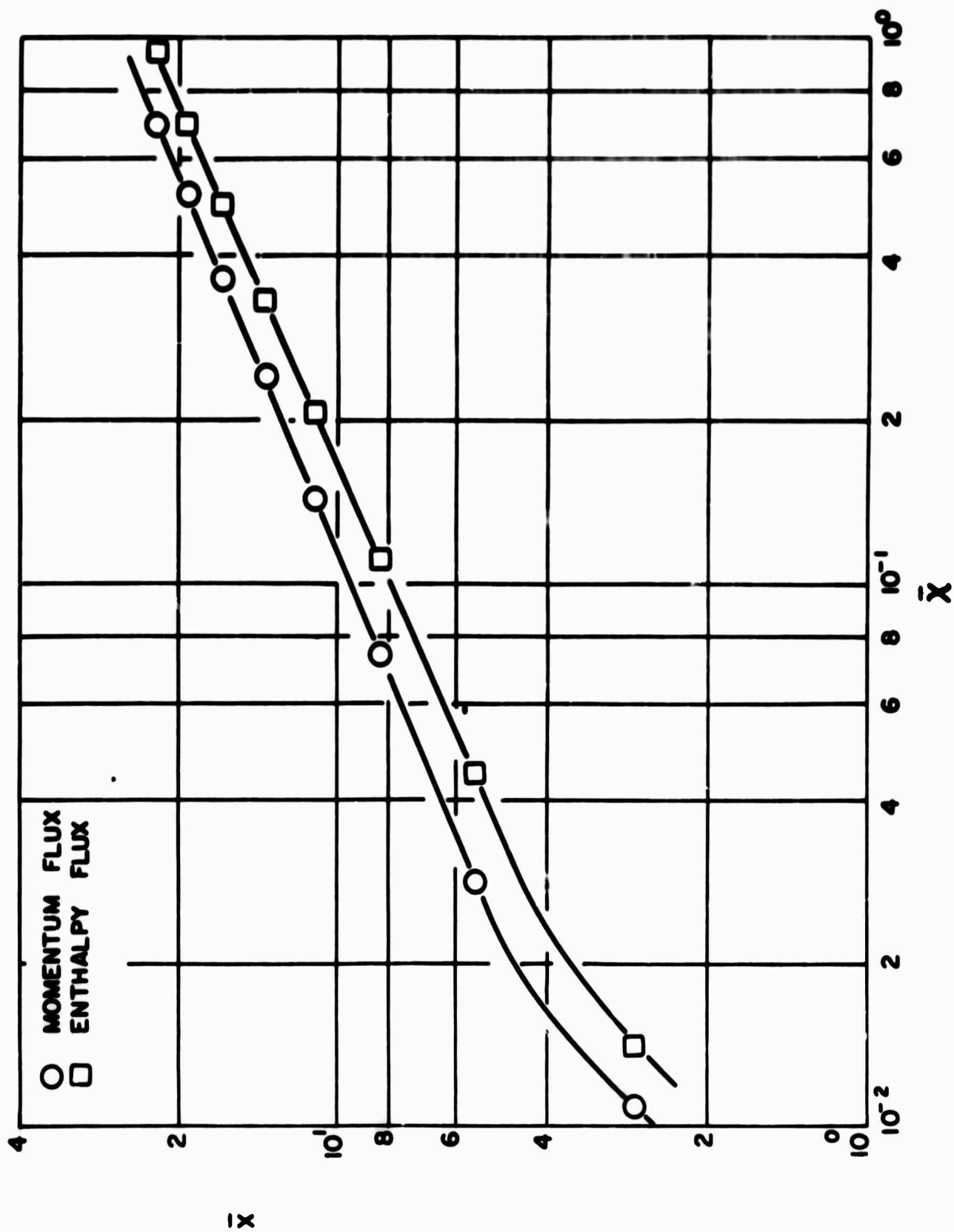


FIGURE 34 TRANSFORMATION BETWEEN PHYSICAL COORDINATE \bar{x} AND TRANSFORM COORDINATE $\bar{\chi}$ FOR MOMENTUM FLUX AND ENTHALPY FLUX FOR HOMOGENEOUS, NON-ISOTHERMAL JET

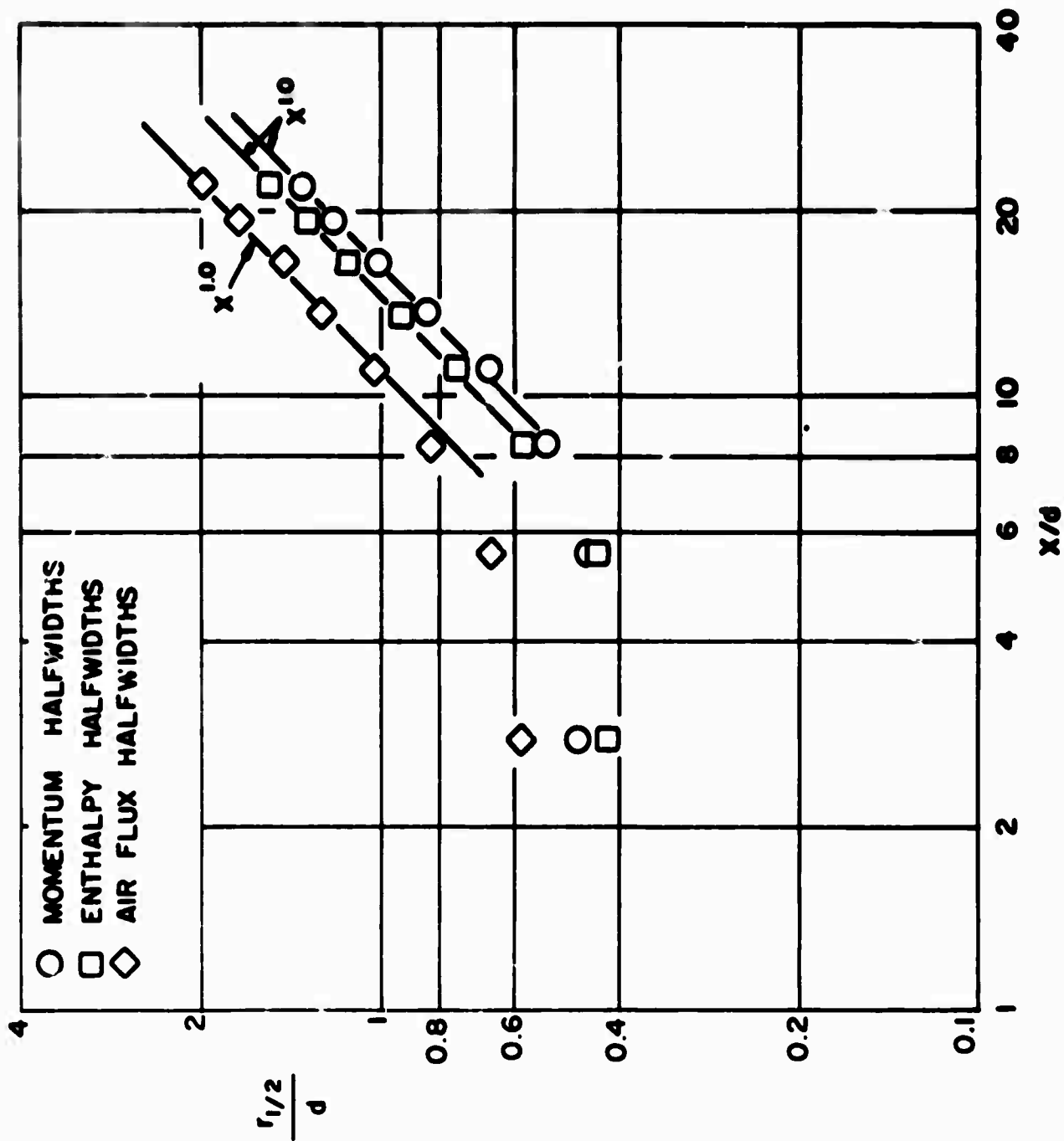


FIGURE 35 HALFWIDTH BEHAVIOR OF ALL FLUX VARIABLES FOR HOMOGENEOUS, NON-ISOTHERMAL JET

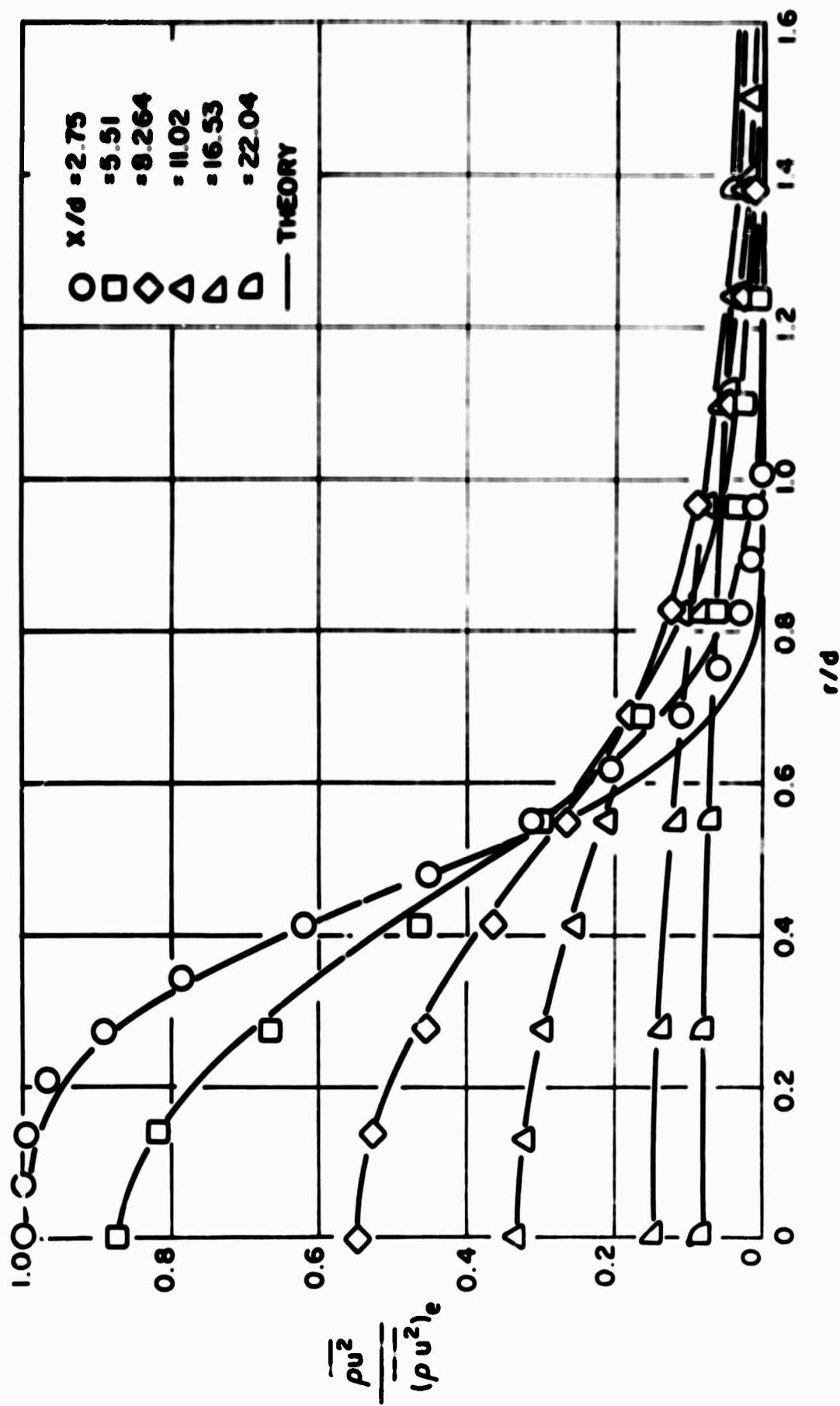


FIGURE 36 COMPARISON BETWEEN THEORY AND EXPERIMENT FOR COMPLETE MOMENTUM FLUX FIELD FOR HOMOGENEOUS, NON-ISOTHERMAL JET

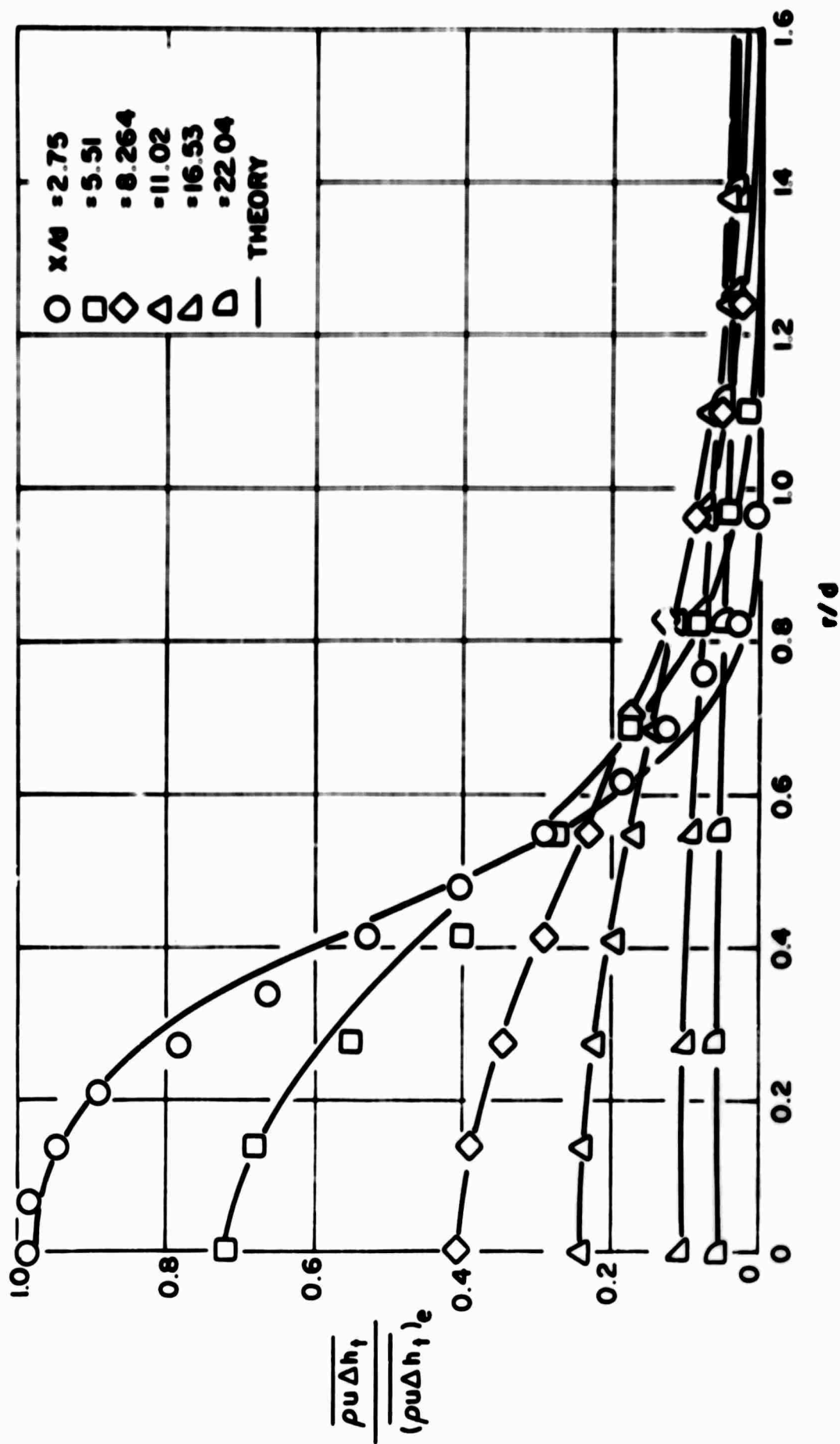


FIGURE 37 COMPARISON BETWEEN THEORY AND EXPERIMENT FOR COMPLETE ENTHALPY FLUX FIELD FOR HOMOGENEOUS, NON-ISOTHERMAL FLOW

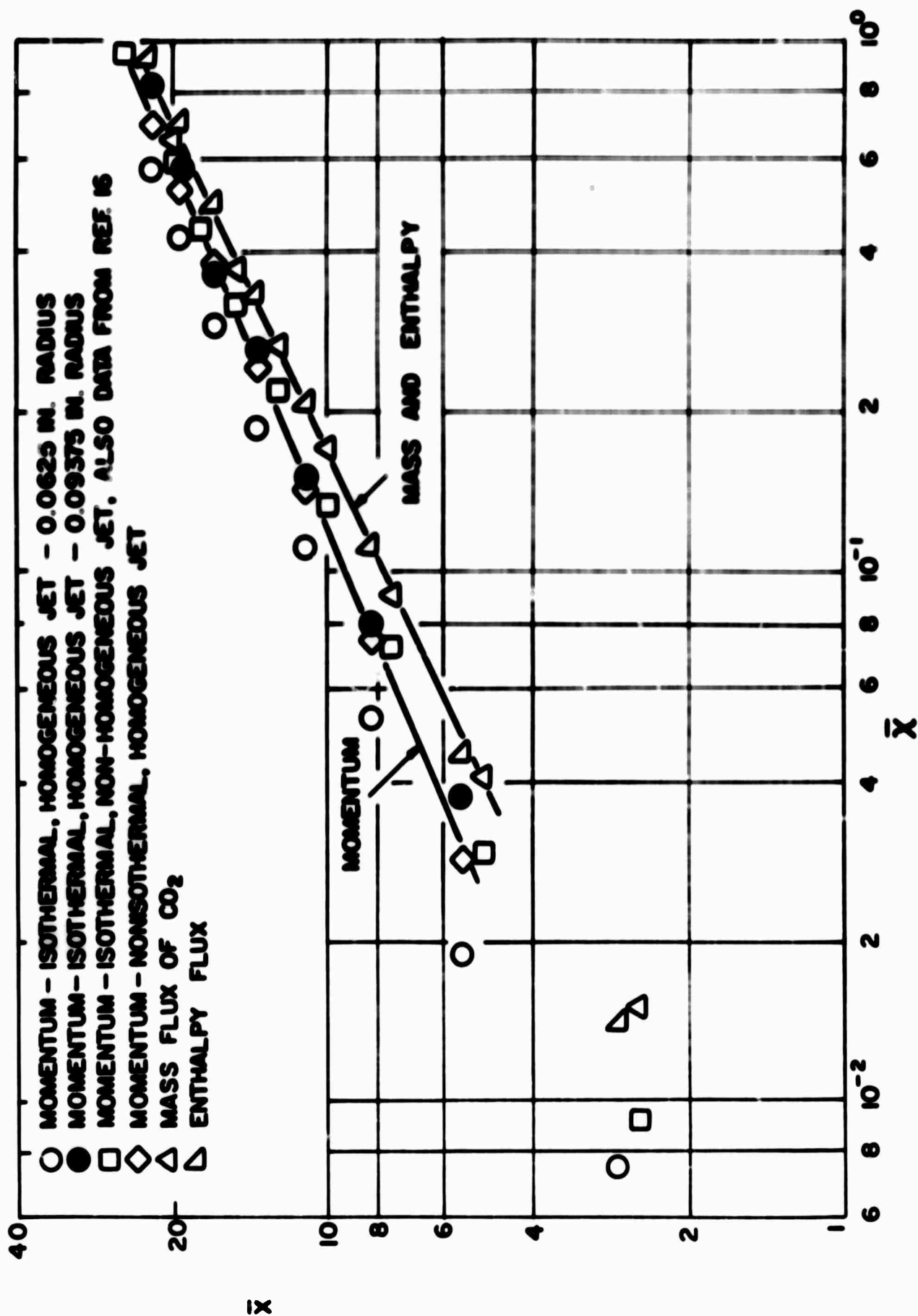


FIGURE 39 COMPARISON OF RELATIVE ENTRAINMENT FOR ALL JETS INVESTIGATED

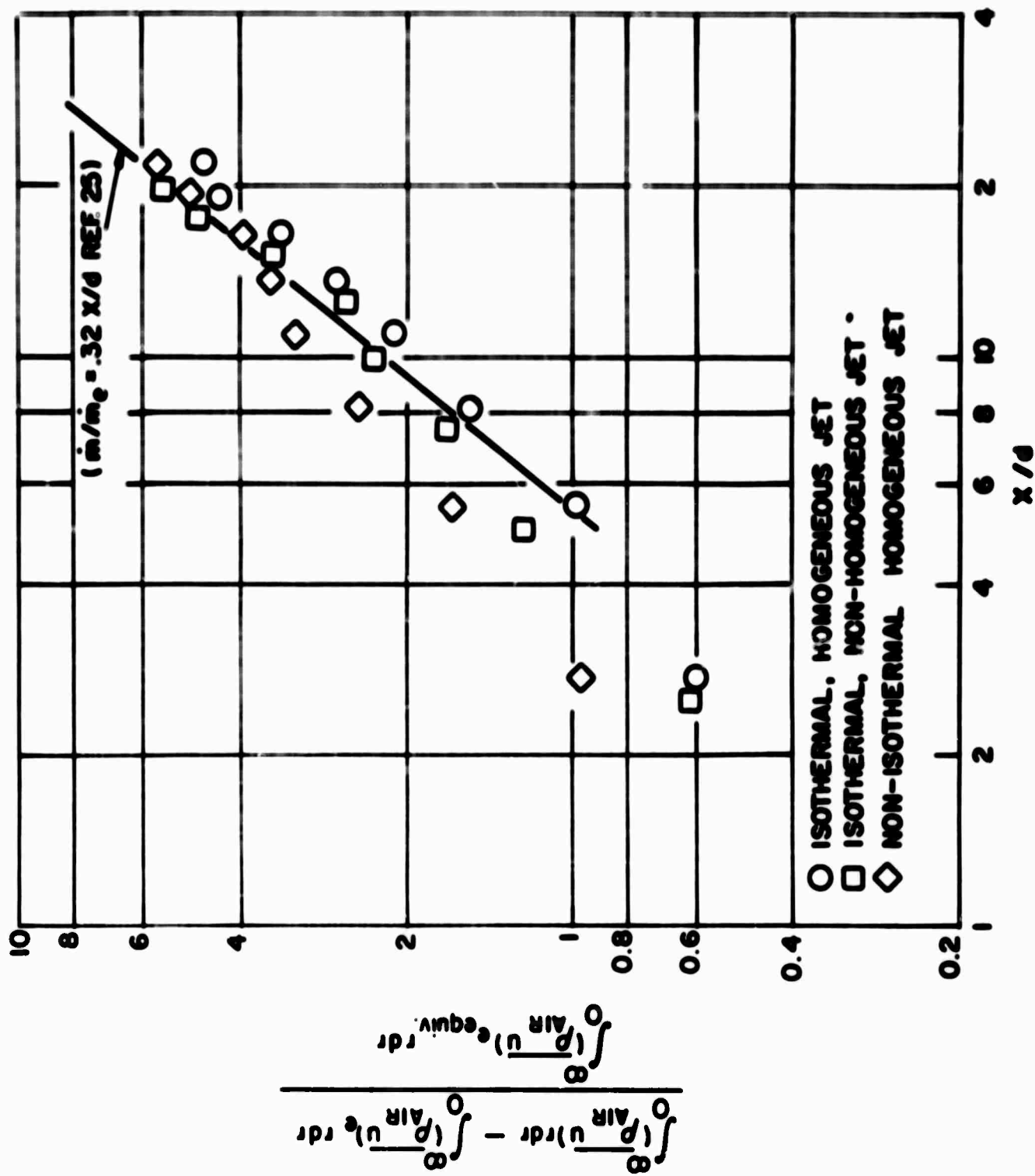


FIGURE 38 COMPARISON OF TRANSFORMATIONS BETWEEN PHYSICAL COORDINATE x AND TRANSFORM COORDINATE \bar{x} FOR ALL JETS INVESTIGATED